PhD Thesis

Surface electromagnetic wave in two-dimensional materials

Muhammad Shoufie Ukhtary

Department of Physics, Graduate School of Science
Tohoku University

September, 2018

Acknowledgments

"You do not see in the creation of the Most Merciful any inconsistency. So return your eyes to the sky; do you see any breaks? Then return your eyes twice again. Your eyes will return to you humbled while they are fatigued."

Quran, 67:3-4

Alhamdulilah, Praise be to the Lord. In this opportunity, I would like to acknowledge everyone that has supported me in finishing my doctoral course and this thesis. I would like to thank my parents and family to keep supporting and praying for the best of me until now. I hope that I can make them proud. I would like also to say my thanks to Saito-sensei for his supervision during my five years study in Japan. I learnt a lot from him, such as how to present something to audience in the most simple way and also how to teach somebody. Thank you for taking care of me and for being patient with me, since I am slow to learn and I am not the brightest student that he might ever had. For Nugraha-san and Hasdeo-san, thanks for being such a great tutors. I would like to say my thanks to Izumida-sensei and Sato-sensei for many discussions during my time as their teaching assistant. It has been a great experience for me to be able to work with you and to understand how to be a good teacher. For Shirakura, Tatsumi, Iwasaki, Nguyen, Pratama, Islam, Maruoka, and Kazu-san, it has been a great time to be your friend and lab mate. For Haihao, Cole, Jakob, Johannes, Ben and Nulli-san, it has been nice time to be your tutor and worked with you. I wish for your success in your future. For my Indonesian friends, thank you for being there and it has been an unforgettable experience for us to struggle together in the land far from home. Thank you for Hasib and Seno-san for sticking around me every day.

And not to forget, *Thank you, Japan,* and Japanese government for the generous scholarship (The MEXT scholarship and JSPS fellowship) and support so that I can finish my duty as a student. It has been a wonderful experience to study and research in Japan. I am incredibly grateful. I will never forget your generosity.

Abstract

Atomic layer material, such as the well-known graphene, has attracted many research interests due to its unique two dimensional (2D) nature of electron. The bounded nature of electron to the surface of atomic layer material gives us one of interesting phenomena, which is known as the surface electromagnetic (EM) wave, or simply surface wave. Surface wave is useful for their capability to transport the EM energy across the surface. There are two polarization of surface wave, the transverse magnetic (TM) and transverse electric (TE). The TE surface wave is unique for its ability to propagate longer than the TM and is not available on the surface of conventional 2D electron gas system or even the surface of bulk metal. Graphene has been predicted to support both TM and TE surface waves within terahertz (THz) frequency range due to the Dirac cone shape of electronic structure. However, it was predicted that the TE surface wave in graphene may only exist for a narrow frequency range. Moreover, the TE surface wave in graphene is less confined to the surface than the TM surface wave. To solve this problem, we may use other 2D material whose electronic structure is similar to graphene, such as silicene. Different to graphene, silicene is single layer of silicon atom and is known to have a band gap that can be controlled by external electric field, which might affects the properties of the TE surface waves.

Another subject of this thesis is phenomenon of the surface plasmon excited by light in graphene. The surface plasmon is collective oscillation of electrons on the surface of material and it can be seen as TM surface wave. Experimentally, the surface plasmon excitation can be observed as a peak on optical absorption spectrum. In order to excite surface plasmon by light, the resonant conditions have to be fulfilled, in which the parallel component of wave vector and frequency of light match with the wave vector and frequency of the surface plasmon. However, it is not clear from only the description of classical electrodynamics, the reason why obtaining the resonant conditions means excitation of surface plasmon and how the resonant conditions give a peak on optical absorption spectra. To answer these questions, we might adopt the quantum picture, in which the surface plasmon and light can be quantized and considered as interacting quasi-particles.

In this thesis, we show the optical conductivity of silicene with several external electric fields obtained from linear response theory. We also compare it with the case of graphene. We show that the frequency range of TE surface wave in silicene is wider compared with the one in graphene with the same Fermi energy. For fixed Fermi energy, increasing the external electric field increases the frequency range and confinement length of TE surface wave in silicene, which is in contrast with the case of graphene, in which they do not change. The TE surface wave in silicene is also found to be much confined to the surface compared with the one in graphene, due to the

more pronounced interband conductivity. We also show that the TE surface wave can propagate much longer compared with the surface plasmon. The TE surface wave can reach distance in order of meter, while the surface plasmon can only reach distance less than one millimeter.

In this thesis, we also discuss the quantum description of the excitation of surface plasmon by light in graphene by explaining the interaction between surface plasmon and external light within second quantization. We derive the matrix element of interaction in which we create one surface plasmon by annihilating one incident photon. From the matrix element, we understand that the parallel wave vector of light should match with the surface plasmon wave vector ($k_{\parallel} = q$) in order to have non zero matrix element. The frequency matching comes from the Fermi golden rule, from which the maximum excitation rate of surface plasmon is obtained in the case of frequency matching. From the Fermi golden rule, we derive the absorption probability of light due to the excitation of surface plasmon in graphene (A_{sp}). The peak of A_{sp} corresponds to the maximum excitation rate of surface plasmon, in which the resonant conditions are fulfilled as explained before. The peak on the optical absorption spectrum comes from the excitation of surface plasmon, since it is coincides with the peak of A_{sp}, where the resonant conditions are fulfilled. For other part of the optical absorption spectrum, the resonant conditions are not fulfilled and the absorption comes from the single particle excitation of electron.

Contents

Chapter 1

Introduction

1.1 Purpose of the study

Nowadays, atomic layer material has attracted many research interests due to its unique two dimensional (2D) nature of electron. Graphene, which is a single layer of carbon atom, is one of the most well-known example of atomic layer material [1, 2, 3, 4, 5, 6, 7]. The bounded nature of electron to the surface of atomic layer material gives us one of interesting phenomena, which is known as the surface electromagnetic (EM) wave, or simply surface wave [1, 8, 9, 10, 11]. Surface wave is electromagnetic wave that propagates on and confined to the surface of material [8, 9, 12, 13, 11]. Surface wave is useful for their capability to transport the EM energy across the surface. There are two polarization of surface wave, the transverse magnetic (TM) and transverse electric (TE). The TE surface wave is unique for its ability to propagate longer than the TM and is not available on the surface of conventional 2D electron gas system or even the surface of bulk metal [8, 9, 10, 12, 13, 14]. Graphene has been predicted to support both TM and TE surface waves within terahertz (THz) frequency range due to the Dirac cone shape of electronic structure [9, 10]. However, it was predicted that the TE surface wave in graphene may only exist for a narrow frequency range. Moreover, the TE surface wave in graphene is less confined to the surface than the TM surface wave. To solve this problem, we may use other 2D material whose electronic structure is similar to graphene, such as silicene. Different to graphene, silicene is single layer of silicon atom and is known to have a band gap that can be controlled by external electric field, which might affects the properties of the TE surface waves [15, 16]. Therefore, detailed study of TE surface wave in silicene must be important to investigate, which is one of subjects of this thesis.

Another subject of this thesis is phenomenon of the surface plasmon excited by light in graphene. The surface plasmon is collective oscillation of electrons on the surface of material [1, 8, 9]. In point of view of electromagnetism, surface plasmon can be seen as TM surface wave [8, 9, 10, 13]. Experimentally, the surface plasmon excitation can be observed as a peak on optical absorption spectrum, which usually gives large optical absorption for doped graphene [8, 10, 13, 17, 18, 19, 20, 21]. In order to excite surface plasmon by light, the resonant conditions have to be fulfilled, in which the parallel component of wave vector and frequency of light match with the wave vector and frequency of the surface plasmon [8, 10, 21]. These conditions have guided the researchers for exciting the surface plasmon and getting large optical absorption.

However, the reason why obtaining the resonant conditions means excitation of surface plasmon and how the resonant conditions gives a peak on optical absorption spectra are not clearly understood by only the description of classical electrodynamics. To answer these questions, we might adopt the quantum picture, in which the surface plasmon and light can be quantized and considered as interacting quasiparticles. The quantum description of surface plasmon excitation by light in graphene should be consistent with the classical electrodynamic one.

The purposes of this thesis are: (1) to investigate the properties of surface wave in graphene and silicene, and (2) to explain by the quantum mechanics the excitation of surface plasmon for doped graphene by light. For discussing the first purpose, we calculate the optical conductivity of graphene and silicene by using the linear response theory. We also solve the Maxwell equations to get the energy of surface wave. For the second purpose, we quantize both photon and surface plasmon, and calculate the interaction between them by using the Fermi golden rule. The calculated results are compared with those by classical electrodynamics. When we discuss the surface wave phenomena, the boundary conditions at the interface are taken into account by the transfer matrix method. The transfer matrix method is very useful and we can solve by this method the optical spectra of the material, such as graphene inside the multilayer or other new emerging material such as the Weyl semimetal.

1.2 Organization of thesis

This thesis is organized as follows. In Sec. 1.3 we present some basic concepts which are important for understanding this thesis. We introduce the atomic layer materials that we study, which are graphene and silicene. We also present the basic concept of surface wave and the previous studies of surface wave for both TM surface wave or surface plasmon and TE surface wave. In Chapter 2, we introduce our methods of calculation. First we show the method for achieving the first purpose as follows. We show the electronic structure of graphene and silicene, which is used to calculate the optical conductivity. The general expression of optical conductivity is derived by using the well-known linear response theory. For the second purpose, we show the method for calculating the optical spectra of graphene within classical electrodynamics. We discuss the method for quantizing photon and surface plasmon. In Chapter 3, we show the calculated results and discussion of the first purpose, which is the TE surface wave in silicene. In Chapter 4, we show the results and discussion of the second purpose, which is the quantum description of surface plasmon excitation by light in graphene. In Chapter 5, we present our interesting findings on the unique transmission of light in the Weyl semimetal, even though this work is not directly related to the main topic of the surface wave phenomena. In Chapter 6, we summarize our works.

1.3 Background

Here we show the basic concepts which are important for understanding this thesis.

1.3.1 The electromagnetic surface wave

The electromagnetic surface wave is electromagnetic wave that propagates in the direction parallel to the surface, but its amplitude decays as a function of z in the direction

perpendicular to surface [8, 10, 13, 11, 21, 20, 22]. Such kind of wave can be considered as a two-dimensionally confined wave. The electromagnetic surface wave, or simply surface wave, might occur at the interface between dielectric medium and bulk metal or between two dielectric media that satisfies appropriate boundary conditions. The works on surface wave started in 1907 in which J. Zenneck and A. Sommerfeld tried to understand the propagation of radio wave on the surface of earth or ocean. They found that the Maxwell equations had a solution related to the confined wave coupled with the flat surface. This surface was understood to be the interface between a dielectric material, that is air, and a weakly conductive medium, that is the ocean or land [13, 11].

Nowadays, the study of surface wave does not focus on the radio communication across the earth, instead it focuses on the potential applications in nanoscale optoelectronic devices, such as for transmitting signal and signal processing with high bandwidth and high transmission rate, which bring the advantages realized by optical fiber to nanoscale [13, 11, 23, 8, 24, 25, 26, 27, 28, 29]. Other application includes a very sensitive biochemical sensor based on the excitation of surface wave [13, 11, 8, 30, 31, 32, 33, 34, 35, 36, 37]. In all applications, the basic principle underlying the surface wave phenomenon is the solution of the Maxwell equations in the interface. The surface wave can be excited by external electromagnetic wave incident to the interface [23, 8, 22]. The polarization of the surface wave is determined by the polarization of the incident wave. Therefore, there are two kinds of surface wave, the transverse magnetic (TM) and transverse electric (TE) surface waves. In the TM surface wave, the incident field has a component of magnetic field perpendicular to the incidence plane, while in the TE surface wave, the incident field has a component of electric field perpendicular to the incidence plane. These conditions determine the components of field for each surface wave. For our convention, it is noted that the surface wave propagates in the direction of x and the field decays in the direction of z as shown in Fig. 1.1.

1.3.1.1 TM surface wave

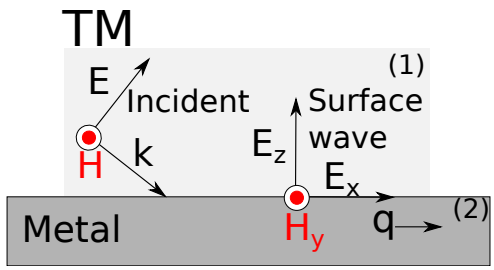

Figure 1.1 The TM surface wave with a component of electric field in the direction of propagation. The direction of propagation of the surface wave is given by **q**, which is the wave vector of surface wave wave vector, while **k** is the wave vector of incident wave.

Fig. 1.1: Fig/Fig1k1a.eps

Let us first discuss the TM surface wave on the surface of a bulk metal shown in Fig. 1.1. For TM surface wave, the field components are the E_x, E_z, H_y. The electromagnetic fields of the TM surface wave are given by [8],

In medium 1

$$\begin{aligned} E_x^{(1)} &= E_1 e^{iqx} e^{-\kappa_1 z} \ , \\ E_z^{(1)} &= \frac{iq}{\kappa_1} E_x^{(1)} \ , \\ H_y^{(1)} &= -\frac{i\omega\varepsilon_0\varepsilon_1}{\kappa_1} E_x^{(1)}, \end{aligned} \tag{1.1}$$

and in medium 2 or metal

$$\begin{aligned} E_x^{(2)} &= E_2 e^{iqx} e^{\kappa_2 z} \ , \\ E_z^{(2)} &= -\frac{iq}{\kappa_2} E_x^{(2)} \ , \\ H_y^{(2)} &= \frac{i\omega\varepsilon_0\varepsilon_1}{\kappa_2} E_x^{(2)}, \end{aligned} \tag{1.2}$$

where $E_i, E_x^{(i)}, E_z^{(i)}, H_y^{(i)}$ $(i = 1, 2)$ denote the amplitude of electric field in the x direction, the magnitude of electric field in the x direction, the magnitude of electric field in the z direction, and the magnitude of magnetic field in the y direction for the i-th medium, respectively. q is the propagating wave vector of the surface plasmon and κ_i is decay constant of the fields inside the i-th medium given by

$$\kappa_i = \sqrt{q^2 - \omega^2\varepsilon_i/c^2}. \tag{1.3}$$

The dielectric constant of the bulk metal can be expressed in the Drude form, given by the following equation.

$$\varepsilon_2(\omega) = 1 - \frac{\omega_{\rm bp}^2}{\omega^2}, \tag{1.4}$$

where ω is frequency of the EM wave and $\omega_{\rm bp}$ is the bulk plasmon frequency of metal defined by [38],

$$\omega_{\rm bp} = \sqrt{\frac{ne^2}{m\varepsilon_0}}, \tag{1.5}$$

where n and m is the density of electron in metal and mass of electron, respectively. The $\omega_{\rm bp}$ is a threshold frequency that determines whether an EM wave is allowed to propagate through the metal ($\omega > \omega_{\rm bp}$) or to be reflected by metal ($\omega < \omega_{\rm bp}$). For example, the plasmon frequency of bulk silver is $\omega_{\rm bp} = 12 \times 10^{15}$ Hz. If $\omega < \omega_{\rm bp}$, the electrons can follow the EM wave and thus the EM wave is reflected due to the screening of the electron field by electrons. On the other hand, if $\omega > \omega_{\rm bp}$, the electrons cannot follow the EM wave, and thus the EM wave can be transmitted through the metal. It is noted that ε_2 is positive (negative) if $\omega > \omega_{\rm bp}$ ($\omega < \omega_{\rm bp}$) [38].

We also use the following relations that relate the magnetic field with electric field,

$$H_y^{(i)} = i\omega\varepsilon_0\varepsilon_i \int E_x^{(i)} dz \tag{1.6}$$

$$E_z^{(i)} = -q/(\omega\varepsilon_0\varepsilon_i) H_y^{(i)}, \tag{1.7}$$

which can be derived from the Maxwell equations [8]. It is understood that the surface of metal is at $z = 0$. The boundary conditions of electromagnetic field tell us that the electric field and the magnetic field parallel to the surface should be continuous at the surface ($z = 0$) if there is no surface current. Therefore we have the following equations,

$$E_x^{(1)} = E_x^{(2)} \tag{1.8}$$

$$H_y^{(1)} = H_y^{(2)}. \tag{1.9}$$

By substituting the EM fields of TM surface wave to Eq. (1.9), we obtain the following equality,

$$\frac{\varepsilon_1}{\kappa_1} = -\frac{\varepsilon_2}{\kappa_2}. \tag{1.10}$$

Equation (1.10) requires the dielectric constant of metal to be negative $\varepsilon_1 < 0$, which can be achieved with $\omega < \omega_{\rm bp}$, shown in Eq. (1.4). By substituting κ_i for each medium given by Eq. (1.3) to Eq. (1.10), we obtain an equation for q, which gives the relation between the wave vector of the TM surface wave and the frequency as follows [8],

$$q = \frac{\omega}{c}\sqrt{\frac{\varepsilon_1\varepsilon_2(\omega)}{\varepsilon_1 + \varepsilon_2(\omega)}}. \tag{1.11}$$

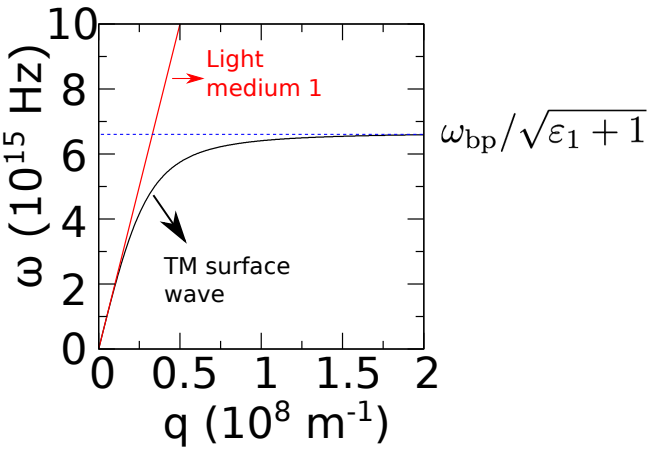

Figure 1.2 The TM surface wave frequency as a function of wave vector obtained from Eq. (1.11) for silver. $\omega_{\rm bp} = 12 \times 10^{15}$ Hz, and $\varepsilon_1 = 1$. The dispersion of light in medium 1 is shown as the red curve. The blue dashed line denotes the $\omega = \omega_{\rm bp}/\sqrt{\varepsilon_1 + 1}$.

In Fig. (1.2), we show the frequency of the TM surface wave as a function of wave vector by substituting Eq. (1.4) to Eq. (1.11) shown by the black curve. We also show the dispersion of light in medium 1 by red line. We can see that the ω linearly increases with increasing q for $q \approx 0$, but it saturates at $\omega = \omega_{\rm bp}/\sqrt{\varepsilon_1 + 1}$, which is obtained by setting $q \approx \infty$ in Eq. (1.11) or $\varepsilon_1 + \varepsilon_2(\omega) = 0$.

Fig. 1.2: Fig/Fig1k2.eps

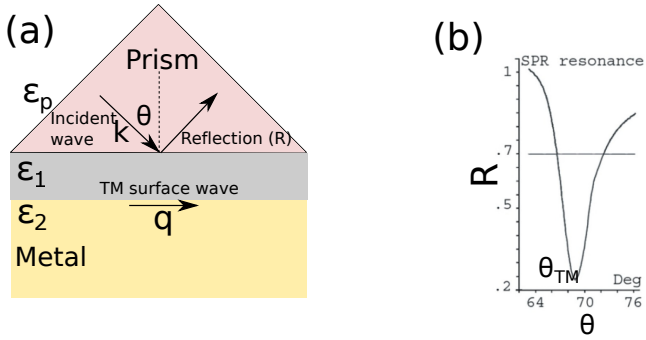

Figure 1.3 (a) the Otto geometry for exciting TM surface wave. q is the wave vector of the excited surface wave. (b) The experimental measurement of reflectance of Otto geometry shown in Fig. 1.3 (a) with gold as metal. The TM surface wave is excited at $\theta_{\rm TM} \approx 68^\circ$.

In the experiment, exciting the TM surface wave requires the resonant conditions, in which the parallel component of wave vector and frequency of the incident EM wave match with the wave vector and frequency of the TM surface wave [8, 10, 21]. To obtain such kind of resonant conditions, a special geometry is generally used. In Fig. 1.3(a) we illustrate the Otto geometry or the attenuated total reflection (ATR) geometry, which is generally used for exciting TM surface wave on the surface of a bulk metal [8, 10, 21, 20, 18]. The incident TM wave comes from a coupling prism whose dielectric constant $\varepsilon_{\rm P}$ larger than the dielectric constant of medium 1 ($\varepsilon_{\rm P} > \varepsilon_1$). This geometry allows us to achieve total internal reflection of light, in which there is no transmission of incident wave to medium 1 if θ is larger than a critical angle θ_c, where $\theta_c = \sin^{-1}\sqrt{\varepsilon_1/\varepsilon_{\rm P}}$. In this case, the TM surface wave is excited on the metal surface, and there is a sudden drop of the measured reflection (R) of incident wave at an angle $\theta_{\rm TM} > \theta_c$ as shown in the case of gold in Fig. 1.3(b) or there will be a peak on the absorption spectrum. As mentioned before, this excitation occurs if the resonant conditions are satisfied. Therefore, we can approximate the incident angle that gives the excitation, $\theta_{\rm TM}$ by using Eq. (1.11) as follows [39],

$$\begin{aligned} k_{\|} &= q \\ \frac{\omega}{c}\sqrt{\varepsilon_{\rm P}}\sin\theta_{\rm TM} &= \frac{\omega}{c}\sqrt{\frac{\varepsilon_1\varepsilon_2(\omega)}{\varepsilon_1+\varepsilon_2(\omega)}}, \end{aligned} \tag{1.12}$$

where $k_{\|}$ is the parallel component of the incident wave in the prism and we assume that the frequency of TM surface wave is equal to the frequency of light ω. We can think that if the resonant conditions in Eq. (1.12) are satisfied, there will be a maximum energy transfer from the incident wave to the metal surface that excites the TM surface wave. Therefore, the reflection is minimum as shown in Fig. 1.3 (b) and the absorption of incident wave is maximum [39].

Fig. 1.3: Fig/Fig1k3.eps

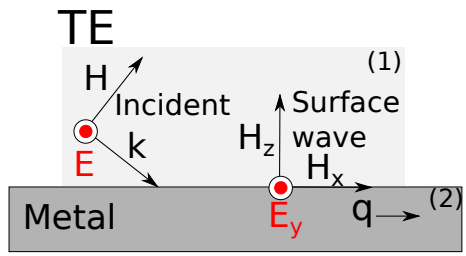

Figure 1.4 The TE surface wave with a component of magnetic field in the direction of propagation. The direction of propagation of the surface wave is given by **q**, which is the wave vector of surface wave wave vector, while **k** is the wave vector of incident wave.

1.3.1.2 TE surface wave

Now let us discuss the second kind of surface wave, which is transverse electric (TE) surface wave as shown in Fig 1.1 (b). For TE surface wave, the field components are the $E_y,\ H_x,\ H_z$. The electromagnetic fields of the TE surface wave are given by, In medium 1

$$\begin{aligned} H_x^{(1)} &= H_1 e^{iqx} e^{-\kappa_1 z}\ , \\ H_z^{(1)} &= \frac{iq}{\kappa_1} H_x^{(1)}\ , \\ E_y^{(1)} &= \frac{i\omega\mu_0\mu_1}{\kappa_1} H_x^{(1)}, \end{aligned} \tag{1.13}$$

and In medium 2 or metal

$$\begin{aligned} H_x^{(2)} &= H_2 e^{iqx} e^{\kappa_2 z}\ , \\ H_z^{(2)} &= -\frac{iq}{\kappa_2} H_x^{(2)}\ , \\ E_y^{(2)} &= -\frac{i\omega\mu_0\mu_2}{\kappa_2} H_x^{(2)}, \end{aligned} \tag{1.14}$$

where μ_0 is the permeability of vacuum, μ_i is the relative permeability of the i-th medium. We use the following relations,

$$E_y^{(i)} = -i\omega\mu_0\mu_i \int H_x^{(i)} dz \tag{1.15}$$

$$H_z^{(i)} = q/(\omega\mu_0\mu_i) E_y^{(i)}. \tag{1.16}$$

By using the boundary conditions of electromagnetic field at the surface $z = 0$, which are the same as the case of TM surface wave given in Eq. (1.9), we obtain the following equation [8, 39],

$$\frac{\mu_1}{\kappa_1} = -\frac{\mu_2}{\kappa_2}. \tag{1.17}$$

Fig. 1.4: Fig/Fig1k1b.eps

Equation (1.17) implies that we should have the medium 2 with negative relative permeability ($\mu_2 < 0$), since κ_i is positive [39]. This condition cannot be fulfilled by a normal bulk metal or any other common material found in nature, due to the weak coupling between the magnetic field to the atom. Therefore, the TE surface wave cannot be excited on the surface of conventional bulk metal or other normal material. Even though we can develop artificial material, which possess the negative permeability, which is known as meta material [39, 40], it is generally complicated to fabricate. However, it is predicted that by simply using 2D material such as graphene instead of bulk metal, TE surface wave can exist on the surface of 2D material [9, 10], which will be discussed in the Section 1.3.3.

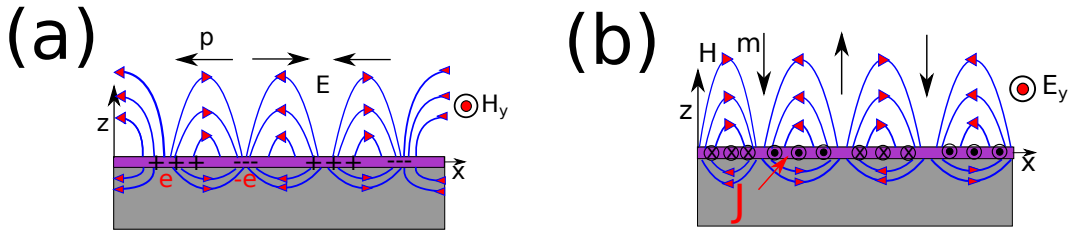

Figure 1.5 (a) The TM surface wave can be seen as the surface plasmon, which is the collective oscillation of electron on the surface of material. Since there is an oscillation of charge density across the surface, surface plasmon can be seen physically as a electric dipole (p) wave. (b) The TE surface wave can be seen a magnetic dipole (m) wave on the surface of the material due to the self-sustained surface current (J) oscillation [40].

Before ending this section, we will briefly discuss the surface wave in the electron point of view. Physically, the TM surface wave can be seen as the surface plasmon [9, 10, 40]. Surface plasmon is a collective oscillation of charge density of electrons that propagates on the surface of a material. This propagating oscillation of charge density creates a wave of electric dipole (p) as shown in Fig. 1.5 (a) as a black arrow. The electric field of the electric dipole is nothing but the electric field the TM surface wave, with one component in the direction of propagation (x) and the other component in the perpendicular direction of propagation (z).

On the other hand, the TE surface wave can be considered as a magnetic dipole (m) wave on the surface of the material due to the self-sustained surface current oscillation (J) [10, 40]. The magnetic dipole, which is shown as black arrow in Fig. 1.5 (b), induces the magnetic field with one component in the direction of propagation (x) and the other compenent in the perpendicular direction of propagation (z), which is nothing but the magnetic field of the TE surface wave. Hence, the to support TE surface wave, the surface current density should be finite on the surface of a material, which is absent in the bulk metal, where we have only bulk current. This condition is satisfied for the 2D material, in which the electric current is always surface current. It is important to note that the radiation loss of magnetic dipole (P_{mag}) is much smaller than that of electric dipole ($P_{\mathrm{el}} \propto c^2 P_{\mathrm{mag}}$) [41, 42]. Therefore, the TE surface wave can propagate longer than the TM surface wave, which makes the TE surface wave desirable for transporting EM energy over long distance [14, 43, 44, 9].

Fig. 1.5: Fig/Fig1k4.eps

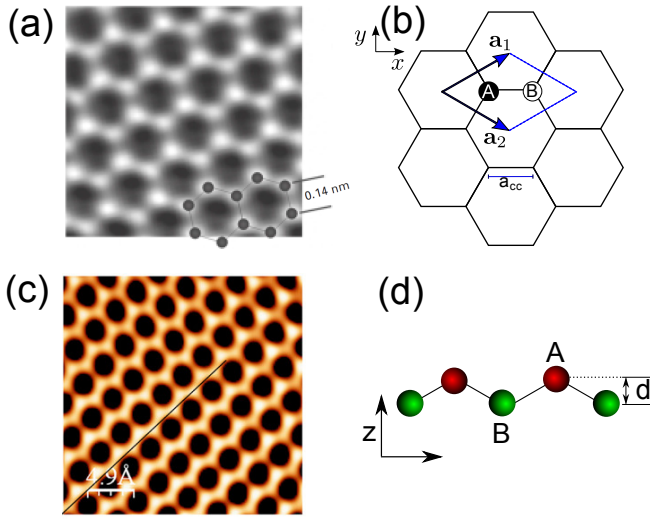

Figure 1.6 (a) Graphene hexagonal lattice observed experimentally by transmission electron aberration-corrected microscope (TEAM). It is shown that carbon-carbon distance is 0.142 nm [3]. (b) The graphene unit cell consisting of two atomic sites A and B. $\mathbf{a_1}$ and $\mathbf{a_2}$ are the unit vectors and $\mathbf{a}_{cc}$ is the nearest neighbor carbon-carbon distance [4]. (c) The silicene hexagonal lattice, shown as bright color, observed experimentally by STM. The lattice of silicene is the same honeycomb lattice of graphene as shown in (b), however it is not planar [45]. (d) Silicene lattice from side view. Sublattice A and B are separated vertically by $d = 0.46$. Sublattice A (B) is depicted by red (green) atom. In graphene atom A and B are carbon atom, while in silicene they are silicon atom.

1.3.2 Graphene and silicene

Before discussing the surface wave in the atomic layer material, first we introduce the atomic materials that we study, which are graphene and silicene. Graphene is a planar allotrope of carbon in a honeycomb lattice structure where all the carbon atoms form covalent bonds in a single plane [3, 4, 46, 47, 48, 49, 5, 6, 7]. Graphene is well-known as the mother of the three carbon allotropes of fullerene, nanotube, and graphite. Several layers of graphene sheets are stacked together by the van der Waals force to form three dimensional (3D) graphite, while by wrapping it up, a 0D fullerene can be made and by rolling it up, a 1D single wall nanotube is made [3, 4]. The first isolation of single layer graphene was done by A. Geim and C. Novoselov at Manchester in 2004, in which they use mechanical exfoliation technique to isolate the 2D crystal from 3D graphite. They obtain single- and few-layer graphene flakes that were attached weakly to the substrate by the van der Waals forces, which can be made free standing by etching away the substrate.

The lattice structure of graphene has been observed experimentally and is shown by Fig. 1.6(a) and (b) [3]. In Fig. 1.6(b) we show the honeycomb lattice of graphene, which consists of two carbon atoms in the unit cell. The covalent bonds between nearest neighbor carbon atoms are called σ-bonds, which are the strongest covalent

Fig. 1.6: Fig/Fig1k5.eps

bond among the materials. The σ-bonds have the electrons localized along the plane connecting two carbon atoms and are responsible for the great strength and mechanical properties of graphene. Due to the unique Dirac cone shape of the electronic structure, graphene acquire zero effective mass of electron, which allows graphene to achieve very high electron mobility ($\mu \approx 10^4$ cm^2 V^{-1}s^{-1}) due to the supression of scattering [47, 48, 49]. This high mobility allows graphene to be used in the future of nanoelectronics at a high frequency of THz [46]. However, the absence of the band gap in graphene might hinder the the possible application of graphene in logic application. Therefore, other 2D material similar to graphene, such as silicene, which has band gap ($\approx 1.55-7.9$ meV for the spin-orbit band gap [50]), might give more advantage than graphene[51, 52].

Silicene is a monolayer of silicon atoms arranged in honeycomb lattice and the stable structure of silicene is not purely planar, but slightly buckled, i.e., the two sublattices are separated by vertical distance $d = 0.046$ nm due to the sp^3-like hybridization as shown in Fig. 1.6 (d) [51, 52, 45, 15, 16, 53, 54, 55, 56]. The honeycomb lattice of silicene observed experimentally by STM as shwon in Fig. 1.6 (c), which clearly shows the hexagonal shape given by the bright color [45]. The buckling of the atoms creates potential difference between two sublattices when an external electric field is applied in the direction perpendicular to the surface. The induced potential difference, along with the non-negligible spin orbit (SO) coupling in silicene due to the larger mass of silicon atom compared with carbon atom, will give a tunable energy gap, which can be tuned by the external electric field [52, 15, 16, 53, 54, 56]. The tunable band gap gives silicene more advantage in logic application compared with graphene. Moreover, silicene will be much more compatible for the integration with the existing silicon-based electronics [51, 52].

1.3.3 The surface waves in 2D material

1.3.3.1 TM surface wave

Now let us return our discussion to the surface wave phenomena in the 2D material, which is predicted to support the TE surface wave due to the presence of surface current. First, let us focus on the TM surface wave or surface plasmon. To discuss the existence of surface wave, let us obtain the dispersion of TM surface wave in the surface of 2D material. We assume that the 2D material is surrounded by two dielectric media 1 and 2 as shown in Fig. 1.7. The TM surface wave propagates on the surface of graphene in the direction of x with wave vector q. Similar to the discussion of TM surface wave in bulk metal, the electromagnetic fields of TM surface wave are given as follows [8, 57],

In medium 1

$$E_x^{(1)} = E_1 e^{iqx} e^{-\kappa_1 z} \ , \tag{1.18}$$

$$E_z^{(1)} = \frac{iq}{\kappa_1} E_x^{(1)} \ , \tag{1.19}$$

$$H_y^{(1)} = -\frac{i\omega\varepsilon_0\varepsilon_1}{\kappa_1} E_x^{(1)}, \tag{1.20}$$

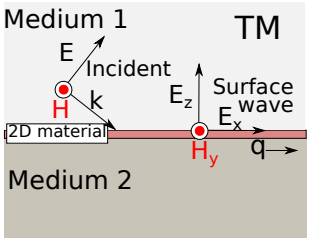

Figure 1.7 TM surface wave in the surface of 2D material. 2D material is shown as red color with negligible thickness.

and in medium 2

$$E_x^{(2)} = E_2 e^{iqx} e^{\kappa_2 z} \,, \tag{1.21}$$

$$E_z^{(2)} = -\frac{iq}{\kappa_2} E_x^{(2)} \,, \tag{1.22}$$

$$H_y^{(2)} = \frac{i\omega\varepsilon_0\varepsilon_1}{\kappa_2} E_x^{(2)}, \tag{1.23}$$

where κ_i $(i = 1, 2)$ is decay constant given by Eq. (1.3). However, due to the presence of surface current that flows on the 2D material, the magnetic fields component in the direction parallel to the surface are not continuous anymore at the surface of 2D material. Therefore, the boundary conditions of electromagnetic wave on the surface of 2D material are given by,

$$E_x^{(1)} = E_x^{(2)} \tag{1.24}$$

$$H_y^{(1)} - H_y^{(2)} = -J, \tag{1.25}$$

where $J = \sigma(\omega) E_x^{(2)}$ is the surface current on the 2D material. In the calculation, we consider that 2D material has a negligible thickness, therefore it appears only in the boundary conditions and $\sigma(\omega)$ is the optical conductivity of 2D material. If we take graphene as the 2D material, the $\sigma(\omega)$ is given by the following equation [9, 58, 59, 57, 60, 61],

$$\begin{aligned} \sigma(\omega) \equiv & \sigma_D + \mathrm{Re}\ \sigma_E + \mathrm{Im}\ \sigma_E \\ = & \frac{E_F e^2}{\pi\hbar} \frac{i}{\hbar\omega + i\Gamma} + \frac{e^2}{4\hbar}\Theta(\hbar\omega - 2E_\mathrm{F}) - \frac{ie^2}{4\pi\hbar} \ln\left|\frac{\hbar\omega + 2E_\mathrm{F}}{\hbar\omega - 2E_\mathrm{F}}\right|. \end{aligned} \tag{1.26}$$

The first term in Eq. (1.26) is the intraband conductivity, which is known as the Drude conductivity σ_D [57, 59, 60]. We add a spectral width Γ as a phenomenological parameter for scattering rate or electron damping due to the impurity or scattering with phonon, and Γ depends on E_F as $\Gamma = \hbar e v_\mathrm{F}^2 / \mu E_\mathrm{F}$, where $v_\mathrm{F} = 10^6$ m/s is the Fermi velocity of graphene, $\mu = 10^4$ cm^2/Vs is the mobility for ideal graphene [57]. The second and the third terms in Eq. (1.26) correspond to the real part and the imaginary

Fig. 1.7: Fig/Fig2DTM.eps

part of interband conductivity σ_E, respectively [59, 9, 60]. The real part and imaginary part of $\sigma(\omega)$ are related with each other by the Kramers-Kronig relation. We have two kinds of optical conductivity corresponding to two possible optical scattering or excitation of electron by photon in graphene, which are the intraband and interband transitions as shown in Figs. 1.8 (a) and (b), respectively. The intraband transition is the transition of electron within the same conduction band, which is dominant if $\hbar\omega < 2E_{\rm F}$. The optical transition of electron with $q \neq 0$ is possible in intraband transition, due to the additional scattering of electron by impurity or phonon, which might modify the momentum of electron. For $\hbar\omega > 2E_{\rm F}$, we might have transition from valence to conduction band, which is called the interband transition [60].

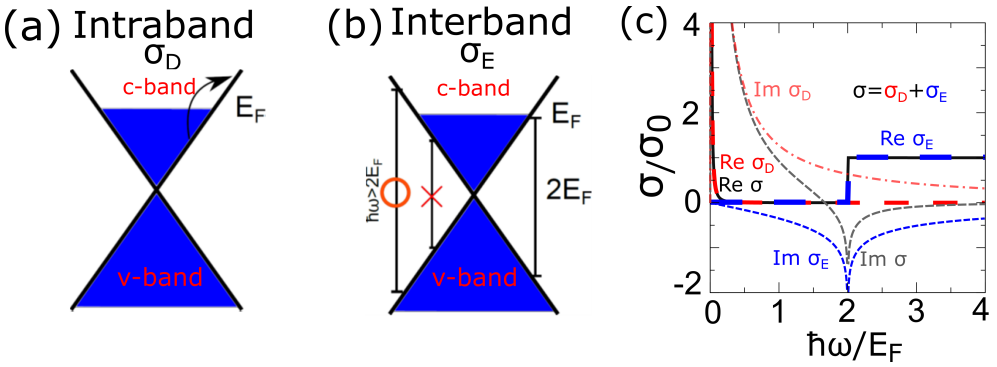

Figure 1.8 (a) The intraband transition of electron (b) The interband transition of electron, which occurs if $\hbar\omega > 2E_{\rm F}$. (c) the optical conductivity of graphene $\sigma(\omega)$ normalized to $\sigma_0 = e^2/4\hbar$. $\sigma(\omega)$ consists of intraband σ_D and interband σ_E conductivity. c and v-bands denote conduction and valence bands, respectively [61]

.

The optical conductivity of graphene is given in Fig. 1.8 (c), where we plot $\sigma(\omega)$ of Eq. (1.26) normalized to real part of σ_E, $\sigma_0 \equiv e^2/4\hbar$. At low frequency ($\hbar\omega << 2E_{\rm F}$), the σ_D is dominant, while the σ_E can be neglected, while σ_E is dominant for large frequency ($\hbar\omega > 2E_{\rm F}$), where the real part of conductivity is constant at σ_0.

It is noted that for 2D electron gas system, such as GaAs/AlGaAs quantum-well structure, the optical conductivity is only described by the the Drude conductivity or intraband conductivity, given by [38, 9]

$$\sigma_{\text{2D gas}} = i\frac{ne^2}{m(\omega + i\gamma)}, \tag{1.27}$$

where n, m, γ are the density, effective mass, and scattering rate of 2D electron gas system.

The dispersion of TM surface wave is obtained by substituting Eqs. (1.18) - (1.23) to boundary conditions of Eqs. (1.24) and (1.25). The following equation is a requirement to have TM surface wave in the 2D material [9, 57, 59, 62].

$$\frac{\varepsilon_1}{\kappa_1} + \frac{\varepsilon_2}{\kappa_2} + \frac{i\sigma(\omega)}{\omega\varepsilon_0} = 0, \tag{1.28}$$

Fig. 1.8: Fig/Fig1k7.eps

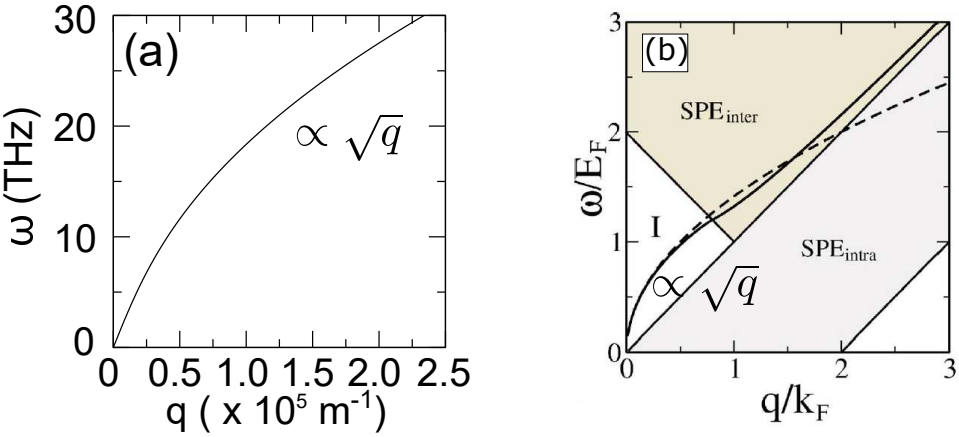

Figure 1.9 (a) The dispersion relation of TM surface wave or surface plasmon in graphene by Eq. (2.98 for $E_{\rm F} = 0.64$ eV. (b) The dispersion relation of TM surface wave or surface plasmon in graphene obtained by calculating the dielectric function of graphene $\varepsilon_g(q,\omega)$ using random phase approximation (RPA) method and solve $\varepsilon_g(q,\omega) = 0$ [58]. It is noted that for $E_{\rm F} = 0.64$ eV, we have $k_{\rm F} = 9.7 \times 10^8$ m^{-1}.

where ε_i, $(i = 1, 2)$ is the dielectric constant of the i-th medium, which surrounds the 2D material. Because ε_i and κ_i are positive values, the imaginary part of the optical conductivity should be positive (Im $\sigma(\omega) > 0$) to satisfy Eq. (1.28). This requirement is satisfied by the conventional 2D electron gas system, since Im $\sigma_{\rm 2D\ gas} = ne^2\omega/(m(\gamma^2+\omega^2)) > 0$ [9]. This condition is also satisfied in the case of graphene, since from Fig. 1.8 (c), Im $\sigma(\omega) > 0$ for $\hbar\omega < 1.667E_{\rm F}$. Therefore, the TM surface wave or surface plasmon can exist in both conventional 2D electron gas system and graphene [9, 59].

We can derive the dispersion relation of TM surface wave for graphene by solving Eq. (1.28). Suppose that $\hbar\omega << 2E_{\rm F}$, for example with $E_{\rm F} = 0.64$ eV, we take the frequency in terahertz (THz) range, the optical conductivity can be taken only as the Drude conductivity ($\sigma(\omega) \approx \sigma_D(\omega)$). The scattering of electron or Γ can be ignored, since it gives only the spectral broadening of the TM surface wave. Since the velocity of light can be considered to be much larger than the group velocity of surface plasmon $v_{\rm sp}$, we can approximate the $q >> \omega/c$ and we get $\kappa_1 = \kappa_2 = q$ in Eq. (1.3). This situation is called the *non-retarded* regime [57, 20, 63]. By substituting σ_D of Eq. (1.26) to Eq. (1.28) and solve for ω, we obtain the dispersion relation [57, 20, 63, 24],

$$\omega = \frac{1}{\hbar}\sqrt{\frac{E_{\rm F}e^2 q}{\pi\varepsilon_0(\varepsilon_1+\varepsilon_2)}}, \tag{1.29}$$

where we have a square-root dependence of q $\omega \propto \sqrt{q}$. The square-root dependence can also be obtained for conventional 2D electron gas by substituting Eq. (1.27) to Eq. (1.28) and solve for ω. Therefore, the $\omega \propto \sqrt{q}$ dependence is the characteristic of

Fig. 1.9: Fig/Fig1k8.eps

TM surface wave or surface plasmon in the 2D material [57, 20, 63, 58]. In Fig. 1.9 (a), we show the dispersion relation of the TM surface wave of graphene.

When we consider graphene as a medium, we can derive the dispersion from the dielectric function of the graphene $\varepsilon_g(q,\omega)$. $\varepsilon_g(q,\omega)$ has been derived by Hwang et al. by using Random Phase Approximation (RPA) method [58]. The dispersion of TM surface wave can be obtained by solving $\varepsilon_g(q,\omega)=0$, in which the surface plasmon is excited [58, 64]. Figure 1.9 (b) shows the TM surface wave or surface plasmon dispersion of graphene obtained by $\varepsilon_g(q,\omega)=0$ as thick black line for graphene surrounded by vacuum. We can clearly see that for $q << k_{\mathrm{F}}$, $\omega \propto \sqrt{q}$ and we return to Eq. (2.98), while for $k >> k_{\mathrm{F}}$, $\omega \propto v_{\mathrm{F}} q$. For $k >> k_{\mathrm{F}}$, the dispersion enters the regime of single particle excitation (SPE) by interband, in which the electron undergoes interband transition and the imaginary part of dielectric function is not zero (Im $\varepsilon_g(q,\omega) > 0$). In this regime, the TM surface wave or surface plasmon experiences damping, known as the Landau damping [58, 64]. The Landau damping is caused purely due to the optical excitation of electron, not due to the scattering of electron by other means. In the white region I in Fig. 1.9(b), where we have $\omega \propto \sqrt{q}$, the Landau damping does not occur, and the lifetime of TM surface wave can be infinity, if we ignore the scattering of electron by impurity or phonon. It is also noted that the TM surface wave disperion for silicene has also been studied by using RPA method by Tabert et al., where they derive the dielectric function of silicene and they got similar results as Fig. 1.9 (b). But, the white region for silicene can be tuned due to the tunable band gap by external electric field [53, 56].

1.3.3.2 TE surface wave

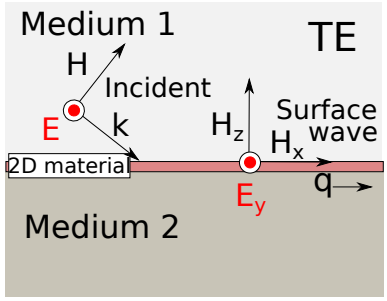

Figure 1.10 TE surface wave in the surface of 2D material. 2D material is shown as red color with negligible thickness.

Now let us discuss the existence of TE surface wave in 2D material as shown in Fig. 1.10 (b). The electromagnetic fields of TE surface wave are expressed as follows [8, 39],

Fig. 1.10: Fig/Fig2DTE.eps

In medium 1

$$H_x^{(1)} = H_1 e^{iqx} e^{-\kappa_1 z} \ ,$$
$$H_z^{(1)} = \frac{iq}{\kappa_1} H_x^{(1)} \ ,$$
$$E_y^{(1)} = \frac{i\omega\mu_0}{\kappa_1} H_x^{(1)}, \tag{1.30}$$

and in medium 2

$$H_x^{(2)} = H_2 e^{iqx} e^{\kappa_2 z} \ ,$$
$$H_z^{(2)} = -\frac{iq}{\kappa_2} H_x^{(2)} \ ,$$
$$E_y^{(2)} = -\frac{i\omega\mu_0}{\kappa_2} H_x^{(2)}, \tag{1.31}$$

where μ_0 is the permeability of vacuum. By using the boundary conditions, which are $E_y^{(1)} = E_y^{(2)}$ and $H_x^{(1)} - H_x^{(2)} = -J$ at $z = 0$, where $J = \sigma(\omega) E_y^{(2)}$, and assuming that the two dielectric media as vaccum ($\varepsilon_1 = \varepsilon_2 = 1$, thus $\kappa_1 = \kappa_2 = \sqrt{q^2 - (\omega/c)^2} \equiv \kappa$), we obtain the following equation [9],

$$2 - \frac{i\sigma(\omega)\omega\mu_0}{\kappa} = 0. \tag{1.32}$$

Since ω is a positive value, Eq. (2.99) requires a negative value of Im σ [9, 10]. Therefore, the TE surface wave cannot be supported by the conventional 2D electron gas system, since the Im $\sigma_{\text{2D gas}} > 0$ as is given by Eq. (1.27) [9]. However, the imaginary part of optical conductivity of graphene can be negative (Im $\sigma(\omega) < 0$) at a certain frequency range as shown in Fig. (1.8) (c). This unusual property has also enabled graphene to have the TE surface wave. However, it was predicted that the TE surface wave in doped graphene may only exist for a narrow frequency range of $1.667 E_{\text{F}} < \hbar\omega < 2E_{\text{F}}$ [9, 10, 65, 59, 66].

Xiao et al. reported that the TE surface wave in graphene is less confined to the surface, but can propagate longer compared with the TM surface wave [43]. Figure 1.11 shows the calculated results of the decay length of TM surface wave in air ($1/\kappa_1$) and the propagation length of TM and TE surface waves in graphene at $T = 3$K. Because TM and TE surface waves cannot occur simultaneously in the same frequency range for fixed E_{F}, $E_{\text{F}} = 0.2$ eV and 8.6 meV are adopted in the calculation and comparison of TM and TE surface waves, respectively. In this case, graphene is surrounded by air (A-G-A) or by air and SiO_2 (A-G-SiO_2). The frequency range for TE surface wave is denoted by the circle, which can only occurs within 3.7 - 9 THz. Within this frequency range, we can see that the decay length of TE surface wave is larger than the TM surface wave, which means that the TE surface wave decays slowly in the air. In other words, TE surface wave is less confined to the surface compared with the TM surface wave. The shortest decay lenght for the TE surface wave is roughly 10^3 μm, while for TM surface wave, it is 10 μm. However, the TE surface wave can propagate longer compared with the TM surface wave in graphene as shown in the inset of Fig. 1.11. The TE surface wave can propagate with maximum distance 1 m, while the TM surface wave can only reach 1 mm.

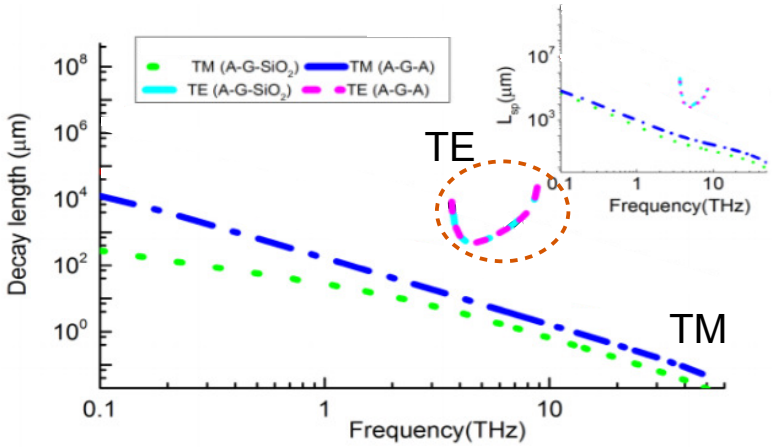

Figure 1.11 The decay length in air ($1/\kappa_1$) for TM and TE surface waves in graphene. The inset gives the propagation length of TM and TE surface waves in graphene. For TM(TE) surface wave calculation, $E_F = 0.2$ (8.6) eV(meV) is adopted so that we can compare TM and TE surface waves within the same frequency range [43]. The temperature is 3K.

The existence of TE surface wave has been proved experimentally by Menabde et al. by monitoring the reflection of TE EM wave coming to graphene, which is put inside the Otto geometry as shown in Fig. 1.12 (a) [10]. They use both TM and TE incident wave with frequency within frequency range of TE surface wave. As the control experiment, they perform the measurement of reflection of TM and TE incident wave without the presence of graphene, in which the reflection coefficient turns unity for both polarizations at angle of incident larger than critical angle due to the total reflection. In the experiment with graphene, they change the doping level of graphene by changing the gate voltage, which is applied to graphene.

Figure 1.12 (c) shows the experiment results of the reflection coefficient of TM and TE incident wave with the presence of graphene. Changing the doping level does not change the reflection of TM incident wave, however, the reflection coefficient of TE wave suddenly drop at incident angle close to critical angle. This dip of reflection coefficient implies that there is a peak on the absorption spectrum of TE incident wave and the TE surface wave is excited on the surface of graphene.

1.3.4 The Weyl semimetal

Graphene and silicene are the two-dimensional Dirac material, since their low energy dispersion is linear to the wavevector. For three-dimensional material, the Dirac material is known as the Dirac semimetal, where the valence and conduction bands touch at so called Dirac point [67, 68, 69]. The examples of Dirac semimetal are Cd_3As_2 and Na_3Bi [68]. In Dirac semimetal, two Dirac cones overlap each other, thus the Dirac point is doubly degenerate. The Dirac semimetal is the consequence of the

Fig. 1.11: Fig/Fig1k9.eps

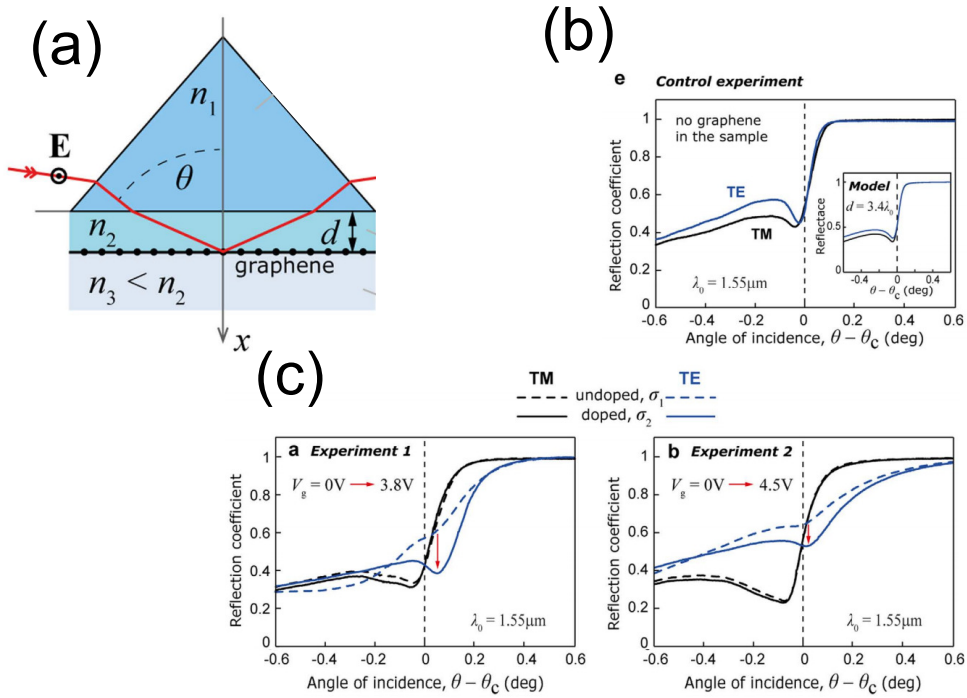

Figure 1.12 (a) The structure to observe the TE surface wave in graphene [10]. (b) The control experiment with no graphene. The reflection turns unity for angle of incident larger than critical angle due to the total reflection. (c) The experimental reflection coefficient for both TM and TE incident wave with changing the gate voltage. There is a sudden drop in reflection coefficient for TE incident wave by changing the gate voltage.

time-reversal and inversion symmetries [67]. When one of the symmetries is broken, the Dirac point is split into a pair of Weyl nodes and we have two separated Dirac cones. This material is called the Weyl semimetal (WSM) [67]. The examples of WSM are $Eu_2Ir_2O_7$ and $YbMnBi_2$ [68]. The WSM possesses topological properties, even though it is not topological insulator, including protected surface states and unusual electromagnetic response [69, 67].

In Fig. 1.13, we show the energy dispersion of the Dirac semimetal and the WSM. Due to the symmetry breaking, two Dirac cones of Dirac semimetal are separated and we have the WSM. The separation can be in momentum [Fig. 1.13 (b)] and in energy [Fig. 1.13 (c)]. The touching points of valence and conduction band are called Weyl nodes for WSM. For our discussion, we focus on the WSM with the Weyl nodes separated in momentum. The separation of two Dirac cones introduces the topological properties in the WSM. The topological properties are characterized by so-called the axion angle given by $\theta = 2(\mathbf{b} \cdot \mathbf{r})$, where $\mathbf{b}$ is a wave vector separating the Weyl nodes [67, 68, 69]. One of unique topological properties is the presence of the Hall current, even without magnetic field [68, 70, 67]. This phenomenon is

Fig. 1.12: Fig/Fig1k10.eps

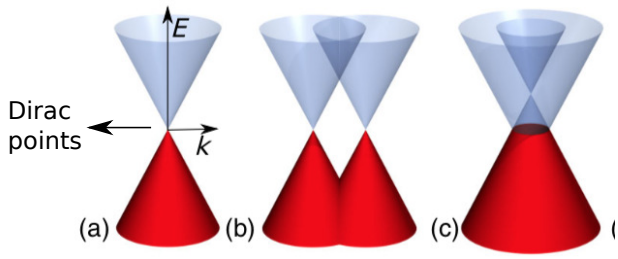

Figure 1.13 (a) The Dirac semimetal with doubly degenerate Dirac points. The Weyl semimetal with two Dirac cones separated in (b) momentum and (c) energy [67].

known as the anomalous Hall effect, which is responsible for the tensor form of the dielectric function of the WSM [71, 68]. The electromagnetic response of WSM can be derived from the formula of action for the electromagnetic field [71, 67, 72]. Here, we will give brief derivation of the electromagnetic response of WSM represented by electric displacement vector **D**. The more detailed derivation is given by Zyuzin and Burkov [69, 73] or Hosur and Qi [74]. The action of electromagnetic field is given by,

$$S_\theta = -\frac{e^2}{8\pi^2\hbar}\int dtd\mathbf{r}\partial_\gamma\theta\epsilon^{\gamma\nu\rho\eta}A_\nu\partial_\rho A_\eta, \tag{1.33}$$

where A_ν is electromagnetic potential, $\epsilon^{\gamma\nu\rho\eta}$ is the Levi-Civita tensor and each index γ, ν, ρ, η takes values $0, 1, 2, 3$. The current density j_ν is given by varying the action with respect to electromagnetic potential,

$$j_\nu \equiv \frac{\delta S_\theta}{\delta A_\nu} = \frac{e^2}{4\pi^2\hbar}\partial_\gamma\theta\epsilon^{\gamma\nu\rho\eta}\partial_\rho A_\eta. \tag{1.34}$$

By writing $\mathbf{E} = -(\nabla A_0) - \partial_0\mathbf{A}$, Eq. (1.34) gives the Hall current $\mathbf{j} = \frac{e^2}{4\pi^2\hbar}\nabla\theta\times\mathbf{E}$, which gives additional terms in **D** of the normal metals as the second term of Eq. (1.35). We can write the electric displacement vector as follows,

$$\mathbf{D} = \varepsilon_0\varepsilon_b\left(1 - \frac{\omega_p^2}{\omega^2}\right)\mathbf{E} + \frac{ie^2}{4\pi^2\hbar\omega}(\nabla\theta)\times\mathbf{E}, \tag{1.35}$$

where ω_p is the plasmon frequency, ε_b is the background dielectric constant ($\varepsilon_b = 13$ for $Eu_2Ir_2O_7$). The first term of Eq. (5.1) is the Drude dielectric function, which is similar to normal metals. The anomalous Hall effect given by the second term of Eq. (1.35). The anomalous Hall current only depends on the structure of the electron dispersion of WSM represented by θ.

Fig. 1.13: Fig/wsm.eps

Chapter 2

Methods of calculation

In this chapter, we will describe formalisms that are useful for the main calculations. We will discuss the electronic structure of graphene and silicene, which is used in the linear response theory for obtaining the optical conductivity. The optical conductivity is useful for discussing the existence of TE surface wave in silicene. We also discuss about the method to quantize the photon and surface plasmon. Finally we show how to calculate the optical spectra of graphene, which is useful for discussion of the quantum description of surface plasmon excitation by light.

2.1 The optical conductivity by linear response theory

The definition of the linear response theory is a theory, in which we consider that the response of a material to the external perturbation is linear to the strength of perturbation. In this section, we will consider the response of a material as electric current $\mathbf{J}$ to the external electric field $\mathbf{E}$. Within the linear approximation, the electric current can be related to the field as follows,

$$\mathbf{J} = \sigma \mathbf{E}, \tag{2.1}$$

where the constant of proportionality σ is conductivity. Equation (2.1) is known as Ohm's law. In this section, we will derive the general expression of σ by linear response theory, which will be used to derive the optical conductivity of silicene in the next chapter.

2.1.1 Kubo formula

Suppose that we measure an observable quantity O, such as the current density $\mathbf{J}$. The relation between the change of an observable quantity δO to the perturbation is described by the Kubo formula [75, 76]. In the perturbed system, the Hamiltonian can be written as follows,

$$H(t) = H_0 + H'(t)\theta(t - t_0), \tag{2.2}$$

where H_0 is the unperturbed Hamiltonian, which does not depend on the time, $H'(t)$ is the perturbation Hamiltonian, which depends on time and $\theta(t - t_0)$ is the step

function, which implies that the perturbation starts at $t = t_0$. The expectation value of an observable quantity O at a given time t is given as follows,

$$\langle O(t)\rangle = \frac{1}{Z_0}\sum_n \langle\psi_n(t)\,|O|\,\psi_n(t)\rangle e^{-\beta E_n}, \tag{2.3}$$

where Z_0 is partition function, $\beta = 1/k_B T$, E_n is the eigenvalue of Eq. (2.2), and $|\psi(t)\rangle$ is the time-dependent state, which is governed by the Schrödinger equation below

$$i\hbar\frac{\partial}{\partial t}|\psi_n(t)\rangle = H(t)|\psi_n(t)\rangle. \tag{2.4}$$

Since the perturbation is weak, it is convenient to work in the interaction picture. In the interaction picture, the evolution of a state is governed by the perturbing Hamiltonian only. The time evolution of a state $|\hat{\psi}_n(t_0)\rangle$ at $t = t_0$ to a state $|\hat{\psi}_n(t)\rangle$ is given by

$$|\hat{\psi}_n(t)\rangle = \hat{U}(t, t_0)|\hat{\psi}_n(t_0)\rangle, \tag{2.5}$$

where $|\hat{\psi}_n(t)\rangle$ is the state in the interaction picture, and $\hat{U}(t, t_0)$ is the unitary operator, which only depends on $H'(t)$. The unitary operator in interaction picture is the solution of the following self-consistent equation,

$$\begin{aligned}\hat{U}(t, t_0) =& 1 + \frac{1}{i}\int_{t_0}^{t} dt'\hat{H}'(t')\hat{U}(t', t_0)\\ =& 1 + \frac{1}{i\hbar}\int_{t_0}^{t} dt_1\hat{H}'(t_1) + \frac{1}{i^2\hbar^2}\int_{t_0}^{t} dt_1\hat{H}'(t_1)\int_{t_0}^{t_1} dt_2\hat{H}'(t_2) + ...\end{aligned} \tag{2.6}$$

If we consider only linear order of perturbing Hamiltonian, then the unitary operator is given only up to the second term of Eq. (2.6).

The state in Schrödinger picture $|\psi(t)\rangle$ is related with the interaction picture $|\hat{\psi}(t)\rangle$ by the following equation,

$$\begin{aligned}|\psi_n(t)\rangle =& e^{iH_0 t/\hbar}|\hat{\psi}_n(t)\rangle\\ =& e^{iH_0 t/\hbar}\hat{U}(t, t_0)|\hat{\psi}(t_0)\rangle,\end{aligned} \tag{2.7}$$

where we use Eq. (2.5) to obtain Eq. (2.7). Therefore, by substituting Eqs. (2.6) and (2.7) up to linear order to Eq. (2.3), we obtain the following equation for the

expectation value of observable quantity A at a given time,

$$\begin{aligned}\langle O(t)\rangle =&\frac{1}{Z_0}\sum_n \left\langle \hat{\psi}_n(t_0)\right| e^{iH_0 t/\hbar}\left(1+\frac{i}{\hbar}\int dt'\hat{H}'(t')\right) O e^{-iH_0 t/\hbar}\\ &\times\left(1-\frac{i}{\hbar}\int dt'\hat{H}'(t')\right)\left|\hat{\psi}_n(t_0)\right\rangle e^{-\beta E_n}\\ =&\left\langle O\right\rangle_0 - \frac{i}{\hbar}\int_{t_0}^{t} dt' \frac{1}{Z_0}\sum_n e^{-\beta E_n}\left\langle \hat{\psi}_n(t_0)\right|\left[\hat{O}(t),\hat{H}'(t')\right]\left|\hat{\psi}_n(t_0)\right\rangle\\ =&\left\langle O\right\rangle_0 - \frac{i}{\hbar}\int_{t_0}^{t} dt' \frac{1}{Z_0}\sum_n e^{-\beta E_n}\left\langle \psi_n(t_0)\right|\left[\hat{O}(t),\hat{H}'(t')\right]\left|\psi_n(t_0)\right\rangle \qquad (2.8)\\ =&\left\langle O\right\rangle_0 - \frac{i}{\hbar}\int_{t_0}^{t} dt' \left\langle\left[\hat{O}(t),\hat{H}'(t')\right]\right\rangle_0, \qquad (2.9)\end{aligned}$$

where all the averages $\langle\cdots\rangle_0$ are taken with respect to the unperturbed Hamiltonian H_0 The term that is not linear to $\hat{H}'$ is neglected in Eq. (2.9) due to the linear approximation. The time dependence of the operator O is taken in the interacting picture as follows,

$$\hat{O}(t) = e^{iH_0 t/\hbar} O e^{-iH_0 t/\hbar}. \qquad (2.10)$$

In Eq. (2.8), we use the fact that $|\hat{\psi}_n(t_0)\rangle = e^{iH_0 t_0/\hbar}|\psi_n(t_0)\rangle = e^{iE_n t_0/\hbar}|\psi_n(t_0)\rangle$. Eq. (2.9) is known as the Kubo formula. By using the Kubo formula, the expected value of an observable quantity in a perturbed system is determined by the average with respect to the unperturbed system. The average in the second term of Eq. (2.9) is known as the retarded correlation function, because the response O appears after the perturbation starts ($t > t'$).

2.1.2 The optical conductivity

In this section, we will use the Kubo formula in Eq. (2.9) to derive the general expression of the optical conductivity of a material [76, 60]. The corresponding response is the current density. We assume that the external field is represented by the vector potential $\mathbf{A}$. The current density operator is give as follows,

$$\begin{aligned}\hat{\mathbf{J}}(r,t) =& -e\hbar\hat{\Psi}^\dagger(r,t)\mathbf{v}\hat{\Psi}(r,t) - \frac{e^2}{m}\hat{\Psi}^\dagger(r,t)\hat{\Psi}(r,t)\mathbf{A}(r,t),\\ =& J_{\mathrm{P}}(r,t) + J_{\mathrm{D}}(r,t), \qquad (2.11)\end{aligned}$$

where $\mathbf{v} = \partial H_0/\partial\mathbf{k}$ is the velocity operator with k is the wave vector of electron. J_{P} and J_{D} are called the paramagnetic and diamagnetic current. The $\hat{\Psi}^\dagger(r,t)$ and $\hat{\Psi}(r,t)$ are the field operator that creates and annihilates electron at position r, respectively. The perturbing Hamiltonian is given by,

$$\begin{aligned}\hat{H}'(t) =& \int d\mathbf{r}\ \hat{\mathbf{J}}(r,t)\cdot\mathbf{A}(r,t)\\ =& -e\hbar\int dr\ \hat{\Psi}^\dagger(r,t)v\hat{\Psi}(r,t)A(r,t), \qquad (2.12)\end{aligned}$$

where we neglect the non-linear term with respect to $A(r,t)$ ($J_{\rm D}(r,t)$). Moreover, the current and field are considered to be parallel to each other. By substituting Eqs. (2.11) and (2.12) to Eq. (2.9), we can determine the expectation value of current density up to linear order of $A(r,t)$, as follows,

$$\begin{aligned}\left\langle J(r,t)\right\rangle =&\left\langle J\right\rangle_0 - ie^2\hbar\int_{t_0}^{t}dt'\int dr' \\ &\times\left\langle\left[\hat{\Psi}^\dagger(r,t)v\hat{\Psi}(r,t),\hat{\Psi}^\dagger(r',t')v'\hat{\Psi}(r',t')A(r',t')\right]\right\rangle_0 \\ =&\left\langle J\right\rangle_0 + \int_{t_0}^{t}dt'\int dr' C^R(r,r',t,t')A(r',t',), \end{aligned} \tag{2.13}$$

where $\langle J\rangle_0$ is the averaged current without perturbation, and it can be taken as zero and $C^R(r,r',t,t')$ is defined as below,

$$C^R(r,r',t,t') = -ie^2\hbar\, T\left\langle\left[\hat{\Psi}^\dagger(r,t)v\hat{\Psi}(r,t),\hat{\Psi}^\dagger(r',t')v'\hat{\Psi}(r',t')\right]\right\rangle_0 \quad , \tag{2.14}$$

where we add time ordering operator T, since perturbation has to start before the response $t > t'$. Suppose that the function $C(r,r',t,t')$ depends only at the time difference $t-t'$, we can write,

$$\left\langle J(r,t)\right\rangle = \int_{t_0}^{t}dt'\int dr' C^R(r,r',t-t')A(r',t'). \tag{2.15}$$

If the perturbation is applied for long time $t >> t_0$, we can take a limit of $t\to\infty$ and $t_0\to-\infty$, and Eq. (2.15) becomes the convolution equation. Thus, we get the current density in frequency domain as follows,

$$\begin{aligned}\left\langle J(r,\omega)\right\rangle =&\int dr' C^R(r,r',\omega)A(r',\omega) \\ =&\frac{1}{i\omega}\int dr' C^R(r,r',\omega)E(r',\omega), \end{aligned} \tag{2.16}$$

where $A(r',\omega) = 1/i\omega\ E(r',\omega)$. By comparing Eq. (2.16) with Ohm's law of Eq. (2.1), we can define the optical conductivity

$$\sigma(r,r',\omega) = \frac{1}{i\omega}C^R(r,r',\omega). \tag{2.17}$$

Let us return to time domain, the function $C(r,r',t-t')$ can be written as

$$C^R(r,r',t-t') = -\frac{i}{\hbar}\, T\left\langle\left[\hat{J}_{\rm P}(r,t),\hat{J}_{\rm P}(r',t')\right]\right\rangle_0. \tag{2.18}$$

Suppose that we have translation invariant system, the $C^R(r,r',t-t')$ depends only on $r-r'$ and we can define it in the momentum domain as follows,

$$\begin{aligned} C^R(\mathbf{q},t-t') =& -\frac{i}{\hbar}\int d\mathbf{r}\frac{1}{S}\sum_{\mathbf{q}_1\mathbf{q}_2} T\Big\langle\Big[\hat{J}_{\rm P}(\mathbf{q}_1,t),\hat{J}_{\rm P}(\mathbf{q}_2,t')\Big]\Big\rangle_0 e^{i\mathbf{q}_1\cdot\mathbf{r}+i\mathbf{q}_2\cdot\mathbf{r}'}e^{-i\mathbf{q}\cdot(\mathbf{r}-\mathbf{r}')} \\ =& -\frac{i}{\hbar}\frac{1}{S}\,T\Big\langle\Big[\hat{J}_{\rm P}(\mathbf{q},t),\hat{J}_{\rm P}(-\mathbf{q},t')\Big]\Big\rangle_0, \end{aligned} \tag{2.19}$$

where S is the area of the system for 2D material. The current operator in the momentum domain can be obtained as follows,

$$\begin{aligned} \hat{J}_{\rm P}(r,t) =& -e\hbar\hat{\Psi}^\dagger(r,t)v\hat{\Psi}(r,t) \\ =& -\frac{1}{S}e\hbar\sum_{kk'}e^{i(\mathbf{k}-\mathbf{k}')\cdot\mathbf{r}}c^\dagger_{\mathbf{k}'}(t)vc_{\mathbf{k}}(t) \\ =& \frac{1}{S}\sum_q\Big\{-e\hbar\sum_{\mathbf{k}}c^\dagger_{\mathbf{k}}(t)vc_{\mathbf{k}+\mathbf{q}}(t)\Big\}e^{i\mathbf{q}\cdot\mathbf{r}} \\ =& \frac{1}{S}\sum_q\hat{J}_{\rm P}(\mathbf{q},t)e^{i\mathbf{q}\cdot\mathbf{r}}. \end{aligned} \tag{2.20}$$

Equation (2.19) is called retarded Green's function that is defined for $t>t'$. To obtain the general expression of Eq. (2.19) and the optical conductivity in frequency domain, it is convenient to work on the imaginary time Green function, known as the Matsubara-Green function [76]. The Matsubara-Green function $C(q,\tau-\tau')$ for Eq. (2.19) is expressed by the following function,

$$C(\mathbf{q},\tau-\tau') = -\frac{1}{\hbar}\frac{1}{S}\,T\Big\langle\hat{J}_{\rm P}(\mathbf{q},\tau)\hat{J}_{\rm P}(-\mathbf{q},\tau')\Big\rangle_0, \tag{2.21}$$

where $\tau=it$ is the imaginary time. Since $C(q,\tau-\tau')$ only depends on the time difference, we can set $\tau'=0$. By using the expression of $\hat{J}_{\rm P}(\mathbf{q},\tau)$ obtained from Eq. (2.20), we rewrite the Matsubara Green function as follows

$$\begin{aligned} C(\mathbf{q},\tau) =& -\frac{e^2\hbar}{S}\sum_{\mathbf{k}\mathbf{k}'}T\Big\langle c^\dagger_{\mathbf{k}}(\tau)vc_{\mathbf{k}+\mathbf{q}}(\tau)c^\dagger_{\mathbf{k}'}(0)v'c_{\mathbf{k}'-\mathbf{q}}(0)\Big\rangle_0 \\ =& -\frac{e^2\hbar}{S}\sum_{\mathbf{k}\mathbf{k}'}\Big(-v\,T\Big\langle c_{\mathbf{k}+\mathbf{q}}(\tau)c^\dagger_{\mathbf{k}'}(0)\Big\rangle_0 v'T\Big\langle c_{\mathbf{k}'-\mathbf{q}}(0)c^\dagger_{\mathbf{k}}(\tau)\Big\rangle_0\Big) \\ =& \frac{e^2\hbar}{S}\sum_{\mathbf{k}\mathbf{k}'}\Big(vG_0(\mathbf{k}+\mathbf{q},\mathbf{k}',\tau)v'G_0(\mathbf{k}'-\mathbf{q},\mathbf{k},-\tau)\Big) \\ =& \frac{e^2\hbar}{S}\sum_{\mathbf{k}}\Big(vG_0(\mathbf{k}+\mathbf{q},\tau)v'G_0(\mathbf{k},-\tau)\Big), \end{aligned} \tag{2.22}$$

where we introduce the Matsubara-Green function of a single electron $G_0(\mathbf{k},\tau)$ and its Fourrier transform $G_0(\mathbf{k},i\omega_n)$, which are defined, respectively, as follows,

$$G_0(\mathbf{k},\tau) = -T\Big\langle c_{\mathbf{k}}(\tau)c^\dagger_{\mathbf{k}}(0)\Big\rangle_0 = \sum_{\mathbf{k}'}G_0(\mathbf{k},\mathbf{k}',\tau)\delta_{\mathbf{k},\mathbf{k}'} \tag{2.23}$$

and

$$G_0(\mathbf{k}, i\omega_n) = \frac{1}{i\omega_n - \epsilon(\mathbf{k})}, \tag{2.24}$$

where $G_0(\mathbf{k}, i\omega_n)$ is the Matsubara Green function in frequency domain, $i\omega_n$ is the Matsubara frequency, and $\epsilon(\mathbf{k})$ is the energy of electron with wave vector $\mathbf{k}$. In Eq. (2.22), we use the Wick's theorem that enables us to interchange the fermion operators. Eq. (2.22) can be written in the frequency domain as follows,

$$C(\mathbf{q}, i\omega_n) = \frac{e^2\hbar}{\beta}\int \frac{d^2\mathbf{k}}{(2\pi)^2}\sum_{i\nu_n} \mathrm{Tr}\Big(vG_0(\mathbf{k}{+}\mathbf{q}, i\nu_n + i\omega_n)v'G_0(\mathbf{k}, i\nu_n)\Big). \tag{2.25}$$

If we have two energy bands of electron, then the Green function can be cast into 2×2 diagonal matrix with component $G_0^{ij}(\mathbf{k}, i\omega_n) = 1/(i\omega_n - \epsilon_i(\mathbf{k}))\delta_{ij}$, where $i = 1, 2$ denotes the band index. Therefore, we can write Eq. (2.25) as follows,

$$\begin{aligned} C(\mathbf{q}, i\omega_n) =& \frac{e^2\hbar}{\beta}\int \frac{d^2\mathbf{k}}{(2\pi)^2}\sum_{i\nu_n} \Big(v^{11}G_0^{11}(\mathbf{k}{+}\mathbf{q}, i\nu_n + i\omega_n)v^{11}G_0^{11}(\mathbf{k}, i\nu_n) \\ &+ v^{22}G_0^{22}(\mathbf{k}{+}\mathbf{q}, i\nu_n + i\omega_n)v^{22}G_0^{22}(\mathbf{k}, i\nu_n) \\ &+ v^{12}G_0^{22}(\mathbf{k}{+}\mathbf{q}, i\nu_n + i\omega_n)v^{21}G_0^{11}(\mathbf{k}, i\nu_n) \\ &+ v^{21}G_0^{11}(\mathbf{k}{+}\mathbf{q}, i\nu_n + i\omega_n)v^{12}G_0^{22}(\mathbf{k}, i\nu_n)\Big). \end{aligned} \tag{2.26}$$

Eq. (2.26) consists of four terms of summation of the Green function over the Matsubara frequency. In general, the summation is done by the following way,

$$\frac{1}{\beta}\sum_{i\nu_n} G_0(\mathbf{k}{+}\mathbf{q}, i\nu_n + i\omega_n)G_0(\mathbf{k}, i\nu_n) = \frac{f_0(\epsilon(\mathbf{k})) - f_0(\epsilon(\mathbf{k}{+}\mathbf{q}))}{i\omega_n + \epsilon(\mathbf{k}) - \epsilon(\mathbf{k}{+}\mathbf{q})}, \tag{2.27}$$

where $f_0(\epsilon)$ is the Fermi distribution function. By using Eq. (2.27) in Eq. (2.26), we obtained the following equation,

$$\begin{aligned} C(\mathbf{q}, i\omega_n) = \frac{e^2\hbar}{(2\pi)^2}\int d^2\mathbf{k}\Big(&(v^{11})^2\frac{f_0(\epsilon_1(\mathbf{k})) - f_0(\epsilon_1(\mathbf{k}{+}\mathbf{q}))}{i\omega_n + \epsilon_1(\mathbf{k}) - \epsilon_1(\mathbf{k}{+}\mathbf{q})} \\ &+(v^{22})^2\frac{f_0(\epsilon_2(\mathbf{k})) - f_0(\epsilon_2(\mathbf{k}{+}\mathbf{q}))}{i\omega_n + \epsilon_2(\mathbf{k}) - \epsilon_2(\mathbf{k}{+}\mathbf{q})} \\ &+v^{12}v^{21}\frac{f_0(\epsilon_1(\mathbf{k})) - f_0(\epsilon_2(\mathbf{k}{+}\mathbf{q}))}{i\omega_n + \epsilon_1(\mathbf{k}) - \epsilon_2(\mathbf{k}{+}\mathbf{q})} \\ &+v^{21}v^{12}\frac{f_0(\epsilon_2(\mathbf{k})) - f_0(\epsilon_1(\mathbf{k}{+}\mathbf{q}))}{i\omega_n + \epsilon_2(\mathbf{k}) - \epsilon_1(\mathbf{k}{+}\mathbf{q})}\Big). \end{aligned} \tag{2.28}$$

The retarded Green function of Eq. (2.19) in frequency domain $C^R(\mathbf{q}, \omega)$ is related to the Matsubara-Green function of Eq. (2.28) by the analytic continuation, which is obtained by replacing the $i\omega_n \to \hbar\omega + i\gamma$ with $\gamma \to 0$,

$$C^R(\mathbf{q}, \omega) = C(\mathbf{q}, \hbar\omega + i\gamma) \tag{2.29}$$

The expression of optical conductivity can be obtained by using Eq. (2.29) in Eq. (2.18). However, when the $\omega = 0$ or the vector potential does not vary with time, the electric field and the current should also be zero. Therefore, we have to substract the contribution of $\omega = 0$ in Eq. (2.29) ($C^R(\mathbf{q}, 0)$) and we arrive at the following expression of optical conductivity,

$$\sigma(\mathbf{q},\omega) = \frac{1}{i\omega}\Big(C^R(q,\omega) - C^R(\mathbf{q},0)\Big) \tag{2.30}$$

$$\begin{aligned}
=&\frac{ie^2\hbar}{(2\pi)^2}\int d^2\mathbf{k}\Big((v^{11})^2\frac{f_0(\epsilon_1(\mathbf{k})) - f_0(\epsilon_1(\mathbf{k}+\mathbf{q}))}{(\epsilon_1(\mathbf{k}+\mathbf{q}) - \epsilon_1(\mathbf{k}))(\hbar\omega + \epsilon_1(\mathbf{k}) - \epsilon_1(\mathbf{k}+\mathbf{q}))}\\
&+(v^{22})^2\frac{f_0(\epsilon_2(\mathbf{k})) - f_0(\epsilon_2(\mathbf{k}+\mathbf{q}))}{(\epsilon_2(\mathbf{k}+\mathbf{q}) - \epsilon_2(\mathbf{k}))(\hbar\omega + \epsilon_2(\mathbf{k}) - \epsilon_2(\mathbf{k}+\mathbf{q}))}\\
&+v^{12}v^{21}\frac{f_0(\epsilon_1(\mathbf{k})) - f_0(\epsilon_2(\mathbf{k}+\mathbf{q}))}{(\epsilon_2(\mathbf{k}+\mathbf{q}) - \epsilon_1(\mathbf{k}))(\hbar\omega + \epsilon_1(\mathbf{k}) - \epsilon_2(\mathbf{k}+\mathbf{q}))}\\
&+v^{21}v^{12}\frac{f_0(\epsilon_2(\mathbf{k})) - f_0(\epsilon_1(\mathbf{k}+\mathbf{q}))}{(\epsilon_1(\mathbf{k}+\mathbf{q}) - \epsilon_2(\mathbf{k}))(\hbar\omega + \epsilon_2(\mathbf{k}) - \epsilon_1(\mathbf{k}+\mathbf{q}))}\Big),
\end{aligned} \tag{2.31}$$

where we neglect the γ. Since we are interested in optical transition, we set $q \to 0$, and we arrive at the general expression of optical conductivity for system with two energy bands [60],

$$\begin{aligned}
\sigma(\omega) = \frac{ie^2\hbar}{(2\pi)^2}\int d^2\mathbf{k}\Big(&-\frac{(v^{11})^2}{\hbar\omega}\frac{df_0(\epsilon_1(\mathbf{k}))}{d\epsilon_1} - \frac{(v^{22})^2}{\hbar\omega}\frac{df_0(\epsilon_2(\mathbf{k}))}{d\epsilon_2}\\
&+v^{12}v^{21}\frac{f_0(\epsilon_1(\mathbf{k})) - f_0(\epsilon_2(\mathbf{k}))}{(\epsilon_2(\mathbf{k}) - \epsilon_1(\mathbf{k}))(\hbar\omega + \epsilon_1(\mathbf{k}) - \epsilon_2(\mathbf{k}))}\\
&+v^{21}v^{12}\frac{f_0(\epsilon_2(\mathbf{k})) - f_0(\epsilon_1(\mathbf{k}))}{(\epsilon_1(\mathbf{k}) - \epsilon_2(\mathbf{k}))(\hbar\omega + \epsilon_2(\mathbf{k}) - \epsilon_1(\mathbf{k}))}\Big).
\end{aligned} \tag{2.32}$$

Equation (2.32) is used to calculate the optical conductivity of silicene and graphene in the next chapter. To derive the optical conductivity, the electronic structure of graphene and silicene have to be obtained beforehand, which is discussed in the next section.

2.2 The electronic structure of graphene and silicene

2.2.1 The electronic structure of graphene

The electronic energy dispersion of graphene is calculated by using simple tight binding (STB) model [4, 2]. The electronic energy dispersion describes the energy E as a function of wave vector $\mathbf{k}$. In the tight binding approximation, the eigenfunctions of electrons are made up by the Bloch function that consists of the atomic orbitals.

In graphene, the valence orbitals (2s, $2p_x$, $2p_y$) of a carbon atom are hybridized to one another and form σ-bonds, while $2p_z$ orbital gives a π bond. The $2p_z$ forms the π band independently from σ bands and the π band lies around the Fermi energy. Hence, the electronic transport and optical properties of graphene originate mainly from the π band. Therefore, hereafter we can adopt the STB method to model the π band for simplicity.

The wave function of an electron in graphene can be written as a linear combination of the atomic orbitals

$$\Psi(\mathbf{k},\mathbf{r}) = C_A(\mathbf{k})\phi_A(\mathbf{k},\mathbf{r}) + C_B(\mathbf{k})\phi_B(\mathbf{k},\mathbf{r}), \tag{2.33}$$

where $\phi_j(\mathbf{k},\mathbf{r})$ with $j = A, B$, is the Bloch wave function made of A or B atom in the unit cell. The C_j $(j = A, B)$ is the coefficient of Bloch wave function . This Bloch wave function consists of the linear combination of atomic orbital, that is $2p_z$ orbital. The Bloch wave function can be written as

$$\phi_j(\mathbf{k},\mathbf{r}) = \frac{1}{\sqrt{N}} \sum_{\mathbf{R_j}}^{N} e^{i\mathbf{k}\cdot\mathbf{R_j}} \varphi(\mathbf{r} - \mathbf{R_j}), \quad (j = A \text{ or } B), \tag{2.34}$$

where $\mathbf{R_A}$ and $\mathbf{R_B}$ are the position of A and B sites in solid as shown in Fig. (2.1), respectively. The electronic energy dispersion $E(\mathbf{k})$ is obtained by minimizing

$$E(\mathbf{k}) = \frac{\langle\Psi|H|\Psi\rangle}{\langle\Psi|\Psi\rangle}, \tag{2.35}$$

in respect to the wave function coefficients. Inserting Eq. (2.33) to Eq.(2.35), a secular equation is obtained [2]

$$\sum_{j'} H_{\mathrm{jj'}} C_{j'}(\mathbf{k}) = E \sum_{j'} S_{\mathrm{jj'}} C_{j'}(\mathbf{k}) \quad (j, j' = \mathrm{A}, \mathrm{B}), \tag{2.36}$$

where $H_{\mathrm{jj'}} = \langle\phi|H|\psi\rangle$ and $S_{\mathrm{jj'}} = \langle\phi|\psi\rangle$ are called the transfer integral matrix and the overlap integral matrices, respectively. Then, Eq. (2.36) has turned into eigenvalue problem, where it can be written explicitly as

$$\begin{pmatrix} H_{\mathrm{AA}}(\mathbf{k}) & H_{\mathrm{AB}}(\mathbf{k}) \\ H_{\mathrm{BA}}(\mathbf{k}) & H_{\mathrm{BB}}(\mathbf{k}) \end{pmatrix} \begin{pmatrix} C_{\mathrm{A}}(\mathbf{k}) \\ C_{\mathrm{B}}(\mathbf{k}) \end{pmatrix} = E(\mathbf{k}) \begin{pmatrix} S_{\mathrm{AA}}(\mathbf{k}) & S_{\mathrm{AB}}(\mathbf{k}) \\ S_{\mathrm{BA}}(\mathbf{k}) & S_{\mathrm{BB}}(\mathbf{k}) \end{pmatrix} \begin{pmatrix} C_{\mathrm{A}}(\mathbf{k}) \\ C_{\mathrm{B}}(\mathbf{k}) \end{pmatrix}. \tag{2.37}$$

Thus, the electron energy dispersion can be obtained by solving the secular equation

$$\det\left[\mathbf{H} - E\mathbf{S}\right] = 0 \quad . \tag{2.38}$$

To solve Eq. (2.38), we need to evaluate the matrix elements of transfer integral matrix and overlap matrix. First, we evaluate the matrix elements of transfer integral matrix. By using Bloch wave function in Eq. (2.34),

$$\begin{aligned} H_{\mathrm{AA}} =& \frac{1}{N} \sum_{\mathbf{R_A},\mathbf{R'_A}} e^{i\mathbf{k}\cdot(\mathbf{R_A}-\mathbf{R'_A})} \left\langle \varphi(\mathbf{r} - \mathbf{R'_A})|H|\varphi(\mathbf{r} - \mathbf{R_A})\right\rangle \\ =& \varepsilon_{2\mathrm{p}} + (\text{terms equal to or more distant than} \\ & \mathbf{R_A} \pm \boldsymbol{a_i}). \end{aligned} \tag{2.39}$$

The high order contribution to H_{AA} can be neglected. Therefore, the value of H_{AA} gives $\varepsilon_{2\mathrm{p}}$, which is the energy of the 2p orbital of a carbon atom. By using the same calculation, H_{BB} also gives $\varepsilon_{2\mathrm{p}}$. As for off-diagonal elements of the transfer integral matrix, the same method is used. Here, the largest contribution comes from three

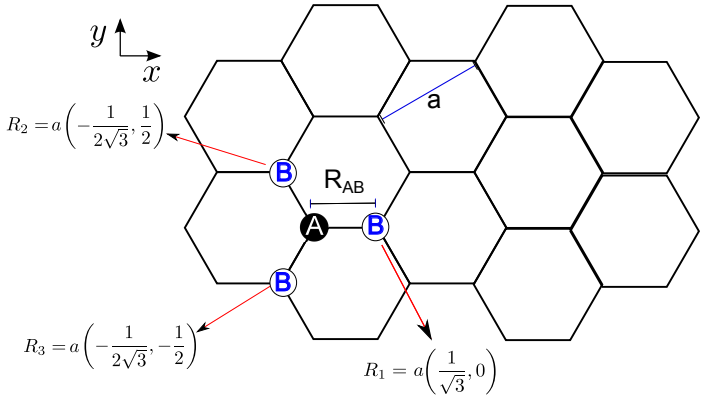

Figure 2.1 The reference atomic site is A. The 3 nearest neighbors (B atomic site) are shown. The positions of nearest neighbors are indicated by $\mathbf{R}_1$, $\mathbf{R}_2$, and $\mathbf{R}_3$ with respect to A site.

nearest-neighbor atoms and we can neglect more distant terms. The three nearest-neighbors vectors $\mathbf{R}_i$ $(i = 1, 2, 3)$ from A atom to three B atoms are shown in Fig. 2.1. The off-diagonal elements for can be written as

$$\begin{aligned} H_{\mathrm{AB}} &= \frac{1}{N} \sum_{\mathbf{R_A}, \mathbf{R_i}} e^{i\mathbf{k}\cdot\mathbf{R}_i} \langle \varphi(\mathbf{r} - \mathbf{R_A}) | H | \varphi(\mathbf{r} - \mathbf{R_A} - \mathbf{R_i}) \rangle \\ &\equiv tf(\mathbf{k}) \quad , \end{aligned} \tag{2.40}$$

where $\langle \varphi(\mathbf{r} - \mathbf{R_A}) | H | \varphi(\mathbf{r} - \mathbf{R_A} - \mathbf{R_i}) \rangle$ denotes contribution of each nearest neighbor atom, denoted by t. By inserting the coordinates of the nearest neighbor atoms, $f(\mathbf{k})$ in Eq. (2.40) can be evaluated

$$\begin{aligned} f(\mathbf{k}) &= \sum_{\mathbf{R_i}} e^{i\mathbf{k}\cdot\mathbf{R_i}}, \quad (i = 1, ...3) \\ &= e^{ik_x a/\sqrt{3}} + 2e^{-ik_x a/2\sqrt{3}} \cos(\frac{k_y a}{2}). \end{aligned} \tag{2.41}$$

Since the transfer integral matrix is a Hermite matrix, we get the $H_{BA}(\mathbf{k}) = H^*_{AB}(\mathbf{k})$. Now we have defined transfer integral matrix. Next let us evaluate the overlap integral matrix. The overlap of same atomic site is 1, $S_{AA}(\mathbf{k}) = S_{BB}(\mathbf{k}) = 1$, while off-site one should be calculated by considering only the nearest neighbors,

$$\begin{aligned} S_{\mathrm{AB}} &= \frac{1}{N} \sum_{\mathbf{R_A}, \mathbf{R_i}} e^{i\mathbf{k}\cdot(\mathbf{R}_i)} \langle \varphi(\mathbf{r} - \mathbf{R_A}) | \varphi(\mathbf{r} - \mathbf{R_A} - \boldsymbol{R_i}) \rangle, \quad (i = 1, ...3) \\ &= sf(\mathbf{k}), \end{aligned} \tag{2.42}$$

where $\langle \varphi(\mathbf{r} - \mathbf{R_A}) | \varphi(\mathbf{r} - \mathbf{R_A} - \boldsymbol{R_i}) \rangle$ denotes contribution of each neighbor atom, denoted by s. This S matrix is also a Hermite matrix, $S_{BA}(\mathbf{k}) = S^*_{AB}(\mathbf{k})$.

Fig. 2.1: Fig/Fig2k1.eps

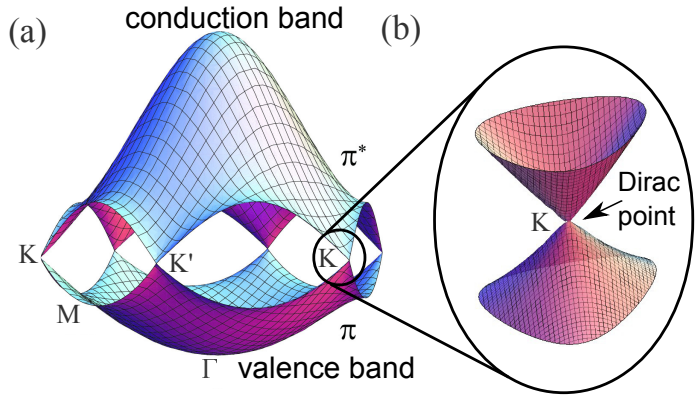

Figure 2.2 (a) The electronic energy dispersion of graphene throughout the whole region of Brillouin zone. (b) The dispersion around K point [4].

After getting all necessary matrices, the electronic energy dispersion can be calculated by Eq. (2.38). The solution is

$$E^{\pm}(\mathbf{k}) = \frac{\mp t\sqrt{f^*(\mathbf{k})f(\mathbf{k})}}{1 \mp s\sqrt{f^*(\mathbf{k})f(\mathbf{k})}} \quad , \tag{2.43}$$

where we set $\varepsilon_{2p} = 0$. The value of $t = -3.033$ eV and $s = 0.129$ [4, 2]. $+(-)$ sign denotes the π (π^*) band, with negative value of t. Hereafter, they will be called valence and conduction band, respectively. The electronic energy dispersion of graphene in the hexagonal Brillouin zone is plotted in Fig. 2.2. We also show the high symmetry points in the energy dispersion. These high symmetry points are defined at the center Γ, the center of an edge M, and the hexagonal corners K and K$'$ of the Brillouin zone. The position of the M and K point can be described with respect of Γ point by vectors

$$\Gamma\mathrm{M} = \frac{2\pi}{a}\left(\frac{1}{\sqrt{3}}, 0\right), \quad \Gamma\mathrm{K} = \frac{4\pi}{3a}\left(0, -1\right), \tag{2.44}$$

where $|\Gamma\mathrm{M}| = 2\pi/\sqrt{3}a$, $|\Gamma\mathrm{K}| = 4\pi/3a$ and $|\mathrm{MK}| = 2\pi/3a$, with $a = \sqrt{3}a_{cc}$ is the lattice constant of graphene unit cell and $a_{cc} = 0.142$ nm is the distance between two carbon atoms. There are six K points (including K$'$ points) and six M points within the Brillouin zone.

If we assume that the orbital wave function is orthogonal or $s = 0$, the energy dispersion is expressed as follows,

$$E^{\pm}(\mathbf{k}) = \pm|t|\sqrt{3 + 2\cos(k_x a) + 4\cos(\frac{k_x a}{2})\cos(\frac{\sqrt{3}}{2}k_y a)} \quad , \tag{2.45}$$

where $+(-)$ sign denotes the conduction (valence) band.

Fig. 2.2: Fig/Fig2k2.eps

2.2.2 Second quantization for the tight binding method

The energy dispersion in Eq. (2.45) can also be obtained using second quantization method. Assuming the tight binding approximation, the Hamiltonian in second quantization form is given as follows,

$$H = -|t| \sum_i \left(a_i^\dagger b_{i+1} + a_i^\dagger b_{i+2} + a_i^\dagger b_{i+3} \right) + h.c, \tag{2.46}$$

where $1, 2, 3$ represent the R_1, R_2, R_3, which are given in Fig. 2.1. $a_i^\dagger$ and a_i are the creation and annihilation operators of electron in the sublattice A located at the site R_i, while $b_i^\dagger$ and b_i are the creation and annihilation operators of electron in the sublattice B located at the site R_i. The term $a_i^\dagger b_{i+1}$ means that we annihilate an electron in the sublattice B located at the site $R_i + R_1$ and then create an electron in the atom A located at the site R_i. In the other words, the electron hops from atom B to atom A. Because there are three nearest neighbors, electron can hops from three different sites of atom B to atom A, therefore we have three terms in the Eq. (2.46). The reverse hopping is included in the term of Hermitian conjugate ($h.c$), where it explains the hopping of electron from atom A to atom B.

To obtain the dispersion relation, we express the Hamiltonian in the momentum space by transforming the creation and annihilation operators as follows,

$$a_i = \frac{1}{\sqrt{N}} \sum_k a_k e^{i\mathbf{k}\cdot\mathbf{R_i}} \qquad , \qquad b_i = \frac{1}{\sqrt{N}} \sum_k b_k e^{i\mathbf{k}\cdot\mathbf{R_i}}. \tag{2.47}$$

By substituting Eq. (2.47) to Eq. (2.46), we get the second quantized Hamiltonian in the momentum space. For example, let us take the first term,

$$\begin{aligned} -|t| \sum_i \; a_i^\dagger b_{i+1} &= - \frac{|t|}{N} \sum_i \sum_{kk'} \; a_k^\dagger b'_k e^{i(\mathbf{k'}-\mathbf{k})\cdot\mathbf{R_i}} e^{i\mathbf{k'}\cdot\mathbf{R_1}} \\ &= - \frac{|t|}{N} \sum_{kk'} \; a_k^\dagger b'_k N \delta_{k',k} e^{i\mathbf{k'}\cdot\mathbf{R_1}} \\ &= - |t| \sum_k \; a_k^\dagger b_k e^{i\mathbf{k}\cdot\mathbf{R_1}} \end{aligned} \tag{2.48}$$

The Hamiltonian of Eq. (2.46) can be written as follows,

$$\begin{aligned} H &= - |t| \sum_k \sum_{R_j=R_1}^{R_3} e^{i\mathbf{k}\cdot\mathbf{R_j}} a_k^\dagger b_k - |t| \sum_k \sum_{R_j=R_1}^{R_3} e^{-i\mathbf{k}\cdot\mathbf{R_j}} b_k^\dagger a_k \\ &= - |t| \sum_k f(\mathbf{k}) a_k^\dagger b_k - |t| \sum_k f^*(\mathbf{k}) b_k^\dagger a_k \\ &= \sum_k \; \begin{pmatrix} a_k^\dagger & b_k^\dagger \end{pmatrix} \begin{pmatrix} 0 & -|t| f(\mathbf{k}) \\ -|t| f^*(\mathbf{k}) & 0 \end{pmatrix} \begin{pmatrix} a_k \\ b_k \end{pmatrix} \end{aligned} \tag{2.49}$$

The 2×2 matrix in Eq. (2.49) is the Hamiltonian matrix in the first quantization discussed in the previous section. The eigen value of this matrix gives the dispersion relation of electron in graphene,

$$E^{\pm}(\mathbf{k}) = \pm |t| \sqrt{f^*(\mathbf{k}) f(\mathbf{k})}, \tag{2.50}$$

which is nothing but Eq. (2.45) with $+(-)$ sign denotes the conduction (valence) band. It is noted that $\mathbf{k}$ is measured from the center of Brillouin zone (Γ point).

Figure 2.2 shows that at the corner of the Brilllouin zone or at the K and K' points, the conduction and valence bands touch each other, which can be proved by substituting K and K' point coordinates to energy dispersion in Eq. (2.45). Coordinates of the K and K' point coordinates are given by $\frac{4\pi}{3a}(0,-1)$ and $\frac{4\pi}{3a}(0,1)$, respectively [4]. The energy at K and K' points is zero for both valence and conduction bands. It is also noted that the the energy dispersion close to K and K' is linear to the wave vector of electron as shown in Fig. (2.2). This linearity can be shown by expanding the $f(\mathrm{k})$ near to K or K' points as follows [4],

$$f(\mathbf{K}+\mathbf{k}) = \frac{\sqrt{3}a}{2}(ik_x + k_y) \tag{2.51}$$

$$f(\mathbf{K}'+\mathbf{k}) = \frac{\sqrt{3}a}{2}(ik_x - k_y), \tag{2.52}$$

where now the $\mathbf{k}$ is measured from K or K', accordingly. Therefore, we can write down the effective Hamiltonian near K and K' points as follows,

$$H(\mathbf{K}+\mathbf{k}) = \frac{\sqrt{3}a|t|}{2}\begin{pmatrix} 0 & e^{-i\pi/2}(k_x - ik_y) \\ e^{i\pi/2}(k_x + ik_y) & 0 \end{pmatrix} \tag{2.53}$$

$$H(\mathbf{K}'+\mathbf{k}) = \frac{\sqrt{3}a|t|}{2}\begin{pmatrix} 0 & e^{-i\pi/2}(k_x + ik_y) \\ e^{i\pi/2}(k_x - ik_y) & 0 \end{pmatrix}. \tag{2.54}$$

By extracting the constants $e^{-i\pi/2}$ and $e^{i\pi/2}$ (which does not affect any physical results, such as energy dispersion), we can obtain the effective Hamiltonian in Eqs. (2.53) and (2.54) can also be expressed by the Pauli matrix ($\boldsymbol{\sigma}$) as follows [16],

$$H(\mathbf{K}+\mathbf{k}) = \frac{\sqrt{3}a|t|}{2}\ \boldsymbol{\sigma}\cdot\mathbf{k} \tag{2.55}$$

$$H(\mathbf{K}'+\mathbf{k}) = \frac{\sqrt{3}a|t|}{2}\ (\boldsymbol{\sigma}\cdot\mathbf{k})^* \tag{2.56}$$

Both of Eqs. (2.53) and (2.54) give the same energy dispersion, which is linear to the wave vector $k = \sqrt{k_x^2 + k_y^2}$,

$$E(\mathbf{K}+\mathbf{k}) = E(\mathbf{K}'+\mathbf{k}) = \hbar v_{\mathrm{F}} k \tag{2.57}$$

where $\hbar v_{\mathrm{F}} = \frac{\sqrt{3}a|t|}{2}$ with $v_{\mathrm{F}} \approx 10^6$ m/s is the Fermi velocity of graphene.

2.2.3 The electronic structure of silicene

The lattice of silicene is similar to that of graphene, which is honeycomb lattice as shown in Fig. 2.3 (a). However, due to the sp^3-like hybridization, the lattice is not planar, but buckled as shown in Fig. 2.3 (b). The sublattice A and B of silicene are vertically separated by distance $d = 0.46$ Å.

It is reported that the intrinsic spin-orbit (SO) coupling in silicene is much larger than in graphene, with SO coupling constant $\Delta_{\mathrm{SO}} = 3.9$ meV for silicene, while it

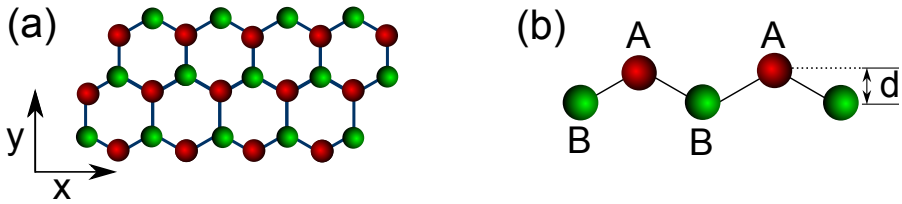

Figure 2.3 (a) Honeycomb lattice of silicene. (b) The buckled lattice of silicene from side view. The sublattice A and B are vertically separated by d. The sublattice A (B) is depicted by red (green) atom.

is $\Delta_{\rm SO} = 10^{-3}$ meV for graphene [50, 53, 16, 15, 77, 78]. The intrinsic SO coupling Hamiltonian in first quantization form is given as follows [77],

$$\begin{aligned} H_{\rm SO} \approx & (-\mathbf{F}_{\parallel} \times \mathbf{p}) \cdot \boldsymbol{\sigma} \\ = & i \frac{\Delta_{\rm SO}}{3\sqrt{3}} v_{ij} \frac{\sigma_z}{2}, \end{aligned} \tag{2.58}$$

where $\mathbf{F}_{\parallel}$ is the force parallel to the surface due to the potential gradient, $\mathbf{p}$ is momentum of an electron, $\boldsymbol{\sigma}$ is the Pauli matrices, which represent the spin of electron. The potential gradient also exist in the perpendicular direction to the surface, which induces another type of SO coupling known as the Rashba coupling [77]. However, we neglect the Rashba coupling, since the coupling constant of Rashba SO is much smaller than the coupling constant of intrinsic SO coupling, roughly 10 times smaller in magnitude [77, 50, 53, 54, 56]. The ij of v_{ij} denotes the next-nearest neighbor site. Here v_{ij} is an integer to select. $v_{ij} = 1$ if the next-nearest neighbor hopping is counterclockwise from i to j sites and $v_{ij} = -1$ if it is clockwise with respect to z axis. Therefore, the Hamiltonian of silicene in second quantization form is given by the following equation,

$$\begin{aligned} H = & -|t| \sum_{\langle ij \rangle \alpha} a^{\dagger}_{i\alpha} b_{j\alpha} - |t| \sum_{\langle ij \rangle \alpha} b^{\dagger}_{i\alpha} a_{j\alpha} + i \frac{\Delta_{\rm SO}}{3\sqrt{3}} \frac{1}{2} \sum_{\langle\langle ij \rangle\rangle \alpha\beta} v_{ij} a^{\dagger}_{i\alpha} \sigma^{z}_{\alpha\beta} a_{j\beta} \\ & - i \frac{\Delta_{\rm SO}}{3\sqrt{3}} \frac{1}{2} \sum_{\langle\langle ij \rangle\rangle \alpha\beta} v_{ij} b^{\dagger}_{i\alpha} \sigma^{z}_{\alpha\beta} b_{j\beta}, \end{aligned} \tag{2.59}$$

where $a^{\dagger}_{i\alpha}$ is a creation operator that creates an electron in the sublattice A at site R_i with spin α. The SO coupling of sublattice B denoted in the fourth term has negative sign, since the direction of the force is opposite to the force for sublattice A. $\langle ij \rangle$ and $\langle\langle ij \rangle\rangle$ denote the summation over the nearest neighbor and next-nearest neighbor, respectively. There are three nearest neighbor atoms and six next-nearest neighbor atoms. To get the dispersion relation, we transform the operators into momentum space. The transformation of the first and second term give the similar form as in graphene, which is given by Eq. (2.49). By using Eq. (2.47), the third and fourth terms of Eq. (2.59) can be written in momentum space, respectively, as follows,

Fig. 2.3: Fig/Figsilicene.eps

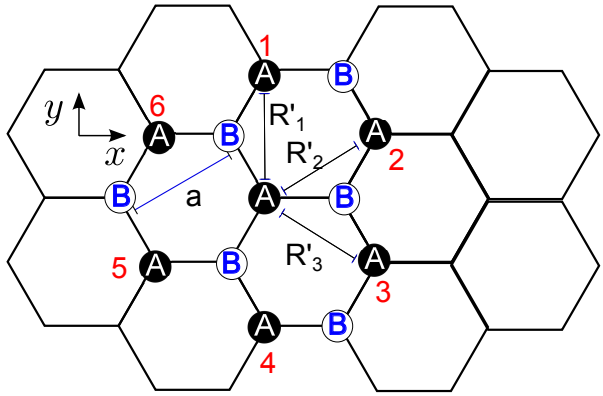

Figure 2.4 The silicene honeycomb lattice. The six next-nearest neighbor atoms of sublattice A at site i ($i = 1, \cdots, 6$) are shown with number. The R'_j is the vector connecting the sublattice A at site i with its six next-nearest neighbors.

$$
\begin{aligned}
i\frac{\Delta_{\mathrm{SO}}}{3\sqrt{3}}\frac{1}{2}\sum_{\langle\langle ij\rangle\rangle\alpha\beta} v_{ij}a^{\dagger}_{i\alpha}\sigma^{z}_{\alpha\beta}a_{j\beta} =& i\frac{\Delta_{\mathrm{SO}}}{3\sqrt{3}}\frac{1}{2}\sum_{i\alpha\beta}\sum_{j=1}^{6} v_{ij}a^{\dagger}_{i\alpha}\sigma^{z}_{\alpha\beta}a_{j\beta} \\
=& i\frac{\Delta_{\mathrm{SO}}}{3\sqrt{3}}\frac{1}{2}\sum_{k}\sum_{\alpha\beta}\sum_{j=1}^{6} a^{\dagger}_{k\alpha}\sigma^{z}_{\alpha\beta}a_{k\beta}v_j e^{i\mathbf{k}\cdot\mathbf{R}'_j} \\
=& i\frac{\Delta_{\mathrm{SO}}}{3\sqrt{3}}\frac{1}{2}\sum_{k}\sum_{\alpha\beta} a^{\dagger}_{k\alpha}\sigma^{z}_{\alpha\beta}a_{k\beta}\nu(\mathbf{k}) \\
=& i\frac{\Delta_{\mathrm{SO}}}{3\sqrt{3}}\frac{1}{2}\sum_{k}\left(a^{\dagger}_{k\uparrow}a_{k\uparrow} - a^{\dagger}_{k\downarrow}a_{k\downarrow}\right)\nu(\mathbf{k}),
\end{aligned}
\tag{2.60}
$$

and

$$
\begin{aligned}
i\frac{\Delta_{\mathrm{SO}}}{3\sqrt{3}}\frac{1}{2}\sum_{\langle\langle ij\rangle\rangle\alpha\beta} v_{ij}b^{\dagger}_{i\alpha}\sigma^{z}_{\alpha\beta}b_{j\beta} =& i\frac{\Delta_{\mathrm{SO}}}{3\sqrt{3}}\frac{1}{2}\sum_{i\alpha\beta}\sum_{j=1}^{6} v_{ij}b^{\dagger}_{i\alpha}\sigma^{z}_{\alpha\beta}b_{j\beta} \\
=& i\frac{\Delta_{\mathrm{SO}}}{3\sqrt{3}}\frac{1}{2}\sum_{k}\sum_{\alpha\beta}\sum_{j=1}^{6} b^{\dagger}_{k\alpha}\sigma^{z}_{\alpha\beta}b_{k\beta}v_j e^{i\mathbf{k}\cdot\mathbf{R}'_j} \\
=& i\frac{\Delta_{\mathrm{SO}}}{3\sqrt{3}}\frac{1}{2}\sum_{k}\sum_{\alpha\beta} b^{\dagger}_{k\alpha}\sigma^{z}_{\alpha\beta}b_{k\beta}\nu(\mathbf{k}) \\
=& i\frac{\Delta_{\mathrm{SO}}}{3\sqrt{3}}\frac{1}{2}\sum_{k}\left(b^{\dagger}_{k\uparrow}b_{k\uparrow} - b^{\dagger}_{k\downarrow}b_{k\downarrow}\right)\nu(\mathbf{k}),
\end{aligned}
\tag{2.61}
$$

Fig. 2.4: Fig/figsil2.eps

where $\nu(\mathbf{k})$ is given by,

$$\begin{aligned}\nu(\mathbf{k}) =& \sum_{j=1}^{6} v_j e^{i\mathbf{k}\cdot\mathbf{R}'_j} \\ =& - e^{i\mathbf{k}\cdot\mathbf{v}_1} - e^{i\mathbf{k}\cdot\mathbf{v}_2} - e^{i\mathbf{k}\cdot\mathbf{v}_3} + e^{-i\mathbf{k}\cdot\mathbf{v}_1} + e^{-i\mathbf{k}\cdot\mathbf{v}_2} + e^{-i\mathbf{k}\cdot\mathbf{v}_3} \\ =& - 2i\Big(\sin(\mathbf{k}\cdot\mathbf{v}_1) + \sin(\mathbf{k}\cdot\mathbf{v}_2) + \sin(\mathbf{k}\cdot\mathbf{v}_3)\Big), \end{aligned} \tag{2.62}$$

and $\mathbf{R}'_j$ $(j = 1, \cdots, 6)$ is the vector of the j-th next-nearest neighbor atoms as shown in Fig. 2.4. It is noted that,

$$\mathbf{R}'_1 = - \mathbf{R}'_4 = \mathbf{v}_1 = (0, a) \tag{2.63}$$

$$\mathbf{R}'_2 = - \mathbf{R}'_4 = \mathbf{v}_2 = \left(\frac{\sqrt{3}a}{2}, \frac{a}{2}\right) \tag{2.64}$$

$$\mathbf{R}'_3 = - \mathbf{R}'_4 = \mathbf{v}_3 = \left(\frac{\sqrt{3}a}{2}, -\frac{a}{2}\right). \tag{2.65}$$

By substituting Eqs. (2.60) and (2.61) to Eq. (2.59), we can obtain the Hamiltonian of silicene in momentum space. Since the creation and annihilation operators for spin up and spin down are decoupled each other, the Hamiltonian can be divided into the Hamiltonian for each spin as follows,

$$\begin{aligned} H_\uparrow =& \sum_k \left(- |t| f(\mathbf{k}) a^\dagger_{k\uparrow} b_{k\uparrow} - |t| f^*(\mathbf{k}) b^\dagger_{k\uparrow} a_{k\uparrow} + i\frac{\Delta_{\rm SO}}{3\sqrt{3}} \frac{\nu(\mathbf{k})}{2} \left(a^\dagger_{k\uparrow} a_{k\uparrow} - b^\dagger_{k\uparrow} b_{k\uparrow} \right) \right) \\ =& \sum_k \begin{pmatrix} a^\dagger_{k\uparrow} & b^\dagger_{k\uparrow} \end{pmatrix} \begin{pmatrix} i\frac{\Delta_{\rm SO}}{3\sqrt{3}} \frac{\nu(\mathbf{k})}{2} & -|t| f(\mathbf{k}) \\ -|t| f^*(\mathbf{k}) & -i\frac{\Delta_{\rm SO}}{3\sqrt{3}} \frac{w(\mathbf{k})}{2} \end{pmatrix} \begin{pmatrix} a_{k\uparrow} \\ b_{k\uparrow} \end{pmatrix} \end{aligned} \tag{2.66}$$

and

$$\begin{aligned} H_\downarrow =& \sum_k \left(- |t| f(\mathbf{k}) a^\dagger_{k\downarrow} b_{k\downarrow} - |t| f^*(\mathbf{k}) b^\dagger_{k\downarrow} a_{k\downarrow} - i\frac{\Delta_{\rm SO}}{3\sqrt{3}} \frac{\nu(\mathbf{k})}{2} \left(a^\dagger_{k\downarrow} a_{k\downarrow} - b^\dagger_{k\downarrow} b_{k\downarrow} \right) \right) \\ =& \sum_k \begin{pmatrix} a^\dagger_{k\downarrow} & b^\dagger_{k\downarrow} \end{pmatrix} \begin{pmatrix} -i\frac{\Delta_{\rm SO}}{3\sqrt{3}} \frac{\nu(\mathbf{k})}{2} & -|t| f(\mathbf{k}) \\ -|t| f^*(\mathbf{k}) & i\frac{\Delta_{\rm SO}}{3\sqrt{3}} \frac{w(\mathbf{k})}{2} \end{pmatrix} \begin{pmatrix} a_{k\downarrow} \\ b_{k\downarrow} \end{pmatrix} . \end{aligned} \tag{2.67}$$

The 2×2 matrix in the Eqs.(2.66) and (2.67) are the Hamiltonian matrix for each spin in the first quantization form, from which the energy dispersion can be obtained. As we mentioned in case of graphene, we can focus only near the K and K' points, whose coordinates are given by $\frac{4\pi}{3a}(0, -1)$ and $\frac{4\pi}{3a}(0, 1)$, respectively. We can approximate the diagonal terms to the first order as follows [77],

$$i\frac{\Delta_{\rm SO}}{3\sqrt{3}} \frac{\nu(\mathbf{K} + \mathbf{k})}{2} \approx -\frac{\Delta_{\rm SO}}{2} \tag{2.68}$$

$$i\frac{\Delta_{\rm SO}}{3\sqrt{3}} \frac{\nu(\mathbf{K}' + \mathbf{k})}{2} \approx \frac{\Delta_{\rm SO}}{2} \tag{2.69}$$

Therefore, we get the effective Hamiltonian near the K or K' points in the first quantization form given by the following matrix,

$$H_{\varsigma\eta} = \begin{pmatrix} -\varsigma\eta\frac{\Delta_{\rm SO}}{2} & \hbar v_{\rm F}(k_x - i\eta k_y) \\ \hbar v_{\rm F}(k_x + i\eta k_y) & \varsigma\eta\frac{\Delta_{\rm SO}}{2} \end{pmatrix} , \tag{2.70}$$

where $\varsigma = +1$ and -1 for spin up and spin down, respectively, and $\eta = +1$ and -1 for K and K' points. The $v_{\rm F} \approx 10^5$ m/s for silicene.

Due to the buckled structure, there is a potential difference between the two sublattices when an electric field is applied perpendicular to the silicene surface. The potential difference between the A and B atom will add an additional term to Eqs. (2.59) and (2.70). The additional term is expressed by $\frac{1}{2}\Delta_z\sigma_z$, where $\Delta_z = eE_z d$. Therefore, the effective Hamiltonian near K or K' points with the applied electric field is expressed by [50, 54, 16, 15, 79],

$$H_{\varsigma\eta} = \begin{pmatrix} -\frac{1}{2}\varsigma\eta\Delta_{\rm SO} + \frac{1}{2}\Delta_z & \hbar v_{\rm F}(k_x - i\eta k_y) \\ \hbar v_{\rm F}(k_x + i\eta k_y) & \varsigma\eta\frac{\Delta_{\rm SO}}{2} - \frac{1}{2}\Delta_z \end{pmatrix} , \tag{2.71}$$

from which we can obtain the energy dispersion of electron in silicene. The energy dispersion of electron is given by $\epsilon_{s\varsigma\eta}(k) = (-1)^{s+1}\epsilon_{\varsigma\eta}(k)$, with s is either 1 or 2 for the conduction or valence band, respectively. $\epsilon_{\varsigma\eta}(k)$ is the energy dispersion for electron with ς spin ($\varsigma = 1$ for up spin and$\varsigma = -1$ for down spin) and at η valley ($\eta = 1$ for K valley and $\eta = -1$ forK' valley), which is given by

$$\epsilon_{\varsigma\eta}(k) = \sqrt{(\hbar v_{\rm F}k)^2 + \frac{1}{4}\Delta^2_{\varsigma\eta}} , \tag{2.72}$$

where $k = \sqrt{k_x^2 + k_y^2}$ and $\Delta_{\varsigma\eta}(\Delta_z) = |\Delta_z - \varsigma\eta\Delta_{\rm SO}|$ denotes the energy gap which is tunable by applying the E_z up to 2.6 V Å^{-1} where the structure of silicene becomes unstable [16]. The energy gap is defined as the energy separation from the top of the valence band to the bottom of the conduction band with the same spin sign. There are only two distinct values of $\Delta_{\varsigma\eta}(\Delta_z)$ for four possible combination of $\Delta_{\varsigma\eta}$, since $\Delta_{++}(\Delta_z) = \Delta_{--}(\Delta_z)$ and $\Delta_{+-}(\Delta_z) = \Delta_{-+}(\Delta_z)$.

In Fig. 2.5, we plot the electron energy dispersions around the K and K' valleys given by Eq. (2.72) for several Δ_z's. We assume that the silicene is doped, with the Fermi energy $E_{\rm F} = 2\Delta_{\rm SO}$ shown as horizontal dotted lines. When we change Δ_z, we can choose three cases for both the K and K' valleys depending on the position of $E_{\rm F}$ relative to the energy gap, which are shown in Fig. 3.2. The first case is $\Delta_z = 2\Delta_{\rm SO}$, in which $E_{\rm F}$ is higher than bottoms of the two conduction bands for spin up and spin down ($E_{\rm F} > \Delta_{++/--}$ and $\Delta_{-+/+-}$) [Figs. 3.2(a) and 2(d)]. The second case is $\Delta_z = 4\Delta_{\rm SO}$, in which $E_{\rm F}$ lies between two bottoms of the conduction bands ($\Delta_{++/--} < E_{\rm F} < \Delta_{-+/+-}$) [Figs. 3.2(b) and 2(e)] and the third case is $\Delta_z = 8\Delta_{\rm SO}$, in which $E_{\rm F}$ exists in energy gaps [Figs. 2.5(c) and (f)]. These three cases will be discussed in Chapter 3 for calculating optical conductivity in silicene.

We can see in Fig. (2.5) that the dispersion relation for each spin is opposite each other for the K and K' valleys. For $\Delta_z > \Delta_{\rm SO}$ as in all case of Fig. (2.5), the band gap increases with increasing Δ_z. The reverse situation occurs if the $\Delta_z < \Delta_{\rm SO}$, where the band gap decreases with increasing Δ_z and reach zero band gap when the $\Delta_z = \Delta_{\rm SO}$ [80, 15, 54]. At this situation, $\Delta_{++/--} = 0$ and one of energy band

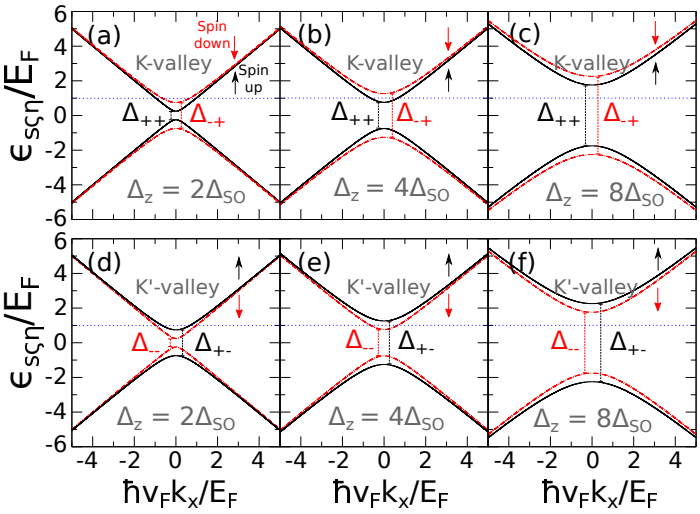

Figure 2.5 Electronic energy dispersions of silicene for [(a)-(c)] K and [(d)-(f)] K' valleys for several Δ_z's ($2\Delta_{SO}$,$4\Delta_{SO}$, and $8\Delta_{SO}$). The solid (dash-dotted) lines correspond to spin up (down) electron dispersion. Positions of $E_F = 2\Delta_{SO}$ are indicated by the horizontal dotted lines.

is gapless. When no external field is applied, the energy bands for both spin are degenerate with spin orbit band gap.

2.3 The optical spectra of graphene

In this section, we will discuss the method on how to obtain the optical spectra of graphene, which is related to the second purpose of this thesis. The optical spectra include the reflection, transmission and absorption of EM wave incident to graphene. For the first case, we assume that graphene is put between two dielectric media and the optical spectra can be obtained by solving the Maxwell equations with boundary conditions. In the second case, we put graphene inside multilayer of dielectric media and the optical spectra can be obtained by using transfer matrix method. These formulations are not restricted to graphene only, but apply to any other 2D material such as silicene.

2.3.1 Graphene between two dielectric media

Let us discuss the formulation of absorption, reflection and transmission probabilities of EM wave penetrating to graphene. A simple way to obtain the probabilities is to solve the amplitude of electric and magnetic fields by solving the Maxwell equations for EM wave with boundary conditions. We consider that graphene is placed between two dielectric media as shown in Fig. 2.6.

Fig. 2.5: Fig/Figsildis.eps

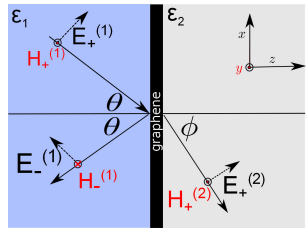

Figure 2.6 Graphene is placed between two dielectric media with dielectric constants ε_1 and ε_2. Thickness of graphene thickness is neglected in the discusion though electric current flows on graphene. The incident EM wave comes at an angle θ in medium 1 (left) and is transmitted at an angle ϕ in medium 2 (right). The EM wave is p-polarized.

Graphene is modeled as a conducting interface with the conductivity σ between two dielectric media with dielectric constants ε_1 and ε_2. When we do not consider the thickness of graphene, the absorption, reflectance and transmittance probabilities for this geometry can be calculated by utilizing the boundary conditions from the Maxwell equations. If we adopt the TM polarization of EM wave as shown in Fig. 2.6, we can obtain two boundary conditions for the electric field $E^{(i)}$ and magnetic field $H^{(i)}$ $(i = 1, 2)$ as follows:

$$E_+^{(1)} \cos\theta + E_-^{(1)} \cos\theta = E_+^{(2)} \cos\phi, \tag{2.73}$$

$$H_+^{(2)} - (H_+^{(1)} - H_-^{(1)}) = -\sigma E_+^{(2)} \cos\phi, \tag{2.74}$$

where $+(-)$ index denotes the right- (left-) going waves according to Fig. 2.6, θ is the incident and reflection angle, ϕ is the refraction angle, and σ is the conductivity of graphene. Eq. (2.73) and (2.74) come from Faraday law and Ampere law, respectively. The E and H fields are also related each other in terms of the EM wave impedance in units of Ohm for each medium:

$$Z_i = \frac{E_i}{H_i} = \frac{377}{\sqrt{\varepsilon_i}} \text{ Ohm}, \quad (i = 1, 2), \tag{2.75}$$

where the constant 377 Ohm is the impedance of vacuum $Z_0 = \sqrt{\mu_0/\varepsilon_0}$, μ_0 and ε_0 are vacuum magnetic susceptibility and permitvity, respectively. Quantities ϕ, θ, and Z_i are related by Snell's law $Z_2 \sin\theta = Z_1 \sin\phi$. Solving Eqs. (2.77)-(2.75), we obtain the reflection R, transmission T, and absorption probabilities A of the EM wave as

Fig. 2.6: Fig/schematic.eps

follows:

$$
\begin{aligned}
R &= \left| \frac{E_1^{(-)}}{E_1^{(+)}} \right|^2 \\
&= \left| \frac{Z_2 \cos\phi - Z_1 \cos\theta - Z_1 Z_2 \sigma \cos\theta \cos\phi}{Z_2 \cos\phi + Z_1 \cos\theta + Z_1 Z_2 \sigma \cos\theta \cos\phi} \right|^2, \\
T &= \frac{\cos\phi}{\cos\theta} \frac{Z_1}{Z_2} \left| \frac{E_2^{(+)}}{E_1^{(+)}} \right|^2 \\
&= \frac{4 Z_1 Z_2 \cos\theta \cos\phi}{\left| Z_2 \cos\phi + Z_1 \cos\theta + Z_1 Z_2 \sigma \cos\theta \cos\phi \right|^2}, \\
A &= 1 - \mathrm{Re}\ R - \mathrm{Re}\ T \\
&= \frac{4 Z_1 Z_2^2 \cos\theta \left|\cos\phi\right|^2 \mathrm{Re}(\sigma)}{\left| Z_2 \cos\phi + Z_1 \cos\theta + Z_1 Z_2 \sigma \cos\theta \cos\phi \right|^2},
\end{aligned}
\tag{2.76}
$$

where the values of R, T, and A are understood to be real quantities and can be denoted in terms of percentage ($0-100\%$). Note that the factor Z_1/Z_2 in T of Eq. (2.76) comes from the different velocities of the EM wave in medium 1 and medium 2. The T should be calculated by the ratio of the Poynting vectors at medium 1 and 2. By calculating the optical conductivity using the Kubo formula of Eq. (2.32), we can obtain the optical spectra of graphene.

2.3.2 Transfer matrix method

In this section, we assume that graphene is put inside the multilayer dielectric media. The optical spectra of graphene can be obtained by using transfer matrix method [81, 82]. To explain the transfer matrix method in a simple way, we assume the structure is given in Fig. 2.7. The graphene system contains two mono-layers of graphene, each placed between two dielectric media, which can be seen as medium 1, 2 and 3 with dielectric constants ε_1, ε_2 and ε_3, respectively, thus creating two conducting interfaces of graphene. The incident EM wave with TM polarization comes from medium 1 and its propagation through medium 2 and 3 is shown in Fig. 2.7, where the EM wave comes from medium 1 with angle θ_1 and propagates through medium 2 with angle θ_2 and medium 3 with angle θ_3. $+(-)$ index denotes the right (left) going waves. The direction of the magnetic fields are shown as the following : red dot (cross) for positive y-direction (negative y-direction). Between two dielectric media, the EM fields can be related each other through the boundary conditions obtained from the Maxwell equations. Since we adopt the TM polarization of the incident EM wave, as shown in Fig. 2.7 for the first interface, we can define the single layer interface's boundary conditions of the electric field $E^{(i)}$ and magnetic field $H^{(i)}$ $(i = 1, 2)$ as follows:

$$E_x^{(1)} = E_x^{(2)}, \tag{2.77}$$

$$H_y^{(2)} - H_y^{(1)} = -\sigma E_x^{(2)}, \tag{2.78}$$

where σ is the conductivity of graphene. Here we can assume, too that the thickness of graphene is sufficiently small compared to the wavelength of the incident light but

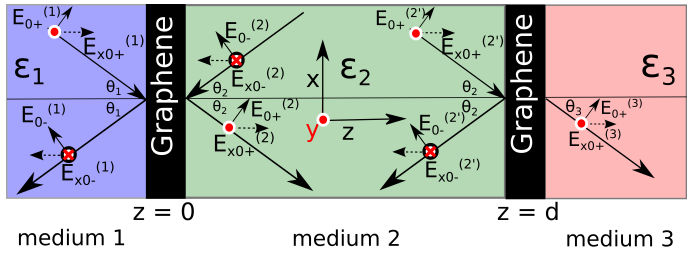

Figure 2.7 The propagation of the wave through the three media and two graphene layers can be expressed by transfer matrices (see the text). Red dot (cross) denote magnetic field in positive (negative) y-direction.

that only finite current density appears in graphene. The electric and magnetic field in medium 1 can be described by the following:

$$\begin{aligned} E_x^{(1)}(z) &= E_{x+}^{(1)}(z) + E_{x-}^{(1)}(z) \\ &= E_{x0+}^{(1)} e^{ik_1 z} + E_{x0-}^{(1)} e^{-ik_1 z}, \end{aligned} \tag{2.79}$$

$$H_y^{(1)}(z) = \frac{\omega\varepsilon_0\varepsilon_1}{k_1}(E_{x0+}^{(1)} e^{ik_1 z} - E_{x0-}^{(1)} e^{-ik_1 z}), \tag{2.80}$$

and for medium 2:

$$\begin{aligned} E_x^{(2)}(z) &= E_{x+}^{(2)}(z) + E_{x-}^{(2)}(z) \\ &= E_{x0+}^{(2)} e^{ik_2 z} + E_{x0-}^{(2)} e^{-ik_2 z}, \end{aligned} \tag{2.81}$$

$$H_y^{(2)}(z) = \frac{\omega\varepsilon_0\varepsilon_1}{k_2}(E_{x0+}^{(2)} e^{ik_2 z} - E_{x0-}^{(2)} e^{-ik_2 z}), \tag{2.82}$$

where $E_x^{(i)}$ is the amplitude of the electric field in the x-axis inside medium i and $+(-)$ index denotes the right- (left-) going waves, ε_i is the dielectric constant of medium i, ω is the angular frequency of the EM wave and k_i is the wave vector on z-direction which is defined as:

$$k_i = \frac{2\pi}{\lambda}\sqrt{\varepsilon_i}\cos\theta_i, \tag{2.83}$$

where λ is the wave length of the EM wave. $E_{x0+}^{(i)}$ and $E_{x0-}^{(i)}$ describe the amplitude of electric field of the EM wave going to right and left direction, respectively. Here we consider $E_{x0-}^{(2)}$ (left going wave in medium 2) since we expect some reflection of the EM wave at the second interface with medium 3. The relationship between H_y and E_x comes from the following equation, $H_y^{(i)} = i\omega\varepsilon_0\varepsilon_i \int E_x^{(i)} dz$. θ_i $(i = 1, 2)$ is the corresponding angle of propagation of the EM wave inside each dielectric medium measured from the z-axis as shown in Fig. 2.7. Quantities θ_i and ε_i between two dielectric media are related by the Snell law $\sqrt{\varepsilon_1}\sin\theta_1 = \sqrt{\varepsilon_2}\sin\theta_2$.

With the well-defined boundary conditions, we can now construct transfer matrices. The transfer matrix method is a method in which we can relate the EM fields between

Fig. 2.7: Fig/schemati2.eps

two different positions within more than two media or layers (multi-layered system). We will use this method because we have three dielectric media (and two graphene layers) in one dimension. Using Eqs. (2.77) through (2.82), we can solve for E_{x0+} and E_{x0-} at the boundary explicitly, and construct the following matrix:

$$\begin{bmatrix} E^{(1)}_{x0+} \\ E^{(1)}_{x0-} \end{bmatrix} = \frac{1}{2} \begin{bmatrix} 1+\beta_1+\alpha_1 & 1-\beta_1+\alpha_1 \\ 1-\beta_1-\alpha_1 & 1+\beta_1-\alpha_1 \end{bmatrix} \begin{bmatrix} E^{(2)}_{x0+} \\ E^{(2)}_{x0-} \end{bmatrix}, \tag{2.84}$$

where α_i and β_i denote

$$\alpha_i = \frac{k_i \sigma}{\omega \varepsilon_0 \varepsilon_i} \ , \quad \beta_i = \frac{k_i}{k_{i+1}} \frac{\varepsilon_{i+1}}{\varepsilon_i} \ . \tag{2.85}$$

The matrix in Eq. (2.84) describes the EM waves in the medium 1 as function of the EM waves in the medium 2 at the first boundary. Next we can construct a second matrix describing the propagation of the wave through the medium 2. The propagation is shown in Fig. 2.7.

$$\begin{bmatrix} E^{(2)}_{x0+} \\ E^{(2)}_{x0-} \end{bmatrix} = \begin{bmatrix} e^{-ik_2 d} & 0 \\ 0 & e^{ik_2 d} \end{bmatrix} \begin{bmatrix} E^{(2')}_{x0+} \\ E^{(2')}_{x0-} \end{bmatrix}, \tag{2.86}$$

where d is the length of the medium 2. Substituting Eq. (2.86) into Eq. (2.84), the total matrix equation now becomes:

$$\begin{bmatrix} E^{(1)}_{x0+} \\ E^{(1)}_{x0-} \end{bmatrix} = [M_1][T_1] \begin{bmatrix} E^{(2')}_{x0+} \\ E^{(2')}_{x0-} \end{bmatrix}, \tag{2.87}$$

where

$$M_i = \frac{1}{2} \begin{bmatrix} 1+\beta_i+\alpha_i & 1-\beta_i+\alpha_i \\ 1-\beta_i-\alpha_i & 1+\beta_i-\alpha_i \end{bmatrix}, \tag{2.88}$$

$$T_i = \begin{bmatrix} e^{-ik_{i+1}d} & 0 \\ 0 & e^{ik_{i+1}d} \end{bmatrix}. \tag{2.89}$$

The far right matrix is the incident and reflected wave of the second interface as shown in Fig. 2.7. Continuing the matrices for the second interface, we will have:

$$\begin{bmatrix} E^{(2')}_{x0+} \\ E^{(2')}_{x0-} \end{bmatrix} = [M_2] \begin{bmatrix} E^{(3)}_{x0+} \\ 0 \end{bmatrix}. \tag{2.90}$$

Finally, by substituting this matrix into Eq. (2.87), the total matrix equation can be written as :

$$\begin{bmatrix} E^{(1)}_{x0+} \\ E^{(1)}_{x0-} \end{bmatrix} = [M_1][T_1][M_2] \begin{bmatrix} E^{(3)}_{x0+} \\ 0 \end{bmatrix}. \tag{2.91}$$

If we multiply these matrices, we can find the total reflection (ρ_{total}) and transmission (τ_{total}) coefficients:

$$\begin{bmatrix} E^{(1)}_{x0+} \\ E^{(1)}_{x0-} \end{bmatrix} = \begin{bmatrix} a & b \\ c & d \end{bmatrix} \begin{bmatrix} E^{(3)}_{x0+} \\ 0 \end{bmatrix}, \tag{2.92}$$

$$\rho_{\text{total}} = \frac{E^{(1)}_{x0-}}{E^{(1)}_{x0+}} = \frac{c}{a}, \text{ and } \tau_{\text{total}} = \frac{E^{(3)}_{x0+}}{E^{(1)}_{x0+}} = \frac{1}{a}, \tag{2.93}$$

where a, b, c and d are the components of total matrix (Eq. (2.91)). We finally get,

$$\begin{aligned} R &= |\rho_{\text{total}}|^2, \\ T &= \frac{\sqrt{\varepsilon_3}\cos\theta_1}{\sqrt{\varepsilon_1}\cos\theta_3}\ |\tau_{\text{total}}|^2, \\ A &= 1 - \text{Re}\ R - \text{Re}\ T, \end{aligned} \tag{2.94}$$

where R, T and A are reflection, transmission and absorption probabilities of EM wave, respectively. The formulation of transfer matrix can be extended for arbitrary number of layers by simply multiplying the matching and propagation matrices correspondingly. Suppose that we have have N layers of dielectric media and the incident EM wave comes from medium 1 and is transmitted to medium N, we have,

$$\begin{bmatrix} E^{(1)}_{x0+} \\ E^{(1)}_{x0-} \end{bmatrix} = [M_1][T_1][M_2][T_2]\cdots[T_{N-2}][M_{N-1}] \begin{bmatrix} E^{(N)}_{x0+} \\ 0 \end{bmatrix}, \tag{2.95}$$

where the propagation matrices depend on the thickness of each layer. The R, T and A can be obtained in the same manner as in Eq. (2.94). If the interface does not have graphene, then we can set $\alpha_i = 0$ in the matching matrix (Eq. (2.88)) of corresponding interface.

2.4 The dispersion of surface plasmon in graphene

In this section, we will describe dispersion of surface plasmon in graphene, from which we can define two kinds of surface plasmon, the non-retarded and retarded surface plasmon. The dispersion has been discussed briefly in section 1.3.3.1. The dispersion of surface plasmon in graphene can be obtained by considering the boundary conditions of electromagnetic wave with TM polarization on the graphene surface and we obtain the following equation [57], which is also given in Eq. (1.28),

$$\frac{\varepsilon_1}{\kappa_1} + \frac{\varepsilon_2}{\kappa_2} + \frac{i\sigma_D(\omega)}{\omega\varepsilon_0} = 0, \tag{2.96}$$

where κ_i is the decay constant of surface plasmon in $i-$th medium given in Eq. (1.3), and $\sigma_D(\omega)$ is the intraband optical conductivity of graphene [57] [see also Eq. (1.26)],

$$\sigma_D(\omega) = i\frac{E_{\text{F}}e^2}{\pi\hbar^2\omega}, \tag{2.97}$$

where E_{F} is the Fermi energy of graphene. The solution of Eq. (2.96) gives the surface plasmon dispersion. Since the velocity of light can be considered to be much larger than the surface plasmon group velocity v_{sp}, we can approximate the $q^2 >> \omega^2\varepsilon/c^2$ and we get $\kappa_1 = \kappa_2 = q$ in Eq. (1.3). This case is called the *non-retarded* regime [57, 63]. By putting the Eq. (2.97) to Eq. (2.96), we can obtain the surface plasmon frequency ω as a function of q in the non-retarded case as follows

$$\omega = \frac{1}{\hbar}\sqrt{\frac{E_{\text{F}}e^2q}{\pi\varepsilon_0(\varepsilon_1+\varepsilon_2)}}, \tag{2.98}$$

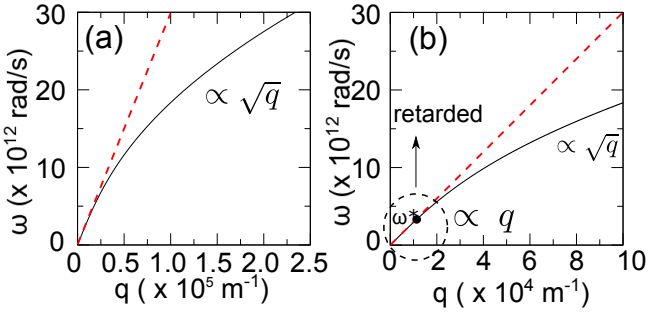

Figure 2.8 (Color online) (a) The surface plasmon dispersion of graphene for $E_F = 0.64$ eV obtained from Eq. (1.28). The dispersion has $\omega \propto \sqrt{q}$ dependence for large q. (non-retarded regime) (b) The surface plasmon dispersion for smaller q showing the retarded region where the dispersion is linear to q. The red dashed line is the dispersion of light incident directly to graphene. Transition frequency (see below) $\omega^* = 3.5 \times 10^{12}$rad s$^-$1 is shown as a black dot.

where we have a $\omega \propto \sqrt{q}$ dependence similar to the case of surface plasmon of 2D electron gas.

From Eq. (2.98), we can say that $v_{sp} \propto 1/\sqrt{q}$, which means that the v_{sp} might exceed the velocity of light for small q. At this region, the non-retarded approximation cannot be used and the v_p is comparable to the velocity of light. This case is called *retarded* regime [63]. For the retarded case, the dispersion of surface plasmon is linear $\omega \propto q$ and very close to the dispersion of light. This dispersion can be obtained by using Eq. (1.3) and solving Eq. (2.96). Supposing that $\varepsilon_1 = \varepsilon_2 = \varepsilon$, we have for retarded regime,

$$\omega \approx \frac{c}{\sqrt{\varepsilon}} q, \tag{2.99}$$

which is independent of properties of graphene.

In Fig. 2.8 we show the dispersion of surface plasmon for $E_F = 0.64$ eV. In Fig. 2.8 (a), we plot the exact solution of Eq. (1.28), where we can clearly see the $\omega \propto \sqrt{q}$ dependence of non-retarded regime and the frequency is in terahertz (THz) range. In Fig. 2.8 (b), we plot the dispersion of surface plasmon for smaller q where we can see the retarded regime with $\omega \propto q$ dependence. The dispersion in retarded regime is close to light dispersion shown as red dashed line. We can also infer that there is a transition point from retarded to non-retarded regime, where the dispersion starts to be $\omega \propto \sqrt{q}$. The transition point (q^*, ω^*) has been discussed by Deng et al. as follows [63],

$$\omega^* = \frac{E_F}{\hbar v_F \sqrt{\pi}} \times 6.5 \times 10^3 \text{ Hz, and } q^* = \frac{\omega^*}{c}, \tag{2.100}$$

where $v_F = 10^6$ m/s is Fermi velocity of graphene. For $E_F = 0.64$ eV, the transition occurs at $\omega^* \approx \omega^* = 3.5 \times 10^{12}$rad s$^-$1, below which we have retarded regime. The concept of retarded and non-retarded in surface plasmon can be useful to determine the method to excite the surface plasmon by light.

Fig. 2.8: Fig/Fig24.eps

2.5 The quantization of free EM wave and surface plasmon

In this section, we will discuss the method on how to quantize the free EM wave and the surface plasmon (or TM surface wave). This discussion is useful for the calculation of matrix element of the interaction between photon and surface plasmon, which will be discussed later. For the quantization of surface plasmon in graphene, we follow the work of Archambault et al., in which they discuss the method to quantize surface plasmon on the surface of bulk metal [83].

2.5.1 Quantization of free EM wave

The quantized free EM wave is called a photon. The quantization can be obtained by quantizing the energy of EM fields, which can be expressed in terms of creation and annihilation operator [76, 75]. We start from the EM wave equation,

$$\nabla^2 \times \mathbf{A}(\mathbf{r},t) - \frac{1}{c^2}\frac{\partial^2}{\partial t^2}\mathbf{A}(\mathbf{r},t) = 0, \tag{2.101}$$

where $\mathbf{A}(\mathbf{r},t)$ is the vector potential. We can solve for $\mathbf{A}(\mathbf{r},t)$ by assuming that the EM wave is enclosed inside a box with volume V with periodic boundary condition. The general solution of Eq. (2.101) is given in form of expansion of plane wave as follows,

$$\mathbf{A}(\mathbf{r},t) = \frac{1}{\sqrt{V}}\sum_{\mathbf{k}} \widehat{\boldsymbol{\epsilon}}\Big(A_k e^{i(\mathbf{k}\cdot\mathbf{r}-\omega_k t)} + A_k^* e^{-i(\mathbf{k}\cdot\mathbf{r}-\omega_k t)} \Big), \tag{2.102}$$

where $\widehat{\boldsymbol{\epsilon}}$ is the polarization vector of the $\mathbf{A}(\mathbf{r},t)$, $\mathbf{k}$ is the wave vector, and A_k is the complex expansion coefficient. The EM fields for a given $\mathbf{A}(\mathbf{r},t)$ can be written in terms of vector potential as follows,

$$\begin{aligned}\mathbf{E}(\mathbf{r},t) =& -\frac{\partial}{\partial t}\mathbf{A}(\mathbf{r},t) \\ =& \frac{i}{\sqrt{V}}\sum_{\mathbf{k}} \widehat{\boldsymbol{\epsilon}}\omega_k \Big(A_k(t) e^{i\mathbf{k}\cdot\mathbf{r}} - A_k^*(t) e^{-i\mathbf{k}\cdot\mathbf{r}} \Big),\end{aligned} \tag{2.103}$$

and

$$\begin{aligned}\mathbf{B}(\mathbf{r},t) =& \nabla \times \mathbf{A}(\mathbf{r},t) \\ =& \frac{i\mathbf{u}_{\mathbf{k}}}{\sqrt{V}}\sum_{\mathbf{k}} \Big(A_k(t) e^{i\mathbf{k}\cdot\mathbf{r}} - A_k^*(t) e^{-i\mathbf{k}\cdot\mathbf{r}} \Big),\end{aligned} \tag{2.104}$$

where $\mathbf{u}_{\mathbf{k}} = \mathbf{k}\times\widehat{\boldsymbol{\epsilon}}$. We will express the Hamiltonian of EM wave in terms of Eq. (2.102). The Hamiltonian of EM wave in vacuum is given by the total energy of EM fields as follows,

$$H = \frac{1}{2}\int d\mathbf{r}\Big(\varepsilon_0 |\mathbf{E}|^2 + \frac{1}{\mu_0}|\mathbf{B}|^2 \Big). \tag{2.105}$$

By inserting Eq. (2.103) to each term of Eq. (2.105), we obtain,

$$\begin{aligned}
\frac{1}{2}\int d\mathbf{r}\varepsilon_0|\mathbf{E}|^2 =& \frac{\varepsilon_0}{2V}\int d\mathbf{r}\sum_{\mathbf{k},\mathbf{k}'}\omega_k\omega_{k'}\Big(A_k(t)e^{i\mathbf{k}\cdot\mathbf{r}} - A_k^*(t)e^{-i\mathbf{k}\cdot\mathbf{r}}\Big)\Big(A_{k'}^*(t)e^{-i\mathbf{k}'\cdot\mathbf{r}} \\
& - A_{k'}(t)e^{i\mathbf{k}'\cdot\mathbf{r}}\Big) \\
=& \frac{\varepsilon_0}{2V}\int d\mathbf{r}\sum_{\mathbf{k},\mathbf{k}'}\omega_k\omega_{k'}\Big(A_k(t)A_{k'}^*(t)e^{i(\mathbf{k}-\mathbf{k}')\cdot\mathbf{r}} - A_k(t)A_{k'}(t)e^{i(\mathbf{k}+\mathbf{k}')\cdot\mathbf{r}} \\
& - A_k^*(t)A_{k'}^*(t)e^{-i(\mathbf{k}+\mathbf{k}')\cdot\mathbf{r}} + A_k^*(t)A_{k'}(t)e^{-i(\mathbf{k}-\mathbf{k}')\cdot\mathbf{r}}\Big) \\
=& \frac{\varepsilon_0}{2}\sum_{\mathbf{k},\mathbf{k}'}\omega_k\omega_{k'}\Big(A_k(t)A_{k'}^*(t)\delta_{\mathbf{k},\mathbf{k}'} - A_k(t)A_{k'}(t)\delta_{\mathbf{k},-\mathbf{k}'} - A_k^*(t)A_{k'}^*(t)\delta_{\mathbf{k},-\mathbf{k}'} \\
& + A_k^*(t)A_{k'}(t)\delta_{\mathbf{k},\mathbf{k}'}\Big) \\
=& \frac{\varepsilon_0}{2}\sum_{\mathbf{k}}\omega_k^2\Big(A_k(t)A_k^*(t) - A_k(t)A_{-k}(t) - A_k^*(t)A_{-k}^*(t) + A_k^*(t)A_k(t)\Big) \\
=& \frac{\varepsilon_0}{2}\sum_{\mathbf{k}}\omega_k^2\Big(2|A_k(t)|^2 - A_k(t)A_{-k}(t) - A_k^*(t)A_{-k}^*(t)\Big), \qquad (2.106)
\end{aligned}$$

and

$$\begin{aligned}
\frac{1}{2\mu_0}\int d\mathbf{r}|\mathbf{B}|^2 =& \frac{1}{2\mu_0 V}\int d\mathbf{r}\sum_{\mathbf{k},\mathbf{k}'}\mathbf{u}_{\mathbf{k}}\cdot\mathbf{u}_{\mathbf{k}'}\Big(A_k(t)e^{i\mathbf{k}\cdot\mathbf{r}} - A_k^*(t)e^{-i\mathbf{k}\cdot\mathbf{r}}\Big) \\
& \times\Big(A_{k'}^*(t)e^{-i\mathbf{k}'\cdot\mathbf{r}} - A_{k'}(t)e^{i\mathbf{k}'\cdot\mathbf{r}}\Big) \\
=& \frac{1}{2\mu_0}\sum_{\mathbf{k}}\Big(2k^2|A_k(t)|^2 + k^2A_k(t)A_{-k}(t) + k^2A_k^*(t)A_{-k}^*(t)\Big) \\
=& \frac{\varepsilon_0}{2}\sum_{\mathbf{k}}\omega_k^2\Big(2|A_k(t)|^2 + A_k(t)A_{-k}(t) + A_k^*(t)A_{-k}^*(t)\Big). \qquad (2.107)
\end{aligned}$$

Therefore, the total Hamiltonian of Eq. (2.105) can be written as

$$\begin{aligned}
H =& \frac{1}{2}\int d\mathbf{r}\Big(\varepsilon_0|\mathbf{E}|^2 + \frac{1}{\mu_0}|\mathbf{B}|^2\Big) \\
=& 2\varepsilon_0\sum_{\mathbf{k}}\omega_k^2|A_k|^2 \\
=& \varepsilon_0\sum_{\mathbf{k}}\omega_k^2\Big(A_kA_k^* + A_k^*A_k\Big). \qquad (2.108)
\end{aligned}$$

Equation (2.108) is similar to the Hamiltonian of quantum harmonic oscillator. Therefore we can think that the electromagnetic wave can be considered as a collection of harmonic oscillators. Then, the Hamiltonian can be expressed in terms of creation

and annihilation operator of photon as follows,

$$\begin{aligned} H =& \varepsilon_0 \sum_{\mathbf{k}} \omega_k^2 \bigg(A_k A_k^* + A_k^* A_k \bigg) \\ =& \sum_{\mathbf{k}} \frac{\hbar\omega_k}{2} \bigg(b_k b_k^\dagger + b_k^\dagger b_k \bigg), \end{aligned} \tag{2.109}$$

with the definition of creation $b_k^\dagger$ and annihilation b_k operator of photon to be,

$$b_k = \sqrt{\frac{2\omega_k \varepsilon_0}{\hbar}} A_k \quad \text{and} \quad b_k^\dagger = \sqrt{\frac{2\omega_k \varepsilon_0}{\hbar}} A_k^*. \tag{2.110}$$

A photon follows the Bose-Einstein statistics, therefore we can define the following creation and annihilation operations,

$$b_k^\dagger \left| n_k \right\rangle = \sqrt{n_k + 1} \left| n_k + 1 \right\rangle, \tag{2.111}$$

$$b_k \left| n_k \right\rangle = \sqrt{n_k} \left| n_k - 1 \right\rangle, \tag{2.112}$$

where n_k is number of photon with wave vector $\mathbf{k}$.

Finally, the vector potential $\mathbf{A}(\mathbf{r}, t)$ can be written in terms of creation and annihilation operators by substituting Eq. (2.119) to Eq. (2.102) as follows,

$$\mathbf{A}(\mathbf{r}, t) = \sum_{\mathbf{k}} \sqrt{\frac{\hbar}{2V\omega_k \varepsilon_0}} \widehat{\boldsymbol{\epsilon}} \bigg(b_k e^{i(\mathbf{k}\cdot\mathbf{r} - \omega_k t)} + b_k^\dagger e^{-i(\mathbf{k}\cdot\mathbf{r} - \omega_k t)} \bigg). \tag{2.113}$$

2.5.2 Quantization of surface plasmon of graphene

Suppose that we have graphene between two dielectric media as shown in Fig. 2.9. The quantization of surface plasmon is similar to the quantization of free EM wave. However, since the surface plasmon is the TM surface wave, therefore the EM wave propagates on the surface and the EM fields should be confined to the surface. Therefore, the the vector potential of Eq. (2.102) is modified into

$$\mathbf{A}(\mathbf{r}, t) = \frac{1}{\sqrt{S}} \sum_{\mathbf{q}} \bigg(A_q \boldsymbol{\nu}_q(z) e^{i(\mathbf{q}\cdot\mathbf{r} - \omega_q t)} + A_q^* \boldsymbol{\nu}_q(z)^* e^{-i(\mathbf{q}\cdot\mathbf{r} - \omega_q t)} \bigg), \tag{2.114}$$

where S is the area of quantization on the surface of graphene, $\mathbf{q} = (q_x, q_y)$ is the surface plasmon wave vector, $\boldsymbol{\nu}_q(z)$ is the polarization vector of surface plasmon, which is given by

$$\boldsymbol{\nu}_q(z) = \alpha e^{-s\kappa_j z} \bigg(\hat{\mathbf{q}} - \frac{q}{is\kappa_j} \hat{\mathbf{z}} \bigg) \qquad (j = 1, 2), \tag{2.115}$$

where α is the normalization constant so that the dimension of $\mathbf{A}$(r,t) for photon and surface plasmon are the same, which will be defined later. The polarization vector of Eq. (2.115) has two directions, the parallel $\hat{\mathbf{q}}$ and perpendicular $\hat{\mathbf{z}}$ to the surface, since surface plasmon is the TM surface wave and it decays in the z direction with a decay constant κ_j. $j = 1, 2$ denotes the surrounding media and $s = 1(-1)$ for medium 1(2).

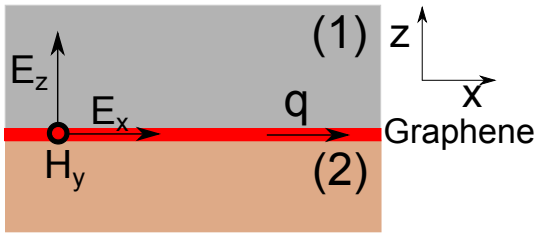

Figure 2.9 Graphene surrounded by two dilectric media 1 and 2. The surface plasmon propagates on the surface of graphene in the direction of x with wave vector q.

The quantization method is similar to that for the photon, in which we express the Hamiltonian of Eq. (2.105) in terms of vector potential of Eq. (2.114). However, for the integration with respect to z should be done separately. Hence, the result of integration in Eq. (2.108) is only for the integration with respect to x and y, since the $\mathbf{q} = (q_x, q_y)$ is two dimensional wave vector for surface plasmon. Therefore, we have the following equation,

$$H = \int dz \sum_{\mathbf{q}} \left(\varepsilon_0 \varepsilon_j \omega_k^2 |\boldsymbol{\nu}_q(z)|^2 + \frac{1}{\mu_0} |\boldsymbol{\eta}_q(z)|^2 \right) |A_q|^2, \tag{2.116}$$

where $\boldsymbol{\eta}_q(z) = \mathbf{q} \times \boldsymbol{\nu}_q(z)$. The integration with respect to z gives,

$$\begin{aligned} H =& \sum_{\mathbf{q}} \omega_q^2 \varepsilon_0 |A_q|^2 \times \alpha^2 \frac{1}{2} \left[\frac{1}{\kappa_1} \left(\varepsilon_1 \left(1 + \frac{q^2}{\kappa_1^2} \right) + \frac{\omega_q^2}{c^2} \frac{\varepsilon_1^2}{\kappa_1^2} \right) \right. \\ & \left. + \frac{1}{\kappa_2} \left(\varepsilon_2 \left(1 + \frac{q^2}{\kappa_2^2} \right) + \frac{\omega_q^2}{c^2} \frac{\varepsilon_2^2}{\kappa_2^2} \right) \right] \\ =& 2\varepsilon_0 \sum_{\mathbf{q}} \omega_q^2 |A_q|^2, \end{aligned} \tag{2.117}$$

where we set α to be,

$$\alpha = \left\{ \frac{1}{4} \left[\frac{1}{\kappa_1} \left(\varepsilon_1 \left(1 + \frac{q^2}{\kappa_1^2} \right) + \frac{\omega_q^2}{c^2} \frac{\varepsilon_1^2}{\kappa_1^2} \right) + \frac{1}{\kappa_2} \left(\varepsilon_2 \left(1 + \frac{q^2}{\kappa_2^2} \right) + \frac{\omega_q^2}{c^2} \frac{\varepsilon_2^2}{\kappa_2^2} \right) \right] \right\}^{-1/2}. \tag{2.118}$$

The relation between ε_1/κ_1 and ε_2/κ_2 can be obtained from the dispersion relation of surface plasmon of graphene, given in Eq. (2.96). Equation (2.117) has the same form of Eq. (2.108), which is the form of quantum harmonic oscillator. Hence, we can define the similar creation and annihilation creation for surface plasmon,

$$a_q = \sqrt{\frac{2\omega_q \varepsilon_0}{\hbar}} A_q \quad \text{and} \quad a_q^\dagger = \sqrt{\frac{2\omega_q \varepsilon_0}{\hbar}} A_q^*. \tag{2.119}$$

A surface plasmon follows the Bose-Einstein statistics, therefore we can define the following creation and annihilation operations,

$$a_q^\dagger |n_q\rangle = \sqrt{n_q + 1} \, |n_q + 1\rangle, \tag{2.120}$$

$$a_q |n_q\rangle = \sqrt{n_q} \, |n_q - 1\rangle, \tag{2.121}$$

Fig. 2.9: Fig/figspgr.eps

where n_q is number of photon with wave vector $\mathbf{q}$.

Finally, the vector potential $\mathbf{A}(\mathbf{r},t)$ of surface plasmon can be written in terms of creation and annihilation operators as follows,

$$\mathbf{A}(\mathbf{r},t)=\sum_{\mathbf{q}}\sqrt{\frac{\hbar}{2S\omega_q\varepsilon_0}}\left(a_q\boldsymbol{\nu}_q(z)e^{i(\mathbf{q}\cdot\mathbf{r}-\omega_q t)}+a_q^{\dagger}\boldsymbol{\nu}_q(z)^*e^{-i(\mathbf{q}\cdot\mathbf{r}-\omega_q t)}\right). \tag{2.122}$$

In the next chapter, we will derive the optical conductivity of silicene and discuss the possibility to have TE surface wave in silicene. In the Chapter 4, we will use the quantization of photon and surface plasmon to describe the excitation of surface plasmon by light in graphene.

Chapter 3

Broadband transverse electric (TE) surface wave in silicene

In this chapter, by using the energy dispersion of silicene in Eq. (2.71), we can calculate the optical conductivity of silicene by using Eq. (2.32). The optical conductivity will be used to show that the silicene might be a better material to support the TE surface wave than graphene. This chapter has been published in Applied Physics Letter [84].

Let us remind the problem of the TE surface wave. The TE surface wave cannot exist on the surface of bulk metal due to the lack of surface current density. Some efforts have been made for designing artificial materials so that the TE surface wave can be generated, such as metamaterials and a cluster of nanoparticles, which are generally complicated [39, 14, 40, 85], hence making them less viable and accessible. The difficulties of generating the TE surface wave can be alleviated by using two-dimensional (2D) materials such like graphene, which is a monolayer of carbon atoms arranged in honeycomb lattice. Mikhailov and Ziegler have shown that, when the imaginary part of optical conductivity of 2D material is negative (positive), the TE (TM) surface wave can propagate on the surface of the 2D materials [9]. Due to the presence of the Dirac cone in the electronic structure, the imaginary part of optical conductivity of graphene can be negative at a certain range of frequency. This is in contrast to usual 2D electron gas systems, which have a positive imaginary part of optical conductivity. This unusual property has also enabled graphene to have the TE surface wave.

However, it was predicted that the TE surface wave in doped graphene may exist only for a narrow frequency range of $1.667E_{\mathrm{F}} < \hbar\omega < 2E_{\mathrm{F}}$, where E_{F} is the Fermi energy [9]. Moreover, the TE surface wave in graphene is less confined in the direction perpendicular to the surface in comparison with the TM surface wave [9, 43]. To solve this problem, we may use other 2D material which is similar in its electronic structure to graphene, such as silicene. Different to graphene, silicene is single layer of silicon atom and is known to have a band gap that can be controlled by external electric field, which might affects the properties of the TE surface waves. Therefore, the more detailed study of TE surface wave in silicene must be important to investigate, which is the subject of this chapter.

3.1 The optical conductivity of silicene

The Kubo formula for optical conductivity is given by Eq. (2.32), and is shown below [60],

$$\sigma(\omega) = \frac{ie^2\hbar}{(2\pi)^2}\int d^2\mathbf{k}\Bigg(- \frac{(v^{11})^2}{\hbar\omega}\frac{df_0(\epsilon_1(\mathbf{k}))}{d\epsilon_1} - \frac{(v^{22})^2}{\hbar\omega}\frac{df_0(\epsilon_2(\mathbf{k}))}{d\epsilon_2} + v^{12}v^{21}\frac{f_0(\epsilon_1(\mathbf{k})) - f_0(\epsilon_2(\mathbf{k}))}{(\epsilon_2(\mathbf{k}) - \epsilon_1(\mathbf{k}))(\hbar\omega + \epsilon_1(\mathbf{k}) - \epsilon_2(\mathbf{k}))} + v^{21}v^{12}\frac{f_0(\epsilon_2(\mathbf{k})) - f_0(\epsilon_1(\mathbf{k}))}{(\epsilon_1(\mathbf{k}) - \epsilon_2(\mathbf{k}))(\hbar\omega + \epsilon_2(\mathbf{k}) - \epsilon_1(\mathbf{k}))}\Bigg), \tag{3.1}$$

where the energy dispersion is obtained by diagonalizing the Hamiltonian given by,

$$H_{\varsigma\eta} = \begin{pmatrix} -\frac{1}{2}\varsigma\eta\Delta_{\mathrm{SO}} + \frac{1}{2}\Delta_z & \hbar v_{\mathrm{F}}(k_x - i\eta k_y) \\ \hbar v_{\mathrm{F}}(k_x + i\eta k_y) & \varsigma\eta\frac{\Delta_{\mathrm{SO}}}{2} - \frac{1}{2}\Delta_z \end{pmatrix}, \tag{3.2}$$

The energy dispersion of electron is given by $\epsilon_{s\varsigma\eta}(k) = (-1)^{s+1}\epsilon_{\varsigma\eta}(k)$, with s is 1 and 2 for the conduction and valence band, respectively. $\epsilon_{\varsigma\eta}(k)$ is the energy dispersion for electron with ς spin and at η valley, which is given by $\epsilon_{\varsigma\eta}(k) = \sqrt{(\hbar v_{\mathrm{F}}k)^2 + \frac{1}{4}\Delta^2_{\varsigma\eta}}$, where $k = \sqrt{k_x^2 + k_y^2}$ and $\Delta_{\varsigma\eta}(\Delta_z) = |\Delta_z - \varsigma\eta\Delta_{\mathrm{SO}}|$ denotes the energy gap which is tunable by applying the E_z. In Fig. 3.1, we plot $\epsilon_{s\varsigma\eta}(k)$ for one spin and near one valley. $\epsilon_{s\varsigma\eta}(0) = +(-)\frac{1}{2}\Delta_{\varsigma\eta}$ at the bottom (top) of conduction (valence) band. The $v^{ss'}$ in Eq. (3.1) is the matrix element of velocity matrix $\widehat{v}(k) = U^{-1}\left(\partial H_{\varsigma\eta}(\mathbf{k})/\hbar\partial\mathbf{k}\right)U$ in the x direction, where U is the unitary matrix which diagonalize $H_{\varsigma\eta}$. Therefore, the $v^{ss'}$ is the velocity in the representation of energy band. The $\widehat{v}(k)$ matrix is explicitly given as follows:

$$\widehat{v}(k) = \frac{\hbar v_{\mathrm{F}}^2 k}{\epsilon_{\varsigma\eta}}\begin{bmatrix} \widehat{\mathbf{x}}\cos\theta + \widehat{\mathbf{y}}\eta\sin\theta & -Z_-\{\widehat{\mathbf{x}}(-\Gamma_- + \mathrm{A}_-) - \widehat{\mathbf{y}}i\eta(\mathrm{B}_- - \mathrm{I}_-)\} \\ Z_+\{\widehat{x}(\Gamma_+ + \mathrm{A}_+) - \widehat{\mathbf{y}}i\eta(\mathrm{B}_+ + \mathrm{I}_+)\} & -\widehat{\mathbf{x}}\cos\theta - \widehat{\mathbf{y}}\eta\sin\theta \end{bmatrix}, \tag{3.3}$$

where we define $\beta_\pm = \epsilon_{\varsigma\eta} \pm 1/2\Delta_{\varsigma\eta}$, $Z_\pm = (\beta_\pm/\beta_\mp)^{1/2}$, $\Gamma_\pm = \Delta_{\varsigma\eta}\cos\theta/\beta_\pm$, $\mathrm{A}_\pm = i2\epsilon_{\varsigma\eta}\sin\theta/\beta_\pm$, $\mathrm{B}_\pm = 2\epsilon_{\varsigma\eta}\cos\theta/\beta_\pm$, and $\mathrm{I}_\pm = i2\Delta_{\varsigma\eta}\sin\theta/\beta_\pm$. Here θ is the angle between k and k_x, while v^{nm} denotes the x-component of the $n-m$ element of $\widehat{v}$ matrix. Eq. (3.3) is derived in the Appendix B.

3.1.1 Intraband conductivity

The first two terms of Eq. (3.1) are called the intraband conductivity [60, 59]. Let us calculate the intraband conductivity for each spin and valley $\sigma^{\mathrm{A}}_{\varsigma\eta}(\omega)$. We consider the case of $T \approx 0$ K and therefore the derivatives of Fermi distribution function are given by,

$$\begin{aligned} \frac{df_0(\epsilon_1(\mathbf{k}))}{d\epsilon_1} &= \frac{d}{d\epsilon_1}\Theta(E_{\mathrm{F}} - \epsilon_1)\Theta(2E_{\mathrm{F}} - \Delta_{\varsigma\eta}) \\ &= -\delta(E_{\mathrm{F}} - \epsilon_1(\mathbf{k}))\Theta(2E_{\mathrm{F}} - \Delta_{\varsigma\eta}), \\ \frac{df_0(\epsilon_2(\mathbf{k}))}{d\epsilon_2} &= \frac{d}{d\epsilon_2}\,1 = 0, \end{aligned} \tag{3.4}$$

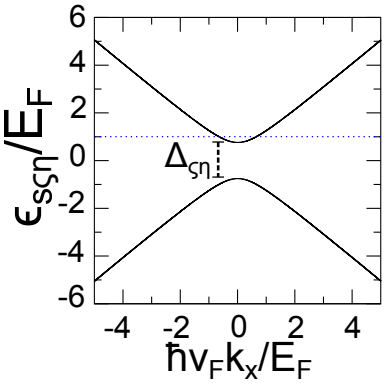

Figure 3.1 The energy band of silicene for one spin and valley $\epsilon_{\varsigma\eta}$ showing the Fermi energy $E_{\rm F}$ in the conduction band as dashed line.

where $\Theta(x)$ is the Heaviside step function and we assume that the $E_{\rm F}$ is located in the conduction band (ϵ_1) or $E_{\rm F} > \frac{\Delta_{\varsigma\eta}}{2}$. Then, the intraband conductivity is given by,

$$\begin{aligned}\sigma^{\rm A}_{\varsigma\eta}(\omega) =& \frac{ie^2}{4\omega\pi^2}\int dk \frac{\hbar^2 v^4 k^3}{\epsilon^2_{\varsigma\eta}} \int_0^{2\pi} d\theta \cos^2\theta \delta(E_{\rm F}-\epsilon_{\varsigma\eta})\Theta(2E_{\rm F}-\Delta_{\varsigma\eta}) \\ =& \frac{ie^2}{4\hbar^2\omega\pi}\int d\epsilon_{\varsigma\eta}\frac{\epsilon^2_{\varsigma\eta}-\frac{1}{4}\Delta^2_{\varsigma\eta}}{\epsilon_{\varsigma\eta}}\delta(E_{\rm F}-\epsilon_{\varsigma\eta})\Theta(2E_{\rm F}-\Delta_{\varsigma\eta}) \qquad (3.5)\\ =& \frac{ie^2}{4\hbar^2\omega\pi}\frac{E^2_{\rm F}-\frac{1}{4}\Delta^2_{\varsigma\eta}}{E_{\rm F}}\Theta(2E_{\rm F}-\Delta_{\varsigma\eta}). \qquad (3.6)\end{aligned}$$

It can be seen from Eq. (3.6) that the $\sigma^{\rm A}_{\varsigma\eta}(\omega)$ has ω^{-1} dependence, which implies the Drude conductivity.

3.1.2 Interband conductivity

The remaining terms in Eq. (3.1) correspond to the interband conductivity per each spin and valley $\sigma^{\rm E}_{\varsigma\eta}(\omega)$. The difference of the Fermi distribution function of conduction and valence band is given as follows,

$$\begin{aligned}f_0(\epsilon_1(\mathbf{k})) - f_0(\epsilon_2(\mathbf{k})) =& -\Theta(\epsilon_1(\mathbf{k})-E_{\rm F})\Theta(2E_{\rm F}-\Delta_{\varsigma\eta}) \\ & -\Theta(\epsilon_1(\mathbf{k})-\Delta_{\varsigma\eta}/2)\Theta(\Delta_{\varsigma\eta}-2E_{\rm F}). \qquad (3.7)\end{aligned}$$

Fig. 3.1: Fig/Figsildis2.eps

The interband conductivity is given by,

$$\begin{aligned}\sigma^{\mathrm{E}}_{\varsigma\eta}(\omega) =& \frac{i\hbar^2\omega e^2}{2\pi^2}\int kdk\int_0^{2\pi} d\theta v^{12}v^{21}\frac{f_0(\epsilon_1(\mathbf{k}))-f_0(\epsilon_2(\mathbf{k}))}{(\epsilon_2(\mathbf{k})-\epsilon_1(\mathbf{k}))(\hbar^2\omega^2-(\epsilon_2(\mathbf{k})-\epsilon_1(\mathbf{k}))^2)}\\ =& \frac{i\hbar^4 v_{\mathrm{F}}^4\omega e^2}{4\pi^2}\int k^3dk\int_0^{2\pi} d\theta\frac{-\cos^2\theta\Delta^2_{\varsigma\eta}-4\epsilon^2_{\varsigma\eta}\sin^2\theta}{\epsilon^2_{\varsigma\eta}-\frac{\Delta^2_{\varsigma\eta}}{4}}\frac{f_0(\epsilon_1(\mathbf{k}))-f_0(\epsilon_2(\mathbf{k}))}{4\epsilon^3_{\varsigma\eta}(\hbar^2\omega^2-4\epsilon^2_{\varsigma\eta})}\\ =& -\frac{i\omega e^2}{4\pi}\int_{\max(E_{\mathrm{F}},\Delta_{\varsigma\eta}/2)}^{\infty} d\epsilon_{\varsigma\eta}\frac{\Delta^2_{\varsigma\eta}+4\epsilon^2_{\varsigma\eta}}{4\epsilon^2_{\varsigma\eta}(4\epsilon^2_{\varsigma\eta}-\hbar^2\omega^2)}.\end{aligned} \tag{3.8}$$

By substituting $p^2 = 4\epsilon^2_{\varsigma\eta} - \hbar^2\omega^2$ and $d\epsilon_{\varsigma\eta} = pdp/(4\epsilon_{\varsigma\eta})$, we obtain,

$$\begin{aligned}\sigma^{\mathrm{E}}_{\varsigma\eta}(\omega) =& -\frac{i\omega e^2}{8\pi}\int_{\sqrt{4\max(E_{\mathrm{F}},\Delta_{\varsigma\eta}/2)^2-\hbar^2\omega^2}}^{\infty} dp\frac{\Delta^2_{\varsigma\eta}+\hbar^2\omega^2+p^2}{p(p^2+\hbar^2\omega^2)^{3/2}}\\ =& -\frac{ie^2}{8\pi\hbar^3\omega^2}\left[\frac{-\Delta^2_{\varsigma\eta}\hbar\omega}{2\max(E_{\mathrm{F}},\Delta_{\varsigma\eta}/2)}+(\Delta^2_{\varsigma\eta}+\hbar^2\omega^2)\ln\left|\frac{\sqrt{\hbar\omega+2\max(E_{\mathrm{F}},\Delta_{\varsigma\eta}/2)}}{\sqrt{2\max(E_{\mathrm{F}},\Delta_{\varsigma\eta}/2)-\hbar\omega}}\right|\right]\\ =& -\frac{ie^2}{16\pi\hbar^3\omega^2}\left[\frac{-\Delta^2_{\varsigma\eta}\hbar\omega}{2\max(E_{\mathrm{F}},\Delta_{\varsigma\eta}/2)}+2(\Delta^2_{\varsigma\eta}+\hbar^2\omega^2)\ln\left|\frac{\sqrt{\hbar\omega+2\max(E_{\mathrm{F}},\Delta_{\varsigma\eta}/2)}}{\sqrt{\hbar\omega-2\max(E_{\mathrm{F}},\Delta_{\varsigma\eta}/2)}}\right|\right]\\ &+\frac{e^2}{16\hbar^3\omega^2}\left[(\Delta^2_{\varsigma\eta}+\hbar^2\omega^2)\right]\Theta(\hbar\omega-2\max(E_{\mathrm{F}},\Delta_{\varsigma\eta}/2)),\end{aligned} \tag{3.9}$$

where we use $\ln i = i\pi/2$. The function of $\max(a, b)$ selects a larger value for a or b. The first two terms of Eq. (3.9) are the imaginary part of intraband conductivity, while the last term of Eq. (3.9) is the real part of intraband conductivity. The real part and imaginary part of intraband conductivity are related each other through Kramers-Kronig relation. If we set the $\Delta_{\varsigma\eta} = 0$ in the real part of interband conductivity, we return to the universal conductivity of graphene Re $\sigma(\omega) = 4 \times \frac{e^2}{16\hbar}$.

3.2 The tunable TE surface wave in silicene

The total optical conductivity is obtained by adding the intraband and interband conductivity for all spin and valley. The total optical conductivity is given by [84],

$$\sigma(\omega,\Delta_z) = \sum_{\varsigma\eta}\left\{\sigma^{\mathrm{A}}_{\varsigma\eta}(\omega,\Delta_z)+\sigma^{\mathrm{E}}_{\varsigma\eta}(\omega,\Delta_z)\right\}, \tag{3.10}$$

$$\sigma^{\mathrm{A}}_{\varsigma\eta}(\omega,\Delta_z) = i\frac{e^2}{16\hbar\pi}\frac{4E_{\mathrm{F}}^2-\left[\Delta_{\varsigma\eta}(\Delta_z)\right]^2}{E_{\mathrm{F}}\hbar\omega}\Theta\left[2E_{\mathrm{F}}-\Delta_{\varsigma\eta}(\Delta_z)\right] \tag{3.11}$$

$$\begin{aligned}\sigma^{\mathrm{E}}_{\varsigma\eta}(\omega,\Delta_z) =& \frac{e^2}{16\hbar}\left\{1+\left(\frac{\Delta_{\varsigma\eta}(\Delta_z)}{\hbar\omega}\right)^2\right\}\Theta\left[\hbar\omega-g(\Delta_z)\right]\\ &- i\frac{e^2}{16\hbar\pi}\left\{1+\left(\frac{\Delta_{\varsigma\eta}(\Delta_z)}{\hbar\omega}\right)^2\right\}\times\ln\left|\frac{\hbar\omega+g(\Delta_z)}{\hbar\omega-g(\Delta_z)}\right|+i\frac{e^2\left[\Delta_{\varsigma\eta}(\Delta_z)\right]^2}{8\hbar^2\pi\omega g(\Delta_z)},\end{aligned} \tag{3.12}$$

where $g(\Delta_z)=\max[2E_{\mathrm{F}},\Delta_{\varsigma\eta}(\Delta_z)]$. If we set $\Delta_{\varsigma\eta}=0$, we get the optical conductivity of graphene given in Eq. (1.26). It noted that we obtain the similar result as in Ref. [54] by Stille et al. However, there is a sign error in the second term of interband conductivity [Eq. (3.12)] in their work, which makes the TE surface wave cannot occur even in graphene and we cannot obtain the optical conductivity of graphene, if we set $\Delta_{\varsigma\eta}=0$. In the subsequent discussion, for simplicity, we fix the $E_{\mathrm{F}}=2\Delta_{\mathrm{SO}}=7.8$ meV, and vary the $\Delta_z=2\Delta_{\mathrm{SO}},4\Delta_{\mathrm{SO}}$, and $8\Delta_{\mathrm{SO}}$, therefore the energy gap is a function of Δ_z ($\Delta_{\varsigma\eta}(\Delta_z)$).

In Fig. 3.2, we plot the electron energy dispersions for K and K' valleys for several Δ_z's. In varying Δ_z, we choose three cases for both the K and K' valleys depending on the position of E_{F} relative to the energy gap, which are shown in Fig. 3.2. The first case is $\Delta_z=2\Delta_{\mathrm{SO}}$, in which E_{F} is higher than bottoms of the two conduction bands for spin up and spin down ($E_{\mathrm{F}}>\Delta_{++/--}$ and $\Delta_{-+/+-}$) [Figs. 3.2(a) and 2(d)]. The second case is $\Delta_z=4\Delta_{\mathrm{SO}}$, in which E_{F} lies between two bottoms of the conduction bands ($\Delta_{++/--}<E_{\mathrm{F}}<\Delta_{-+/+-}$) [Figs. 3.2(b) and (e)] and the third case is $\Delta_z=8\Delta_{\mathrm{SO}}$, in which E_{F} exists in energy gaps [Figs. 3.2(c) and (f)].

In Fig. 3.3, we plot the optical conductivity σ of silicene as a function of frequency where the solid and dashed lines are the imaginary and real parts of σ, respectively, for the three Δ_z. We also plot the σ of graphene in black lines for a comparison. The logarithmic singularities in Im σ in Eq. (3.12) correspond to the lowest excitation energies for interband transitions of electrons between energy bands having the same spin directions and the same valleys. Im σ is logaritmichally singular ln $|\hbar\omega-g(\Delta_z)|$ for any frequency which satisfies condition $\hbar\omega=g(\Delta_z)$ as shown in Eq. (3.12).Since there are two distinct values of $\Delta_{\varsigma\eta}(\Delta_z)$, there are two possible singularity points, $\omega_1=2E_{\mathrm{F}}/\hbar$ and $\omega_2=\Delta_{-+}/\hbar$ if $\Delta_{++}/2<E_{\mathrm{F}}<\Delta_{-+}/2$ [$\Delta_z=4\Delta_{\mathrm{SO}}$] or $\omega_1=\Delta_{++}/\hbar$ and $\omega_2=\Delta_{-+}/\hbar$ if $E_{\mathrm{F}}<\Delta_{++}/2$ and $\Delta_{-+}/2$ [$\Delta_z=8\Delta_{\mathrm{SO}}$]. When $E_{\mathrm{F}}>\Delta_{-+}/2$ and $\Delta_{++}/2$ there is only one singularity point at $\omega=2E_{\mathrm{F}}/\hbar$. These singularities correspond to the minimum photon energy for having interband transition of electron.

Since the σ of silicene depends on Δ_z, σ of silicene can be tuned not only by E_{F} but also by E_z (Δ_z). As mentioned in Eq. (1.32), the negative value of Im σ correspond to the condition for TE surface wave. The TE surface wave cannot exist

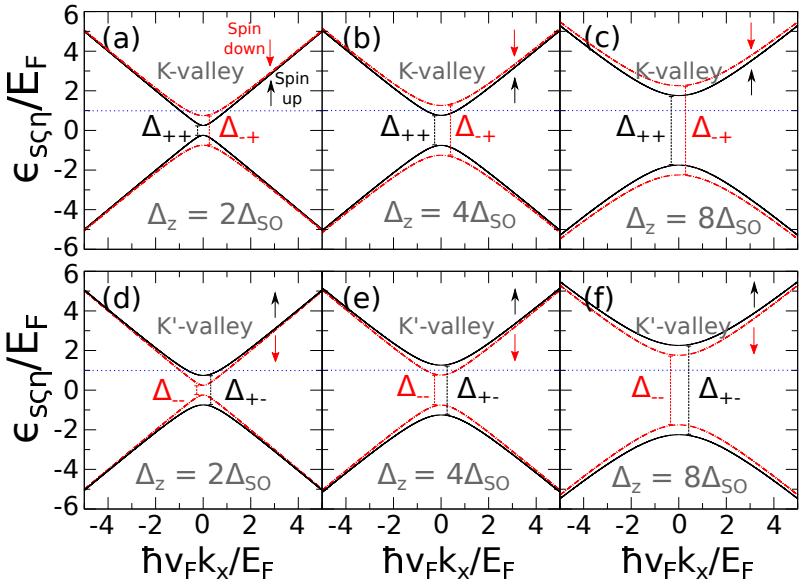

Figure 3.2 Electronic energy dispersions of silicene for [(a)-(c)] K and [(d)-(f)] K' valleys for several Δ_z's ($2\Delta_{SO}$,$4\Delta_{SO}$, and $8\Delta_{SO}$). The solid (dash-dotted) lines correspond to spin up (down) electron dispersion. Positions of $E_F = 2\Delta_{SO}$ are indicated by the horizontal dotted lines.

for the region that Im $\sigma > 0$. In the following discussion, we call the frequency range of Im $\sigma < 0$ as the frequency range of TE surface wave or Δf^{TE}. Furthermore we focus only on the frequency range where Re $\sigma = 0$ in which the TE surface wave is not damped, since the wave vector of TE surface wave q, which can be obtained from Eq. (1.32) is real quantity if Re $\sigma = 0$. For graphene ($\Delta_{s\eta} = 0$), the Δf^{TE} is fixed at $1.667E_F < \hbar\omega < 2E_F$ ($3.14 < f < 3.77$ THz), which reproduces the previous results [9, 10, 59].

In general, the Δf^{TE} in silicene is wider than that in graphene for the same E_F and it is tunable by Δ_z as shown in Fig. 3.3 [84]. For example, for $\Delta_z = 2\Delta_{SO}$ ($E_z = 16.96$ mV Å^{-1}), the TE frequency range lies within $1.4E_F < \hbar\omega < 2E_F$ ($2.64 < f < 3.77$ THz). When we increase Δ_z, $\Delta_{s\eta}$ increases, too. From Eq. (3.11)-(3.12) we know that increasing $\Delta_{s\eta}$ not only makes Im $\sigma^E_{s\eta}$ more negative, but also reduces Im $\sigma^A_{s\eta}$ whose value is always positive. Altogether, Im σ decreases, hence the Δf^{TE} becomes wider when we increase Δ_z. The Im $\sigma^A_{s\eta}$ can be suppressed when $\Delta_{s\eta} > 4\Delta_{SO}$, or the Fermi level is located in $\Delta_{s\eta}$ as shown in Figs. 3.1 (b) and (c). This occurs for $\Delta_z = 4\Delta_{SO}$ ($E_z = 33.92$ mV Å^{-1}) and $\Delta_z = 8\Delta_{SO}$ ($E_z = 67.84$ mV Å^{-1}) (see Figs. 3.2(b) and (c) respectively). For $\Delta_z = 4\Delta_{SO}$, only Im σ^A_{-+} and Im σ^A_{+-} are suppressed, therefore we still have Im $\sigma > 0$ at certain frequency and Re $\sigma \neq 0$ for $\hbar\omega \geq 2E_F$ ($f \geq 3.77$ THz, see Eqs. (3.11) and (3.12)). Hence, the Δf^{TE} becomes $1.61 < f < 3.77$ THz. But in the case of $\Delta_z = 8\Delta_{SO}$, all Im $\sigma^A_{s\eta}$ vanish and Im σ has negative value at all frequency. Re $\sigma \neq 0$ for $\hbar\omega \geq \Delta_{++}$ ($f \geq 6.60$ THz). Therefore,

Fig. 3.2: Fig/Figsildis.eps

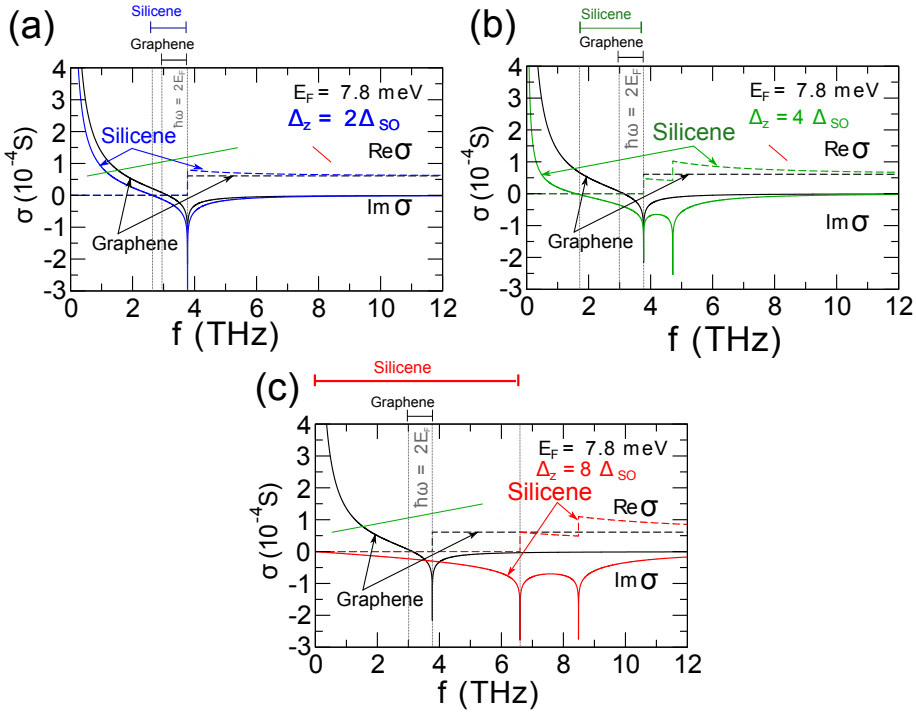

Figure 3.3 Optical conductivity (σ) of silicene for three different Δ_z values and compared with that of graphene. The condition that the TE surface wave exists without damping ($\Delta f^{\rm TE}$) are (1) Im $\sigma < 0$ and (2) Re $\sigma = 0$. The range of frequency, in which TE surface wave exist without damping are shown for silicene (color) and graphene (black) at the top of each figure. The solid lines represent the imaginary part of σ and the dashed lines represent the real part of σ. Position of $\hbar\omega = 2E_{\rm F}$ is fixed at $f = 3.77$ THz.

the $\Delta f^{\rm TE}$ becomes $0 < f < 6.60$ THz. Re σ appears at higher frequency than that for $\Delta_z = 4\Delta_{\rm SO}$, because the Fermi level exists in all of the energy gaps, in which we need a higher excitation energy for interband transition.

Another interesting finding is that the undoped silicene ($E_{\rm F} = 0$) may also support TE surface wave [84]. From Eqs. (3.10)-(3.12), when we put $E_{\rm F} = 0$ we get Im σ as follows,

$$\text{Im }\sigma(\omega,\Delta_z) = -\frac{e^2}{16\hbar\pi}\sum_{\varsigma\eta}\left\{\left[1+\left(\frac{\Delta_{\varsigma\eta}(\Delta_z)}{\hbar\omega}\right)^2\right] \times \ln\left|\frac{\hbar\omega+\Delta_{\varsigma\eta}(\Delta_z)}{\hbar\omega-\Delta_{\varsigma\eta}(\Delta_z)}\right| - \frac{2\Delta_{\varsigma\eta}(\Delta_z)}{\hbar\omega}\right\} . \tag{3.13}$$

In this case, the $\Delta f^{\rm TE}$ lies within $0 < \hbar\omega < \Delta_{++/--}$. It is noted that Im $\sigma(\omega)$ vanishes at $E_{\rm F} = 0$ in graphene that corresponds to $\Delta_{\varsigma\eta}(\Delta_z) = 0$, hence the TE surface wave does not exist for undoped graphene. We have known that the $\Delta f^{\rm TE}$ in silicene

Fig. 3.3: Fig/fig3.pdf

is tunable by the external electric field. The Δf^{TE} is wider by increasing the external electric field. If the E_{F} is located in both of or one of conduction band as shown in the case of Figs. 3.3 (a) and (b), the Δf^{TE} is given by $\hbar\omega_0 < \hbar\omega^{\mathrm{TE}} < 2E_{\mathrm{F}}$, where ω_0 is the lowest frequency for supporting TE mode at which Im $\sigma(\omega_0, \Delta_z) = 0$.

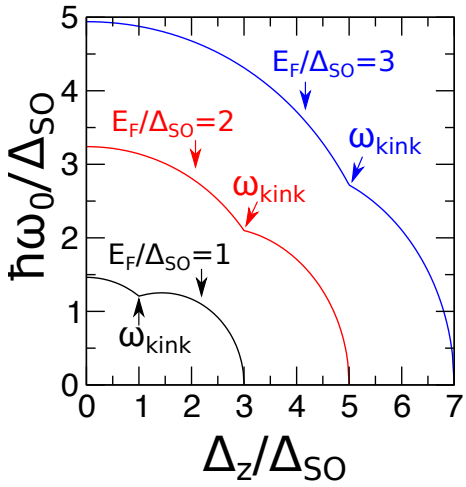

Figure 3.4 The ω_0, which is the frequency that makes Im $\sigma(\omega_0, \Delta_z) = 0$, as a function of Δ_z for several E_{F}'s.

In Fig. 3.4, we show the ω_0 as a function of Δ_z for several E_{F}'s. We can see that as we increase the electric field, the ω_0 gets lower, which means that the frequency range increases with increasing electric field. For each E_{F}, we get a kink at $\hbar\omega_{\mathrm{kink}} = 2E_{\mathrm{F}} - \Delta_{\mathrm{SO}}$, which corresponds to the Fermi level located at the bottom of $\epsilon_{-+/+-}$ [see step function $\Theta(2E_{\mathrm{F}} - \Delta_{\varsigma\eta})$ in Eq. (3.11)]. For $\Delta_z < \hbar\omega_{\mathrm{kink}}$, the all the energy bands in the conduction band contribute to the total optical conductivity Im σ [Eqs. (3.11) and (3.12)], which is the case of Figs 3.2 (a), (d) and 3.3 (a). For $\Delta_z > \hbar\omega_{\mathrm{kink}}$, only Im σ_{++} and Im σ_{--} contribute to the total optical conductivity Im σ, which is the case of Figs 3.2 (b), (e) and 3.3 (b). When the Fermi level is located inside the both of energy gaps as shown in Figs 3.2 (c) and (f), the frequency range lies within $0 < \hbar\omega < \Delta_{++/--}$, and it is clear to say that the Δf^{TE} increases linearly with increasing Δ_z, since $\Delta_{++/--} = |\Delta_z - \Delta_{\mathrm{SO}}|$.

3.3 The properties of TE surface wave in silicene

3.3.1 The confinement length

From Eq. (1.32), we can define a confinement length of TE surface wave $1/\kappa$, as follows

$$\frac{1}{\kappa} = \frac{2}{i\omega\sigma(\omega, \Delta_z)\mu_0} \quad . \tag{3.14}$$

A smaller value of $1/\kappa$ corresponds to better confinement. In Fig. 3.5, we plot $1/\kappa$ of the TE surface wave in graphene and silicene for comparison. The plot starts at

Fig. 3.4: Fig/figrange.eps

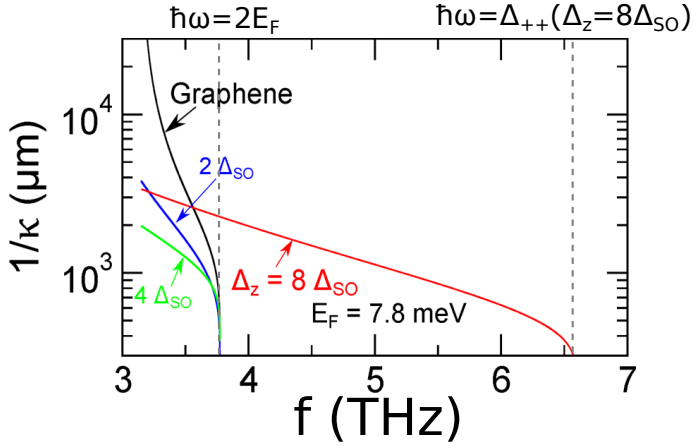

Figure 3.5 Confinement length $1/\kappa$ for silicene and graphene as a function of frequency. Inset : $\Delta\lambda$ as a function of frequency for graphene and silicene.

$f = 3.15$ THz ($\hbar\omega = 1.667E_{\rm F}$), which is the lower bound of the frequency range of TE surface wave in graphene. We can see that the TE surface wave in silicene is much more confined than in graphene and tunable by Δ_z [84]. For example, at $f = 3.25$ THz ($\hbar\omega = 1.725E_{\rm F}$), in case of graphene, $1/\kappa = 13994$ μm, while in case of silicene, $1/\kappa = 2906.2$ μm for $\Delta_z = 2\Delta_{\rm SO}$, $1/\kappa = 1747.7$ μm for $\Delta_z = 4\Delta_{\rm SO}$, and $1/\kappa = 3146.7$ μm for $\Delta_z = 8\Delta_{\rm SO}$.

The value of $1/\kappa$ gets smaller as the frequency approach the $\hbar\omega = 2E_{\rm F}$, at which the Im σ is singular for the case of $\Delta_z = 2\Delta_{\rm SO}$ and $\Delta_z = 4\Delta_{\rm SO}$. In the case of $\Delta_z = 8\Delta_{\rm SO}$, we might get a larger $1/\kappa$ for $\hbar\omega < 2E_{\rm F}$. This is because Im σ is singular at higher frequency [at $\hbar\omega = \Delta{+}{+}(\Delta_z = 8\Delta_{\rm SO})$], which makes $1/\kappa$ for $\Delta_z = 8\Delta_{\rm SO}$ slowly diverge.

3.3.2 The shrinking of wavelength

By solving Eq. (1.32) for $\lambda = 2\pi/q$, we can define the difference between the wavelength of TE surface wave λ and the wavelength of freely propagating EM wave in vacuum $\lambda_0 = 2\pi c/\omega$ as $\Delta\lambda = \lambda - \lambda_0$. The negative value of $\Delta\lambda = \lambda - \lambda_0$ means that there is shrinkage of the wavelength of TE surface wave, which is the preferable feature of surface wave since more information can be compressed in the wave. In the Fig. 3.6, we plot $\Delta\lambda$ as a function of frequency for graphene and silicene for the case of $\Delta_z = 4\Delta_{\rm SO}$. We can see that $\Delta\lambda$ is sufficiently small, which means that λ is almost the same as λ_0 (3 THz corresponds to $\lambda_0 = 100\mu$m). However, $\Delta\lambda$ for silicene is more negative compared with that for graphene, which is almost zero. Although $\Delta\lambda$ of silicene is negligible ($\Delta\lambda/\lambda_0 \approx 10^{-4}$), from Fig. 3.6, we can see more shrinkage of the wavelength in silicene compared with that in graphene [84].

Fig. 3.5: Fig/figloc.eps

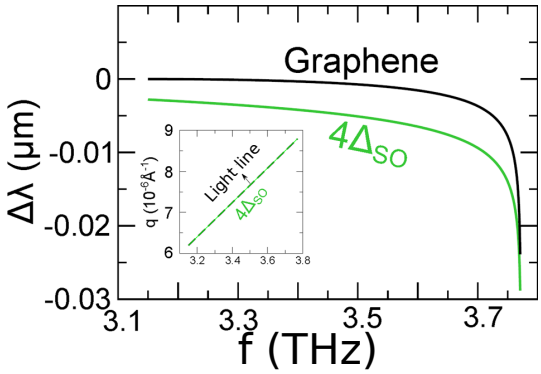

Figure 3.6 The shrinkage of wavelength of TE surface wave in silicene and graphene. Inset: the dispersion of TE surface wave.

3.4 Temperature effect

To investigate the damping of TE surface wave, we consider the case of finite temperature $T \neq 0$, therefore the $\Theta\left[\hbar\omega - g(\Delta_z)\right]$ in the Re σ of Eq. (3.12) is not a step-like function anymore, since the Fermi distribution function is a function of temperature. Hence, within the frequency range of TE surface wave that has been discussed before, the conductivity is not purely imaginary, but might have non-zero component of Re σ. From Eq. (1.32), if the conductivity is complex, the wave vector of TE surface wave q is also complex. The imaginary part of q corresponds to the damping of the TE surface wave. We will show that TE surface wave might propagate longer compared with TM surface wave by taking one case of $\Delta_z = 4\Delta_{\rm SO}$ with $E_{\rm F} = 2\Delta_{\rm SO}$ for TE surface wave and comparing it with the case of TM surface wave in silicene.

3.4.1 The optical conductivity

Let us first calculate the optical conductivity if $T \neq 0$. We follow the method that is used to calculate the optical conductivity of graphene with $T \neq 0$ [86]. From Eq. (3.5), the intraband conductivity for each spin and valley can be expressed by,

$$\sigma^{\rm A}_{\varsigma\eta}(\omega, T) = -\frac{ie^2}{4\pi\hbar^2\omega}\int\limits_{\frac{\Delta_{\varsigma\eta}}{2}}^{\infty} d\epsilon \frac{\epsilon^2_{\varsigma\eta} - \frac{\Delta^2_{\varsigma\eta}}{4}}{\epsilon_{\varsigma\eta}}\left(\frac{df(\epsilon_{\varsigma\eta}, T)}{d\epsilon_{\varsigma\eta}} - \frac{df(-\epsilon_{\varsigma\eta}, T)}{d\epsilon_{\varsigma\eta}}\right), \tag{3.15}$$

where $f(\epsilon_{\varsigma\eta}, T) = (\mathrm{Exp}[(\epsilon_{\varsigma\eta} - E_{\rm F})/k_{\rm B}T] + 1)^{-1}$ is the Fermi distribution function. By substituting $p = k_{\rm B}T/(\epsilon_{\varsigma\eta} - E_{\rm F})$ and $p = k_{\rm B}T/(\epsilon_{\varsigma\eta} + E_{\rm F})$ to the first and second term

Fig. 3.6: Fig/figsh.eps

of Eq. (3.15), respectively, we obtain,

$$\sigma^{\mathrm{A}}_{\varsigma\eta}(\omega,T) = \frac{ie^2}{4\pi\hbar^2\omega}\Bigg[\int_0^{k_{\mathrm{B}}T/(\Delta_{\varsigma\eta}/2-E_{\mathrm{F}})} dp\frac{1}{p^2}\frac{(k_{\mathrm{B}}T/p+E_{\mathrm{F}})^2-\Delta^2_{\varsigma\eta}/4}{k_{\mathrm{B}}T/p+E_{\mathrm{F}}}\frac{e^{1/p}}{(e^{1/p}+1)^2} + \int_0^{k_{\mathrm{B}}T/(\Delta_{\varsigma\eta}/2+E_{\mathrm{F}})} dp\frac{1}{p^2}\frac{(k_{\mathrm{B}}T/p-E_{\mathrm{F}})^2-\Delta^2_{\varsigma\eta}/4}{k_{\mathrm{B}}T/p-E_{\mathrm{F}}}\frac{e^{-1/p}}{(e^{-1/p}+1)^2}\Bigg]. \quad (3.16)$$

The integration in Eq. (3.16) can be solved numerically. From Eq. (3.8), the interband conductivity for each spin and valley is given by,

$$\begin{aligned}\sigma^{\mathrm{E}}_{\varsigma\eta}(\omega) =& \frac{i\omega e^2}{4\pi}\int_{\Delta_{\varsigma\eta}/2}^{\infty} d\epsilon_{\varsigma\eta}\frac{\Delta^2_{\varsigma\eta}+4\epsilon^2_{\varsigma\eta}}{4\epsilon^2_{\varsigma\eta}(\hbar^2\omega^2-4\epsilon^2_{\varsigma\eta})}G(\epsilon_{\varsigma\eta},T)\\ =& \frac{i\omega e^2}{4\pi}\int_{\Delta_{\varsigma\eta}/2}^{\infty} d\epsilon_{\varsigma\eta}\frac{\Delta^2_{\varsigma\eta}+4\epsilon^2_{\varsigma\eta}}{4\epsilon^2_{\varsigma\eta}(\hbar^2\omega^2-4\epsilon^2_{\varsigma\eta})}\Big(G(\epsilon_{\varsigma\eta},T)-G(\frac{\hbar\omega}{2})+G(\frac{\hbar\omega}{2})\Big) \quad (3.17)\\ =& \frac{i\omega e^2}{4\pi}\int_{\Delta_{\varsigma\eta}/2}^{\infty} \frac{\Delta^2_{\varsigma\eta}+4\epsilon^2_{\varsigma\eta}}{4\epsilon^2_{\varsigma\eta}(\hbar^2\omega^2-4\epsilon^2_{\varsigma\eta})}\Big(G(\epsilon_{\varsigma\eta},T)-G(\frac{\hbar\omega}{2})\Big)d\epsilon_{\varsigma\eta}\\ &+\frac{e^2}{16\hbar}G(\frac{\hbar\omega}{2})\Big(1+(\frac{\Delta_{\varsigma\eta}}{\hbar\omega})^2\Big)\Theta(\hbar\omega-\Delta_{\varsigma\eta})\\ &+\frac{ie^2}{4\hbar}G(\frac{\hbar\omega}{2})\Big(\frac{\Delta_{\varsigma\eta}}{\hbar\omega\pi}-\frac{1}{4\pi}(1+(\frac{\Delta_{\varsigma\eta}}{\hbar\omega})^2)\ln\Big|\frac{\hbar\omega+\Delta_{\varsigma\eta}}{\hbar\omega-\Delta_{\varsigma\eta}}\Big|\Big), \quad (3.18)\end{aligned}$$

where $G(\epsilon_{\varsigma\eta},T) = f(-\epsilon_{\varsigma\eta},T) - f(\epsilon_{\varsigma\eta},T)$ is given by,

$$G(\epsilon_{\varsigma\eta},T) = \frac{\sinh\left(\frac{\epsilon_{\varsigma\eta}}{kT}\right)}{\cosh\left(\frac{\epsilon_{\varsigma\eta}}{kT}\right)+\cosh\left(\frac{E_{\mathrm{F}}}{kT}\right)}. \quad (3.19)$$

The integration of the last term of Eq. (3.17), which involves $G(\frac{\hbar\omega}{2})$ term, is done analytically and given by the last two terms of Eq. (3.18). The result of remaining integration is done numerically.

Figure 3.7 shows the optical conductivity of silicene with $\Delta_z = 4\Delta_{\mathrm{SO}}$ for $k_{\mathrm{B}}T = 0$ and 0.1 E_{F} (For $E_{\mathrm{F}} = 7.8$ meV, $T = 9$ K). We also add the scattering time of electron τ to the intraband conductivity by substituting $\omega \to \omega + i/\tau$ with $\hbar/\tau = 0.01$ meV. It is clear that by increasing the temperature, the smearing of the real part of conductivity occurs at $\hbar\omega = 2E_{\mathrm{F}}$. This implies that the electron in the conduction band with energy close to but less than the Fermi level is thermally excited and leaves unoccupied state. This unoccupied state can be filled by the electron excited from the valence band by the EM wave with energy less than $2E_{\mathrm{F}}$. This excitation is not possible if the temperature is zero, since the all the state below Fermi level is occupied. The smearing in Re σ induces the damping of the TE surface wave, since the conductivity is now complex

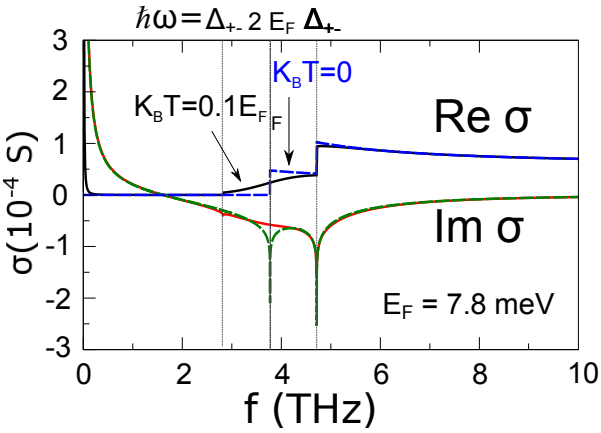

Figure 3.7 The optical conductivity of silicene with $\Delta_z = 4\Delta_{\rm SO}$ for $k_{\rm B}T = 0$ (dashed line) and 0.1 $E_{\rm F}$ (thick line). We also add the scattering time of electron τ to the intraband conductivity by substituting $\omega \to \omega + i/\tau$ with $\hbar/\tau = 0.01$ meV for the case of non zero T.

within the frequency range of TE surface wave ($1.61 < f < 3.77$ THz $[2E_{\rm F}]$). The wave vector of TE surface wave will be complex, too, based on the Eq. (1.32). Since the distribution function of electron is a function of $E_{\rm F}$ as shown in Eq. (3.19), the smearing of the real part of conductivity does not occur at $\hbar\omega = \Delta_{+-/-+}$, which remains step-like function.

3.4.2 The propagation length of TE surface wave in silicene

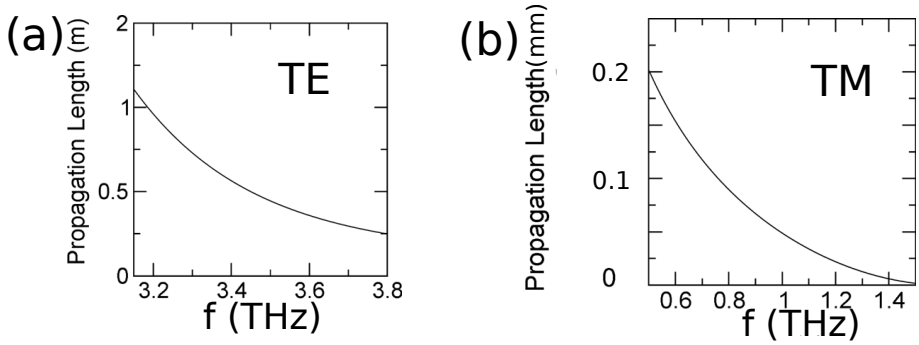

Figure 3.8 The propagation length of (a) TE and (b) TM surface waves in silicene for $T = 9$K.

Due to the smearing of the real part of conductivity, the conductivity of silicene within the frequency range of TE surface wave discussed previously ($1.61 < f <$

Fig. 3.7: Fig/figopttem.pdf
Fig. 3.8: Fig/figprop.eps

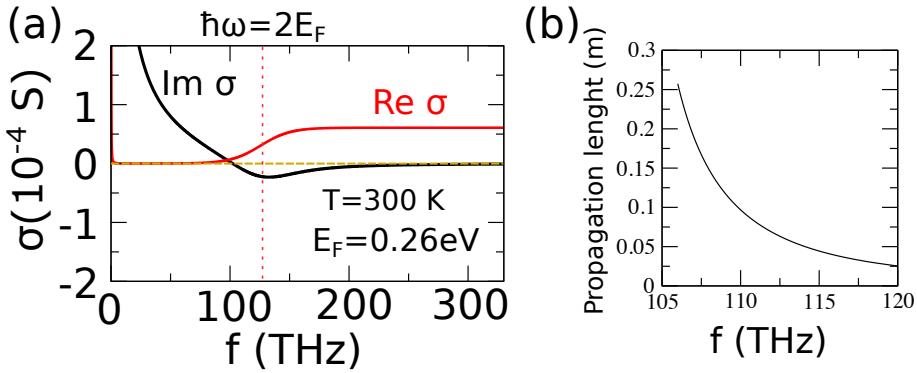

Figure 3.9 (a) The optical conductivity of silicene at T=300K with $E_{\rm F}$ = 0.26. (b) The propagation length of TE surface wave. The position of $2E_{\rm F}$ is indicated by the dashed line at f = 126 THz

3.77 THz [$2E_{\rm F}$]), becomes complex number. Therefore, Eq. (3.19) implies that the wave vector of TE surface $q = \sqrt{(i\omega\sigma\mu_0/1)^2 + (\omega/c)^2}$ is complex, too. The imaginary part of the q corresponds to the damping of TE surface wave, where $1/(\text{Im } q)$ is defined as the propagation length, which is the effective length before the amplitude of surface wave is damped out.

Figure 3.8(a) shows the propagation length of TE surface wave within $3.1 < f < 3.8$ THz. The propagation length is in order of one meter and decreasing with increasing frequency since the real part of conductivity also increases. This propagation length of TE surface wave is significantly longer compared with that of TM surface wave. Figure 3.8(b) gives the propagation length of TE surface wave within $0.5 < f < 1.4$ THz, where the silicene support TM surface wave (Im $\sigma > 0$). The propagation length of TM surface wave is in order of 0.1 mm, which is 10^4 times shorter than that of TE surface wave. The longer propagation length of TE surface wave gives it more advantage in application of transmission of EM signal over large distance and also nano-circuit, compared with using TM surface wave.

For room temperature (T=300K) without changing the $E_{\rm F}$, the Re σ becomes much smeared and Im σ becomes zero. Thus the frequency range of TE surface wave cannot be defined anymore. Therefore, for T=300K, we increase the $E_{\rm F}$ to be 0.26 eV so that the frequency range of TE surface wave can be well defined. The optical conductivity for T=300 K with $E_{\rm F}$ = 0.26 eV is given in Fig. 3.9 (a), where we get the similar smearing of the Re σ as in Fig. 3.7, although at higher frequency, since the $2E_{\rm F}$ is located at 126 THz. In contrast to case of Fig. 3.7, where we have two step-like functions (one of them is smeared), we have only one step-like function in the case of room temperature. Since the $\Delta_{\varsigma\eta} << E_{\rm F}$, we only have one step like function at $2E_{\rm F}$ due to the interband transition and it is smeared due to the temperature. The lower bound of frequency range of TE surface wave is similar to graphene, which is at $\hbar\omega \equiv 1.667E_{\rm F} \approx 105$ THz. In Fig. 3.9 (b), we show the propagation length of TE surface wave at frequency $106 < f < 120$ THz. The propagation length is in order of 10 cm.

Fig. 3.9: Fig/t300.eps

In conclusion, silicene is theoretically proved to be a versatile platform for utilizing TE surface wave. We have shown that silicene supports the TE surface wave propagation and it exhibits more preferable surface wave properties compared with those of graphene, such as the tunable broadband frequency and smaller confinement length. The TE surface wave in silicene is tunable by the Fermi energy as well as by the external electric field. These characteristics originate from the two-dimensional buckled honeycomb structure.

Chapter 4

The quantum description of surface plasmon excitation by light in graphene

In this chapter, we will discuss quantum mechanically the coupling between photon and surface plasmon in graphene. The surface plasmon can be seen as the transverse magnetic (TM) surface wave. In the real experiment, to excite the surface plasmon, we can use external TM EM wave which is incident to the surface of a material. The excitation of surface plasmon can be monitored by observing the reflection of the incident light. The sharp dip in the reflection indicates the excitation of surface plasmon, which also corresponds to the peak of absorption of incident light [39, 8, 20]. Therefore, there is an exchange of energy from the incident light to the surface plasmon due to the coupling between them.

The absorption peak appears if the resonant conditions for exciting surface plasmon are fulfilled, in which are the frequency and parallel component of wave vector of light should be the same as the frequency and wave vector of the surface plasmon, respectively [8]. In other words, the dispersion of light should intersect with the dispersion of surface plasmon. These conditions have guided the researchers for exciting the surface plasmon. Fulfilling the resonant conditions means that there is coupling between the light and surface plasmon. However, (1) the reason for the necessity to satisfy the resonant conditions to have coupling between light and surface plasmon and (2) the reason why the coupling makes the absorption peak cannot be explained clearly by only the classical description of electrodynamics. To answer these questions, in this chapter we will discuss the excitation of surface plasmon within the quantum picture, in which the surface plasmon and light can be quantized and considered as interacting particles.

It is noted that the results of this chapter are to be published by Physica Status Solidi B.

4.1 Excitation of surface plasmon in graphene by light

As mentioned before, to excite surface plasmon by light, the resonant conditions or energy - momentum conservation between light and surface plasmon must be fulfilled.

The resonant conditions mean that the frequency and parallel component of wave vector of light should be the same as the frequency and wave vector of plasmon, respectively. In other words, the dispersion of light should intersect with the surface plasmon's dispersion. The excitation of surface plasmon can be done by shining the light to graphene. However, by simply shining the light directly to graphene in the non-retarded regime, the intersection cannot occur, because for a given wave vector, the frequency of incident light is always larger than the frequency of surface plasmon, which can be seen in Fig. 2.8 (a) [8, 66]. Therefore, some coupling mechanism to increase the wave vector of light should be employed for non-retarded regime. One of mechanism is attenuated total reflection (ATR) method [8, 66], where we put another additional dielectric medium to increase the light wave vector of light as shown in Fig. 4.1 (a) as ε_m, where $\varepsilon_m > \varepsilon$. This additional medium is referred as coupling medium.

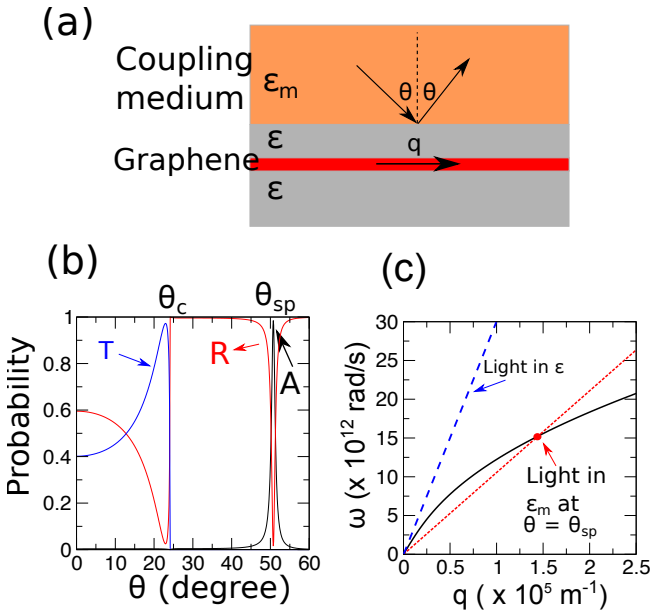

Figure 4.1 (a) The Otto geometry for exciting surface plasmon in non-retarded regime. Here $\varepsilon_m > \varepsilon$. (b) The calculated transmission (T), reflection (R), and absorption (A) probabilities of light.The absorption is maximum if the surface plasmon is excited. Here the $\theta_{\rm sp} = 50.7^\circ$. (c) the dispersion of light in ε_m intersects with surface plasmon dispersion at $\theta = \theta_{\rm sp}$. In the calculation, we use $E_{\rm F} = 0.64$ eV, $\varepsilon_m = 13.5$, $\varepsilon = 2.25$ and $\omega = 15$ THz.

In Fig. 4.1 (a), we show the geometry of ATR method, which is also known as the Otto geometry [8, 66, 20, 18]. The coupling medium has a dielectric constant larger than the media surrounding graphene $\varepsilon_m > \varepsilon$. The excitation can be observed by monitoring the reflection spectrum of light. For a fixed frequency of light, the excitation occurs at an angle of incident $\theta_{\rm sp}$ larger than critical angle $\theta_{\rm c}$ in which we should have total internal reflection as shown in Fig. 4.1 (b). At the excitation angle $\theta_{\rm sp}$, there is a sharp drop in reflection probability (R) or equivalently there is a peak on

Fig. 4.1: Fig/Fig34.eps

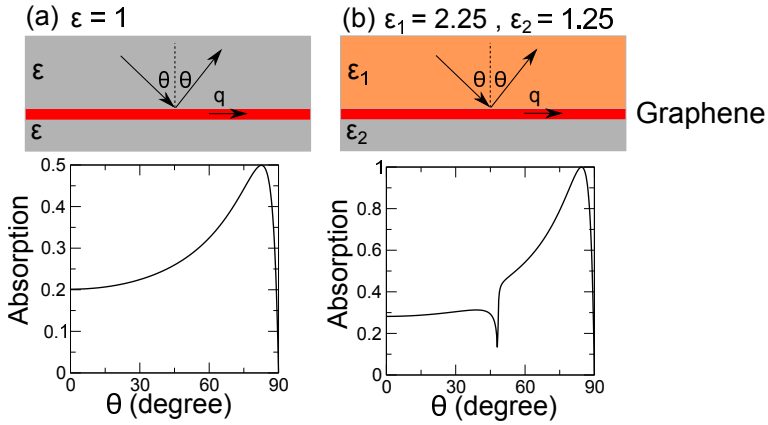

Figure 4.2 The absorption probability of light when the light incident directly to graphene in retarded regime. We adopt $\omega = 144.5 \times 10^9$ rad s^{-1}, $E_{\rm F} = 0.64$ eV and $\Gamma = 1$ meV. (a) Graphene is surrounded by medium with $\varepsilon = 1$. (b) Graphene is surrounded by medium with $\varepsilon_1 > \varepsilon_2$. The excitation occurs at θ close to 90°.

the optical absorption probability (A) of graphene. In this geometry, the light incident to graphene does not behave as a propagating wave, but as an evanescent wave, which means that the wave vector is determined by the wave vector in ε_m, not in ε as shown in Fig. 4.1 (a). This is the reason why we can increase the wave vector of light and we get the resonant conditions.

In Fig. 4.1 (b), we show the calculated transmission (T), reflection (R), and absorption (A) probabilities of light coming to the structure of Fig. 4.1 (a), which is done by solving the Maxwell equations with transfer matrix method, which has been discussed in the Chapter 2. In the calculation, we use $\omega = 15 \times 10^{12}$ rad s^{-1}, $E_{\rm F} = 0.64$ eV, $\varepsilon_m = 13.5$, and for simplicity we assume that graphene is surrounded by only kind of dielectric medium $\varepsilon = 2.25$. We can see at $\theta_{\rm sp} = 50.7°$, there is a sudden drop of R and we have a peak on A. This peak on A corresponds to the excitation of surface plasmon. We can verify it by calculating the parallel component of wave vector of incident light inside the coupling medium, $k_{\parallel}$, given by

$$k_{\parallel} = \frac{\omega}{c}\sqrt{\varepsilon_m}\sin\theta. \tag{4.1}$$

For $\theta_{\rm sp} = 50.7°$, where we have the peak on A, we have $k_{\parallel} = 1.42 \times 10^5 {\rm m}^{-1}$, which matches with the surface plasmon wave vector q at $\omega = 15 \times 10^{12}$ rad s^{-1} THz shown in Fig. 4.1 (c). The dispersion of light coming to graphene surface is now determined by the incident light in the coupling medium and it can intersect with the surface plasmon dispersion shown as red dashed-dot line in Fig. 4.1 (c). The incident light in ε_m with other θ will intersect at other frequency. It is noted that in order to observe optical absorption, the optical conductivity of graphene should have real component, therefore we substitute $\hbar\omega \to \hbar\omega + i\Gamma$ in Eq. (2.97), where Γ corresponds to damping of electron which depends on electron's mobility. In this non-retarded calculation, we adopt $\Gamma = 0.07$ meV. As discussed in Eq. (2.100), below the transition frequency ω^*,

Fig. 4.2: Fig/Fig44.eps

the surface plasmon is retarded and we expect linear dispersion of surface plasmon. In the retarded regime, we have a strong light-surface-plasmon coupling because the surface plasmon dispersion is close to the dispersion of light for any frequencies. Hence, we expect that we can have resonant conditions for any frequency in the retarded regime and the surface plasmon can be excited by simply shining the light directly to graphene. If we measure the optical absorption, we have a peak on the absorption spectrum as the surface plasmon is excited.

In Fig. 4.2, we plot the absorption spectra of light as a function of θ for light incident directly to graphene, which are calculated by solving the Maxwell equations, which is discussed in Chapter 2. In Fig. 4.2 (a), graphene is surrounded by vacuum and we have absorption peak up to 50% at $\theta \approx 83°$. By modifying the surrounding media, such as having $\varepsilon_1 > \varepsilon_2$ shown in Fig. 4.2 (b), we can increase the absorption probability up to 100% at $\theta \approx 85°$ by suppressing the light transmission through the structure [61]. In both case of Fig. 4.2, the peak of absorption appears close to $\theta = 90°$.

From this discussion, we see that when we get the resonant conditions, the optical absorption will reach maximum where we excite the surface plasmon. In the next section, we will discuss the reason why the resonant conditions are needed to excite surface plasmon and why we have an absorption peak, quantum mechanically.

4.2 The quantum description of surface plasmon excitation by light

To understand excitation process of the surface plasmon, we have to consider both the surface plasmon and light as interacting quasiparticles. The interaction might annihilate photon and create surface plasmon. The quantization of light is expressed as a photon. The surface plasmon can be seen as the quantization of collective oscillation of electron on the surface of material, which is in form of harmonic oscillator. The quantization allows us to use the Fermi golden rule for calculating the transition rate between photon and surface plasmon. The interaction Hamiltonian is given by [76, 87]

$$H_{\text{sp-op}} = \int dr\ \mathbf{j}(r,t) \cdot \mathbf{A}(r,t), \tag{4.2}$$

where $\mathbf{j}(r,t)$ is the surface current density of surface plasmon and $\mathbf{A}(r,t)$ is the "total" vector potential of the photon. Here "total" means as follows: we include the reflected vector potential, since the interaction occurs on the surface of a material, the $\mathbf{A}(r,t)$ includes not only the field of incident photon, but also the reflected one (See Fig. 2.6). By using Eq. (4.2), we can calculate the excitation probability by using the Fermi's golden rule, which will be shown as below.

The $\mathbf{j}(r,t)$ and $\mathbf{A}(r,t)$ can be written in terms of creation and annihilation operator of the quasiparticles, which is discussed in Chapter 2. Here, we briefly give the expression of $\mathbf{A}(r,t)$ and $\mathbf{j}(r,t)$ in second quantization, as follows,

$$\begin{aligned}\mathbf{A}(\mathbf{r},t) = &\sum_{\mathbf{k}} (1+r_p)\cos\theta \sqrt{\frac{\hbar}{2V\omega_k\varepsilon_0}}\widehat{\boldsymbol{\epsilon}}_{\parallel}\left(b_k e^{i(\mathbf{k}\cdot\mathbf{r}-\omega_k t)} + b_k^{\dagger} e^{-i(\mathbf{k}\cdot\mathbf{r}-\omega_k t)}\right) \\ &+ \sum_{\mathbf{k}} (1-r_p)\sin\theta \sqrt{\frac{\hbar}{2V\omega_k\varepsilon_0}}\widehat{\boldsymbol{\epsilon}}_{\perp}\left(b_k e^{i(\mathbf{k}\cdot\mathbf{r}-\omega_k t)} + b_k^{\dagger} e^{-i(\mathbf{k}\cdot\mathbf{r}-\omega_k t)}\right),\end{aligned} \tag{4.3}$$

where $\widehat{\boldsymbol{\epsilon}}_{\parallel}(\widehat{\boldsymbol{\epsilon}}_{\perp}), \mathbf{k}, \omega_k$, V are, respectively the unit vector of polarization of the photon in the direction parallel (perpendicular) to graphene, wave vector of the photon, frequency of the photon and volume occupied by the photon. $b_k^{\dagger}(b_k)$ is the creation (annihilation) operator of photon. The reflection coefficient for TM polarized light r_p is given by

$$r_p = \frac{Z_2 \cos\phi - Z_1 \cos\theta - Z_1 Z_2 \sigma_D(\omega) \cos\phi \cos\theta}{Z_2 \cos\phi + Z_1 \cos\theta + Z_1 Z_2 \sigma_D(\omega) \cos\phi \cos\theta}, \tag{4.4}$$

where $Z_i = Z_0/\sqrt{\varepsilon_i}$ is the impedance of medium ε_i, with vacuum impedance $Z_0 = 377\ \Omega$ and ϕ is the angle of refraction.

The $\mathbf{j}(r,t)$ is given by $\mathbf{j}(r,t) = \sigma_D(\omega)\mathbf{E}_{\parallel}(r,t)\delta(z)$, where $\mathbf{E}_{\parallel}(r,t)$ is the electric field of surface plasmon in the direction parallel to graphene surface and graphene is located at $z = 0$. The detailed formulation of quantization of surface plasmon is discussed in Chapter 2, in which the electromagnetic energy of surface plasmon is quantized and can be casted into energy of quantum harmonic oscillator. The electric field of surface plasmon can be written as

$$\begin{aligned}\mathbf{E}(r,t) =& i\sum_{\mathbf{q}} \sqrt{\frac{\hbar\omega_q}{2\varepsilon_0 S}} \left(\boldsymbol{\nu}_{\boldsymbol{q}}(z) e^{i\mathbf{q}\cdot\mathbf{r}} e^{-i\omega_q t} a_q + \boldsymbol{\nu}^{*}_{\boldsymbol{q}}(z) e^{-i\mathbf{q}\cdot\mathbf{r}} e^{i\omega_q t} a_q^{\dagger} \right), \\ =& E_{\parallel}(r,t)\widehat{\mathbf{q}} + E_{\perp}(r,t)\widehat{\mathbf{z}} \end{aligned} \tag{4.5}$$

where ω_q is frequency of the surface plasmon, S is the area of quantized surface plasmon, $\mathbf{q}$ is wave vector of the surface plasmon and $a_q^{\dagger}(a_q)$ is the creation (annihilation) operator of the surface plasmon. The vector $\boldsymbol{\nu}_{\boldsymbol{q}}(z)$ is given by Eq. (2.115). By using Eq. (4.2) and Fermi's golden rule, we can calculate the excitation rate of surface plasmon γ_k for photon wave vector k, given by

$$\gamma_k = \frac{2\pi}{\hbar} \sum_q \left| \langle 1_q, 0_k \left| H_{\text{sp-op}} \right| 0_q, 1_k \rangle \right|^2 \delta(\hbar\omega_k - \hbar\omega_q). \tag{4.6}$$

It is clear from the delta function in Eq. (4.6) that the excitation peak appears if the light frequency matches the surface plasmon frequency (resonant condition). In Eq. (4.6), we consider a joint states consisting of n_k photon and n_q surface plasmon, denoted by $|n_q, n_k\rangle$. $\langle 1_q, 0_k \left| H_{\text{sp-ph}} \right| 0_q, 1_k \rangle$ is called the matrix element of surface plasmon-photon coupling in which a surface plasmon is created by annihilating a photon. Eq. (4.6) gives the generating rate of surface plasmon.

By using Eqs. (4.2) - (4.5), we can write the matrix element $M_{\text{sp-op}}$ as follows,

$$\begin{aligned}
M_{\text{sp-op}} &= \langle 1_q, 0_k \left| H_{\text{sp-op}} \right| 0_q, 1_k \rangle \\
&= i \sum_{k,q} (1 + r_p) \sigma_D(\omega_q) \cos\theta \sqrt{\frac{\hbar}{2V\omega_k \varepsilon_0}} \sqrt{\frac{\hbar\omega_q}{2\varepsilon_0 S}} \times \int dr \; \nu_q^{\parallel}(z) \widehat{\mathbf{q}} \cdot \widehat{\boldsymbol{\epsilon}}_{\parallel} \delta(z) e^{-i(\mathbf{q}-\mathbf{k})\cdot\mathbf{r}} \\
&\quad \times e^{i(\omega_q - \omega_k)t} \left\langle 1_q, 0_k \left| a_q^{\dagger} b_k \right| 0_q, 1_k \right\rangle \\
&= i \sum_{k,q} (1 + r_p) \sigma_D(\omega_q) \cos\theta \sqrt{\frac{\hbar}{2V\omega_k \varepsilon_0}} \sqrt{\frac{\hbar\omega_q}{2\varepsilon_0 S}} e^{i(\omega_q - \omega_k)t} \times \int dx dy e^{-i(\mathbf{q}-\mathbf{k}_{\parallel})\cdot\mathbf{r}} \\
&\quad \times \int dz \nu_q^{\parallel}(z) \widehat{\mathbf{q}} \cdot \widehat{\boldsymbol{\epsilon}}_{\parallel} \delta(z) e^{ik_z z} \\
&= i \sum_{k,q} (1 + r_p) \sigma_D(\omega_q) \cos\theta \sqrt{\frac{\hbar}{2V\omega_k \varepsilon_0}} \sqrt{\frac{\hbar\omega_q}{2\varepsilon_0 S}} \nu_q^{\parallel}(0) \widehat{\mathbf{q}} \cdot \widehat{\boldsymbol{\epsilon}}_{\parallel} e^{i(\omega_q - \omega_k)t} S \delta_{q,k_{\parallel}}, \quad (4.7)
\end{aligned}$$

where $\nu_q^{\parallel}(z)$ is the in-plane component of vector $\boldsymbol{\nu_q}(z)$. Eq. (4.7) shows us that the parallel wave vector of light should match with the surface plasmon wave vector ($k_{\parallel} = q$) in order to have non zero matrix element. In other words, the transition between states with ($k_{\parallel} \neq q$) cannot occur due to the vanishing $M_{\text{sp-op}}$. Hence, Eq. (4.6) can now be calculated by using Eq. (4.7). It is noted from Eq. (4.7) that, if the photon polarization is exactly perpendicular to the surface, the $M_{\text{sp-op}} = 0$, because $\cos\ 90^\circ = 0$. The $M_{\text{sp-op}}$ also vanishes if we have s polarized incident wave, since the $\widehat{\mathbf{q}} \cdot \widehat{\boldsymbol{\epsilon}}_{\parallel}$=0.

In the next section we will use Eq. (4.6) to calculate the excitation probability and relate it with optical absorption spectrum. We will see that if we have the resonant conditions ($k_{\parallel} = q$ and $\hbar\omega_k = \hbar\omega_q$), we will have a peak on absorption spectrum.

4.3 Quantum description of optical absorption

The absorption probability of light that is incident to graphene can be obtained by solving the Maxwell equations on the graphene surface, whose solution is given by Eq. (2.76). However, the physical process related to the transition of electron cannot be understood well. Physically, the optical absorption in graphene is due to the excitation of electron. To show this excitation probability, we may use the Fermi's golden rule for the interaction between photon and electron. The interaction Hamiltonian for electron near the K point of graphene's Brillouin zone can be written as,

$$\begin{aligned}
H_{\text{e-op}} &= \sum_j e v_{\text{F}} \boldsymbol{\sigma} \cdot \mathbf{A}(r_j, t) \\
&= \sum_{ll'pp'} \langle l'p' \left| e v_{\text{F}} \boldsymbol{\sigma} \cdot \mathbf{A} \right| lp \rangle \, c_{l'p'}^{\dagger} c_{lp}, \quad (4.8)
\end{aligned}$$

where $\boldsymbol{\sigma}$ are the Pauli matrices, $\mathbf{A}(r_j, t)$ is vector potential of light for the j-th electron and $v_{\text{F}} \approx 10^6$ m/s is the Fermi velocity of graphene. In Eq. (4.8), we use the second quantization picture and introduce the creation and annihilation operators of electron in state $|lp\rangle$, the $c_{lp}^{\dagger}$ and c_{lp}, respectively. $l = +(-)$ denotes the conduction (valence) band and p denotes the wave vector of electron measured from the K point. It is noted

again that $\mathbf{A}(r_j,t)$ is the total vector potential on the graphene surface which consist of, not only the incident one, but also reflected or transmitted one. By using Eq. (4.3) for TM polarized light and $\boldsymbol{\epsilon} = (\cos\theta, 0, \sin\theta)$, $\langle l'p'\,|ev_{\mathrm{F}}\overrightarrow{\sigma}\cdot\mathbf{A}|\,lp\rangle$ in Eq. (4.8) can be calculated as follows,

$$\begin{aligned}\langle l'p'\,|ev_{\mathrm{F}}\boldsymbol{\sigma}\cdot\mathbf{A}|\,lp\rangle =& \sum_{\mathbf{k}}\frac{ev_{\mathrm{F}}}{2}\sqrt{\frac{\hbar}{2V\omega_k\varepsilon_0}}\left[le^{i\theta_p}+l'e^{-i\theta_{p'}}\right](1+r_p)\cos\theta b_k\delta_{p',p+k_\parallel}\\ &\times e^{-i\omega_k t},\end{aligned} \tag{4.9}$$

where the wave function of electron near the K point is given by $|lp\rangle = \frac{1}{\sqrt{2}}(1 \quad le^{i\theta_k})^t$ and we only consider the annihilation of photon (b_k). Here k denotes the wave vector of photon and p is the wave vector of an electron. By substituting Eq. (4.9) to Eq. (4.8), we have

$$\begin{aligned}H_{\text{e-op}} =& \sum_{ll'pk}(1+r_p)\frac{ev_{\mathrm{F}}}{2}\sqrt{\frac{\hbar}{2V\omega_k\varepsilon_0}}\cos\theta\left[le^{i\theta_p}+l'e^{-i\theta_{p+k_\parallel}}\right]c^\dagger_{l'p+k_\parallel}c_{lp}b_k\\ &\times e^{-i\omega_k t}.\end{aligned} \tag{4.10}$$

Eq. (4.10) gives us the electron-photon interaction Hamiltonian in second quantization form. Hence, we are able to calculate the transition rate between the joint states $|n_{l'p'}, n_{lp}\ n_k\rangle$, which contains n_k photon with wave vector k and $n_{lp}(n_{l'p'})$ electron with wave vector $p(p')$ in $l(l')$ band, by using Fermi's golden rule. The absorption rate for light with wave vector k due to the electron transition γ^e_k is given by,

$$\gamma^e_k = \frac{2\pi}{\hbar}\sum_{ll'p}\left|\left\langle 1_{l'p+k_\parallel},0_{lp},0_k\,|H_{\text{e-op}}|\,0_{l'p+k_\parallel},1_{lp},1_k\right\rangle\right|^2\delta(\hbar\omega_k-\Delta E), \tag{4.11}$$

where ΔE is the energy difference between electronic states. For $\hbar\omega_k \ll E_{\mathrm{F}}$, we have only intraband transition of electron, therefore the transition is between conduction band and $\Delta E = \hbar v_{\mathrm{F}}k_\parallel$. By substituting Eq. (4.10) to Eq. (4.11), the absorption rate for intraband transition is given by,

$$\begin{aligned}\gamma^{e,\text{intra}}_k =& \frac{\pi}{V\omega_k\varepsilon_0}|1+r_p|^2\cos^2\theta\frac{(v_{\mathrm{F}}e)^2}{2}\sum_p\left(1+\cos(\theta_p+\theta_{p+k})\right)\delta(\hbar\omega_k-\hbar v_{\mathrm{F}}k_\parallel)\\ =& \frac{S}{V\omega_k\varepsilon_0}|1+r_p|^2\cos^2\theta(v_{\mathrm{F}}e)^2\delta(\hbar\omega_k-\hbar v_{\mathrm{F}}k_\parallel)\int_{p_{\mathrm{F}}-\frac{\omega_k}{v_{\mathrm{F}}}}^{p_{\mathrm{F}}}pdp\\ =& \frac{S}{V\omega_k\varepsilon_0}|1+r_p|^2\cos^2\theta(v_{\mathrm{F}}e)^2p_{\mathrm{F}}\frac{\omega_k}{v_{\mathrm{F}}}\delta(\hbar\omega_k-\hbar v_{\mathrm{F}}k_\parallel),\end{aligned} \tag{4.12}$$

where p_{F} is the Fermi wave vector of graphene. The $\hbar\omega_k - \hbar v_{\mathrm{F}}k_\parallel$ in the delta function of Eq. (4.12) cannot be zero for $k \neq 0$, because $\hbar\omega_k - \hbar v_{\mathrm{F}}k_\parallel = \hbar k(c - v_{\mathrm{F}}\sin\theta)$, where $c \approx 10^2 v_{\mathrm{F}}$. However, if $k \to 0$, the $\hbar\omega_k - \hbar v_{\mathrm{F}}k_\parallel$ approaches zero, thus we can neglect $\hbar v_{\mathrm{F}}k_\parallel$ and $\delta(\hbar\omega_k - \hbar v_{\mathrm{F}}k_\parallel) \approx \delta(\hbar\omega_k)$. Therefore, we can further calculate the Eq. (4.12),

$$\begin{aligned}\gamma^{e,\text{intra}}_k =& \frac{S}{V\omega_k\varepsilon_0}|1+r_p|^2\cos^2\theta(v_{\mathrm{F}}e)^2p_{\mathrm{F}}\frac{\omega_k}{v_{\mathrm{F}}}\delta(\hbar\omega_k)\\ =& \frac{S}{V\varepsilon_0}\cos^2\theta\,|1+r_p|^2\,\frac{e^2E_{\mathrm{F}}}{\hbar}\delta(\hbar\omega_k)\end{aligned} \tag{4.13}$$

Eq. (4.13) tells us that the $\gamma_k^{e,\text{intra}}$ vanishes if $\hbar\omega_k \neq 0$, or in other words, the intraband optical excitation of electron is not possible. However, if we introduce the broadening of $\delta(\hbar\omega_k)$, we will have value of $\gamma_k^{e,\text{intra}}$ for $\hbar\omega_k \neq 0$. The $\delta(\hbar\omega_k)$ is expressed as Lorentzian function, with broadening factor Γ, as follows,

$$\begin{aligned}\gamma_k^{e,\text{intra}} =& \frac{S}{V\omega_k\varepsilon_0}\left|1+r_p\right|^2\cos^2\theta(v_{\text{F}}e)^2 p_{\text{F}}\frac{\omega_k}{v_{\text{F}}}\frac{1}{\pi}\frac{\Gamma}{(\hbar\omega_k)^2+\Gamma^2}\\ =& \frac{S}{V\varepsilon_0}\cos^2\theta\left|1+r_p\right|^2\frac{e^2E_{\text{F}}}{\pi\hbar}\frac{\Gamma}{(\hbar\omega_k)^2+\Gamma^2}\\ =& \frac{S}{V\varepsilon_0}\cos^2\theta\left|1+r_p\right|^2\text{Re}[\sigma_D(\omega_k+i\frac{\Gamma}{\hbar})],\end{aligned} \tag{4.14}$$

where $E_{\text{F}} = \hbar v_{\text{F}} p_{\text{F}}$ and $\frac{e^2E_{\text{F}}}{\pi\hbar}\frac{\Gamma}{(\hbar\omega_k)^2+\Gamma^2}$ is nothing but real part of the intraband conductivity in Eq. (2.97) if we substitute $\hbar\omega \to \hbar\omega + i\Gamma$. The intraband excitation of electron can only occur if we consider the scattering of electron by impurity or with phonon, which is represented by Γ. Otherwise, we return to Eq. (4.13) with vanishing value of $\gamma_k^{e,\text{intra}}$ if $\hbar\omega_k \neq 0$.

Here we consider the case where graphene is surrounded by vacuum as shown in Fig. 3.5(a), the optical absorption probability by electron $A_{\text{e,intra}}$ can be obtained by dividing $\gamma_k^{e,\text{intra}}$ with photon flux,

$$\begin{aligned}A_{\text{e,intra}} =& \frac{\gamma_k^{e,\text{intra}}}{c\frac{S}{V}\cos\theta} \qquad (4.15)\\ =& \frac{\left|1+r_p\right|^2}{c\varepsilon_0}\text{Re}[\sigma_D(\omega_k+i\frac{\Gamma}{\hbar})]\cos\theta\\ =& \frac{4Z_0\cos\theta\ \text{Re}[\sigma_D(\omega_k+i\frac{\Gamma}{\hbar})]}{\left|2+Z_0\cos\theta\sigma_D(\omega_k+i\frac{\Gamma}{\hbar})\right|^2}, \qquad (4.16)\end{aligned}$$

where $Z_0 \equiv (c\varepsilon_0)^{-1} = 377\ \Omega$ is the impedance of vacuum. Therefore, the optical absorption by electron is proportional to the real part of conductivity, which conforms with the common understanding. Equation (4.16) is nothing but the absorption probability solved by the Maxwell equation that is given by Eq. (2.76), which is plotted in Fig. 4.2 (a), though the physical process involving electron excitation cannot be explained if only the electrodynamics description is employed. The peak in Fig. 4.2 (a) can be understood as the excitation of surface plasmon, where the electrons are excited collectively, which is discussed in the following section.

4.3.1 Absorption due to the surface plasmon

The presence of surface plasmon in graphene is given by the pole of Im $1/\varepsilon_g(\omega,q)$, where $\varepsilon_g(\omega,q)$ is the dielectric function of graphene. The Im $1/\varepsilon_g(\omega,q)$ is given by,

$$\text{Im}\ \frac{1}{\varepsilon_g(\omega,q)} = -\frac{\text{Im}\ \varepsilon_g(\omega,q)}{(\text{Re}\ \varepsilon_g(\omega,q))^2+(\text{Im}\ \varepsilon_g(\omega,q))^2}. \tag{4.17}$$

When we apply the EM wave with the frequency ω and parallel wave vector q to graphene, if Im $\varepsilon_g(\omega,q) \to 0$, then Im $\frac{1}{\varepsilon_g(\omega,q)} \to \delta(\text{Re}\ \varepsilon_g(\omega,q))$, where we have a

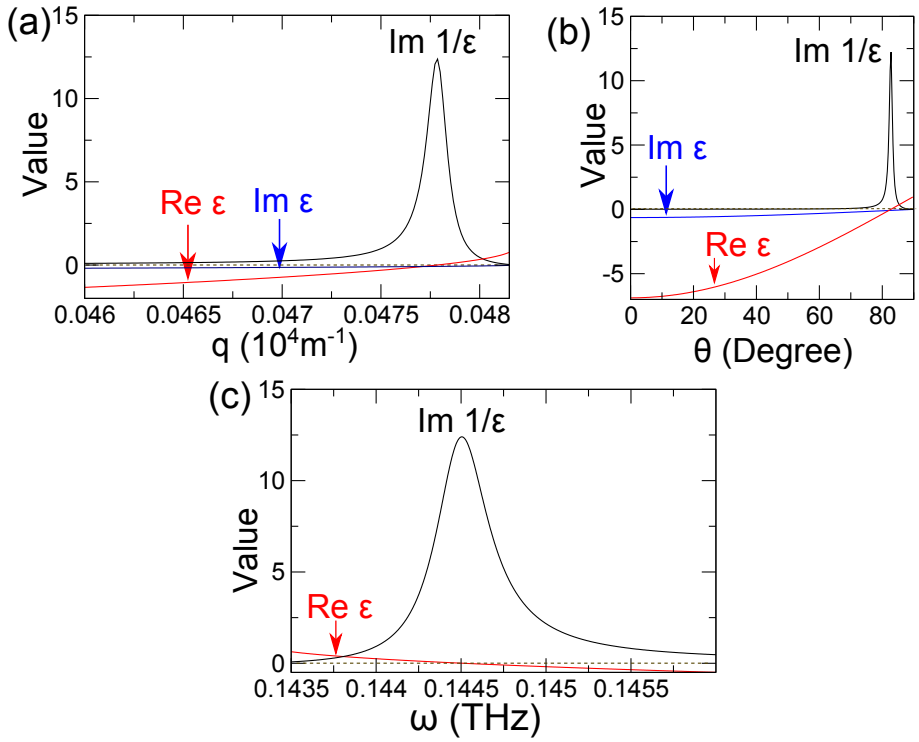

Figure 4.3 The Im $1/\varepsilon_g(\omega, q)$, Re $\varepsilon_g(\omega, q)$, Im $\varepsilon_g(\omega, q)$ as a function of (a) wave vector q, (b) incidence angle θ, (c) frequency ω. For (a) we fix the $\omega = 0.1445$ THz, while for (b) we fix the $q = 0.0477 \times 10^4$ m^{-1}.

peak if Re $\varepsilon_g(\omega, q) = 0$. Therefore, surface plasmon exists if Re $\varepsilon_g(\omega, q) = 0$ and Im $\varepsilon_g(\omega, q) \to 0$. These conditions can be understood from Eq. (1.28). The dielectric function of graphene can be obtained by dividing the left hand side term of Eq. (1.28) with $\frac{\kappa_1 \kappa_2}{\kappa_1 \varepsilon_2 + \kappa_2 \varepsilon_1}$,

$$\varepsilon_g(\omega, q) = 1 + \frac{i\kappa\sigma_D(\omega + i\frac{\Gamma}{\hbar})}{2\omega\varepsilon_0}, \tag{4.18}$$

where we assume that graphene is surrounded by vacuum and $\kappa = \sqrt{q^2 - \omega^2/c^2}$. Let us use the case of Fig. 4.2 (a). Figure 4.3 (a) shows that there is a peak of the Im $\frac{1}{\varepsilon_g(\omega,q)}$ at $q \approx 0.0477 \times 10^4$ m^{-1}, where the Re $\varepsilon_g(\omega, q) = 0$ and Im $\varepsilon_g(\omega, q) \approx 0$. By using Eq. (4.1), we can convert the parallel wave vector q to incidence angle θ, which is given in Fig. 4.3 (b). The peak in Fig. 4.3 (a) corresponds to the excitation of retarded surface plasmon by light incident to graphene with $\theta \approx 82.7°$. Therefore, we can safely say that the absorption peak in Fig. 4.2 (a) comes from the excitation of retarded surface plasmon. In Fig. 4.3 (c), we plot Im $\frac{1}{\varepsilon_g(\omega,q)}$ as a function of ω for $q = 0.0477 \times 10^4$ m^{-1}, where we can see the peak at $\omega \approx 0.1445 \times 10^{12}$ rad s^{-1}.

Fig. 4.3: Fig/epsg.eps

Since we have scattering of electron $\Gamma = 1$ meV, the surface plasmon is damped, which causes the broadening of Im $\frac{1}{\varepsilon_g(\omega,q)}$ as shown in Figs. 4.3 (a)-(c).

We now turn our discussion to the absorption of light due to the excitation of surface plasmon. Eq. (4.6) enables us to calculate the excitation rate of surface plasmon by light. As an example for the theory, we take the case of retarded regime as shown in Fig (4.2). We assume that graphene is surrounded by vacuum and that light propagates to graphene at incident angle θ, as shown in Fig. 4.2 (a). We fixed $\omega_k = 144.5 \times 10^9$ rad s^{-1}, which corresponds to the retarded regime. The absorption probability of light due to the excitation of surface plasmon $A_{\rm sp}$ can be obtained by dividing the γ_k of Eq. (4.11) by the photon flux,

$$\begin{aligned} A_{\rm sp} =& \frac{\gamma_k}{c\frac{S}{V_R}\cos\theta} \\ =& \sum_q |1+r_p|^2 \frac{\alpha^2\pi}{2c\varepsilon_0^2} \left|\sigma_D\left(\omega + i\frac{\Gamma}{\hbar}\right)\right|^2 \frac{\omega_q}{\omega_k}\cos\theta \\ & \times \frac{\eta}{\pi((\omega_k-\omega_q)^2+\eta^2)}\delta_{q,k_\parallel}. \end{aligned} \tag{4.19}$$

In Eq. (4.19), we approximate the delta function $\delta(\hbar\omega_k - \hbar\omega_q)$ to be a Lorentzian, with the broadening parameter η. The $\delta_{q,k_\parallel}$ implies that for each θ, we have one q, which is determined by Eq. (4.1). The ω_q can be obtained from the peak position of Im $\frac{1}{\varepsilon_g(\omega,q)}$. If the ω_q matches the ω_k, we have a peak of $A_{\rm sp}$ coming from the $\delta(\hbar\omega_k - \hbar\omega_q)$ that corresponds to the surface plasmon excitation.

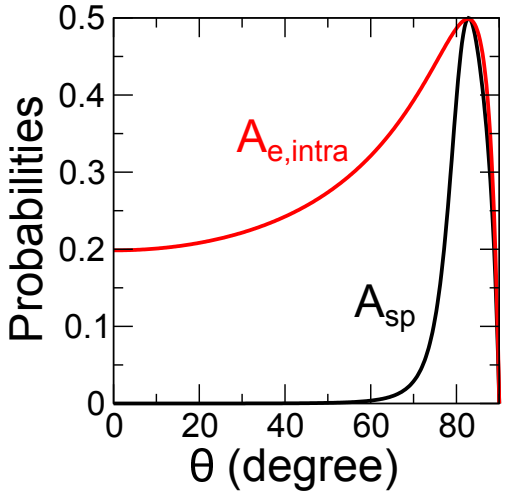

Figure 4.4 The optical absorption due to the surface plasmon ($A_{\rm sp}$) and the total absorption ($A_{\rm e,intra}$)

Figure 4.4 shows the absorption probability of light due to the surface plasmon $A_{\rm sp}$ based on Eq. (4.19) and the total absorption probability based on Eq. (4.16). We can see that the $A_{\rm sp}$ peak coincides with the peak in absorption spectrum, which

Fig. 4.4: Fig/asp.eps

means that the absorption peak in Fig. 4.2 corresponds to the excitation of surface plasmon. It is noted that in Eq. (4.19), the $\eta = 2.27 \times 10^9$ rad s^{-1} is chosen so that the magnitude of the $A_{\rm sp}$ peak is equal with the magnitude of $A_{\rm e,intra}$ peak.

4.3.2 Absorption due to the single particle excitation

Equation (4.16) can be rewritten as follows [76, 75],

$$A_{\rm e,intra} = \frac{Z_0 \cos\theta \ {\rm Re}[\sigma_D(\omega_k + i\frac{\Gamma}{\hbar})]}{\left|1 + \frac{Z_0}{2}\cos\theta\sigma_D(\omega_k + i\frac{\Gamma}{\hbar})\right|^2}. \tag{4.20}$$

The physical meaning of Eq. (4.20) can be compared with the polarization function of interacting electron system $\Pi(q,\omega)$, which is given as follows,

$$\Pi(q,\omega) = \frac{\Pi^0(q,\omega)}{1 - v(q)\Pi^0(q,\omega)} = \frac{\Pi^0(q,\omega)}{\varepsilon_g(q,\omega)}, \tag{4.21}$$

where $\Pi^0(q,\omega)$ and $v(q)$ are polarization function of non-interacting electron system and Coloumb interaction in q space, respectively. In interacting system, the electons interact with each other through Coloumb interaction. The imaginary part $\Pi(q,\omega)$ is the measure of energy dissipation in electron system due to the excitation of the quasi-particle [76], while the Im $\Pi^0(q,\omega)$ measures the dissipation of energy by the non-interacting electron system, which is only due to the excitation of electron-hole or we refer it as single particle excitation [76]. In the interacting electron system, there are not only single particle excitation, but also collective excitation or plasmon, which comes from the pole of Im $1/\varepsilon_g(q,\omega)$. In interacting system, the $\Pi^0(q,\omega)$ is normalized by the $\varepsilon_g(q,\omega)$ to get the polarization function of the system. Hence, the imaginary part $\Pi(q,\omega)$ gives the energy dissipation through the single particle excitation, but at certain values of (q,ω), which give the pole of Im $1/\varepsilon_g(q,\omega)$, the energy dissipation might also comes from the plasmon excitation.

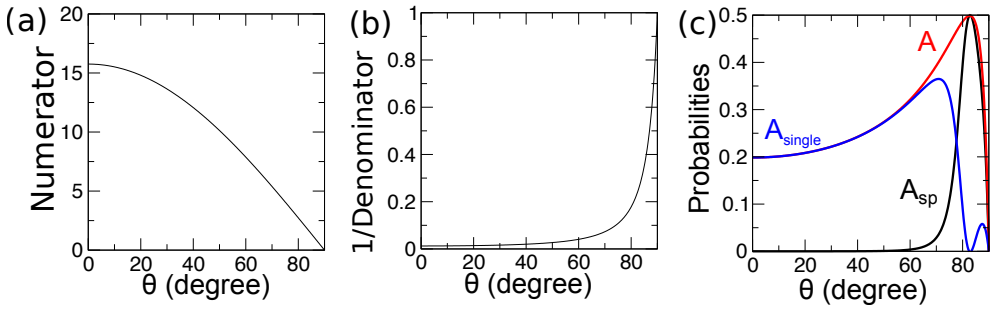

Figure 4.5 The numerator (a) and denominator (b) of Eq. (4.20). (c) The contribution of single particle and collective excitation to the total absorption of light.

In analogy of polarization function of interacting system, the $A_{\rm e,intra}$ is the absorption of light energy used for excitation of quasi-particle in the electron system. The numerator of $A_{\rm e,intra}$ in Eq. (4.20) refers to the Im $\Pi^0(q,\omega)$, which is the absorption

Fig. 4.5: Fig/asp2.eps

of light in the non-interacting electron system due to the single particle excitation. The numerator of $A_{\mathrm{e,intra}}$ in Eq. (4.20) is plotted in Fig. 4.5 (a) as a function θ, where it shows a monotonically decreasing function. The magnitude of the numerator of $A_{\mathrm{e,intra}}$ is normalized by the denominator of $A_{\mathrm{e,intra}}$ in Eq. (4.20) so that the maximum magnitude does not exceed 1. We can say that the normalization is due to the interaction between electrons. The denominator is shown in Fig. 4.5 (b), which is a monotonically increasing function. The surface plasmon appears if only we consider the normalization by the denominator of Eq. (4.20), where we can find a peak of $A_{\mathrm{e,intra}}$.

Therefore, $A_{\mathrm{e,intra}}$ gives the absorption of light due to the single particle excitation, but at certain θ, the surface plasmon appears which is shown by the pole of Im $1/\varepsilon_g(q,\omega)$ and the electrons are excited collectively. In the case of Fig. 4.2 (a), the pole appears at $\theta = 82.7^\circ \equiv \theta_{\mathrm{sp}}$ as shown in Fig. 4.3 (b). At this angle, the numerator of $A_{\mathrm{e,intra}}$ has very low value compared with other angle, therefore we can neglect the contribution of single particle excitation to the total absorption A_{single}. At $\theta = \theta_{\mathrm{sp}}$, the main contribution comes from the surface plasmon or A_{sp}. Therefore, the A_{single} can be obtained by subtracting the total absorption $A_{\mathrm{e,intra}}$ with the A_{sp} as shown in Fig. 4.5 (c). As we see in Fig. 4.5 (c), approaching the θ_{sp}, the A_{single} drops and reaches minimum at θ_{sp}, in which we can say that the electron is not excited individually, but collectively as surface plasmon.

Chapter 5

Negative refraction in Weyl semimetal

In this chapter, we discuss the other work done during the doctoral course, but we do not include it into the main results since the topic is slightly different. In this chapter, we discuss the unique propagation of TM light within a material called the Weyl semimetal (WSM). We found that in certain frequency range of incident TM wave, the wave is refracted negatively within the WSM [88]. This chapter has been published by Journal of the Physical Society of Japan [88].

5.1 Introduction

In recent years, many researchers have developed artificial structures, called as metamaterials, to realize negative refraction as was originally proposed by Veselago [89], in which the light coming to the surface of the materials will be bent with an angle of refraction negative to the normal direction of the surface. Negative refraction requires a material having both negative electric permittivity and magnetic permeability, which has not been found in nature so far. Materials supporting negative refraction could give some interesting applications. For example, superlens proposed by Pendry could have resolution smaller than the light wave length, in contrast to the normal lens whose best resolution is the same as the light wave length [90, 91, 92]. However, fabrication of metamaterials is usually very complicated, involving dielectric photonic crystals or an array of split ring resonators[92, 93, 94, 95] .

To overcome the difficulties in obtaining negative refraction, in this paper, we propose that a WSM may also show negative refraction under some certain conditions, even without having negative magnetic permeability and constructing complicated structure [88]. The WSM is a three-dimensional material having a pair of Dirac cones separated in the k space in its energy dispersion shown in Fig. 5.1 (a)[68, 96]. Example of WSM is phyrochlore ($Eu_2Ir_2O_7$) [68, 97]. We predict that the light can propagate through WSM even though the frequency is smaller than plasmon frequency and this propagation requires the refractive index of the WSM to be negative in order to conserve the energy.

5.2 Model and methods

We can write the electric displacement vector of the WSM as follows [68, 70, 67],

$$\mathbf{D} = \varepsilon_0 \varepsilon_b \left(1 - \frac{\omega_p^2}{\omega^2}\right) \mathbf{E} + \frac{ie^2}{4\pi^2 \hbar \omega} (\nabla\theta) \times \mathbf{E}, \tag{5.1}$$

where ω_p is the plasmon frequency, ε_b is the background dielectric constant. Hereafter, we consider a particular value of the dielectric constant, $\varepsilon_b = 13$, which was measured in pyrochlore. The term θ is called the axion angle given by $\theta = 2(\mathbf{b} \cdot \mathbf{r})$, where $\mathbf{b}$ is a wave vector separating the Weyl nodes [see Figure 5.1(a)] The first term of Eq. (5.1) is the Drude dielectric function, which is similar to normal metals (NMs). The appearance of Hall current without external magnetic field is known as anomalous Hall effect [71, 68] given by the second term of Eq. (5.1). The anomalous Hall current only depends on the structure of the electron dispersion of WSM represented by θ. Due to the anomalous Hall effect, the dielectric tensor has non-zero off-diagonal terms, which can be written as

$$\varepsilon = \begin{bmatrix} \varepsilon_1 & 0 & i\varepsilon_2 \\ 0 & \varepsilon_1 & 0 \\ -i\varepsilon_2 & 0 & \varepsilon_1 \end{bmatrix} \tag{5.2}$$

where we assume that $\mathbf{b}$ lies in the direction of y, $\mathbf{b} = b\hat{\mathbf{y}}$, and that ε_1 and ε_2 are expressed by

$$\varepsilon_1 = \varepsilon_0 \varepsilon_b \left(1 - \frac{1}{\Omega^2}\right), \tag{5.3}$$

$$\varepsilon_2 = \varepsilon_0 \varepsilon_b \left(\frac{\Omega_b}{\Omega}\right), \tag{5.4}$$

with $\Omega = \omega/\omega_p$ and $\Omega_b = e^2 b/(2\pi^2 \varepsilon_0 \varepsilon_b \hbar \omega_p)$ as dimensionless quantities. We take $\Omega_b = 0.5$ as a fixed parameter throughout this paper, otherwise it will be mentioned. Similar to NMs, in the WSM we have $\varepsilon_1 > 0$ ($\varepsilon_1 < 0$) if $\Omega > 1$ ($\Omega < 1$).

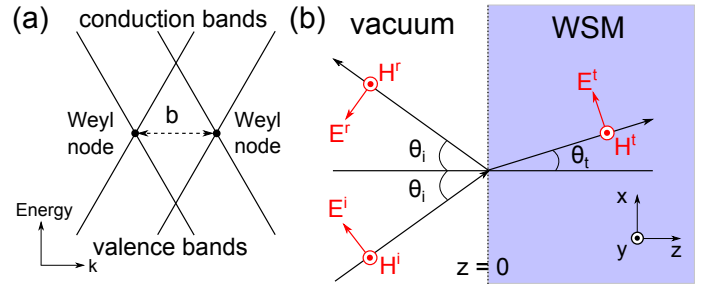

Figure 5.1 (a) Schematic of energy dispersion of WSM showing a pair of Dirac cones with two Weyl nodes represented by dots, separated by the wave vector b. (b) A TM wave coming to xy surface of WSM at angle θ_i and transmitted to WSM at angle θ_t.

Fig. 5.1: Fig/Fig1c.pdf

In order to calculate the reflection and transmission spectra of a bulk WSM, we will determine the refractive index of the WSM (n_w). Suppose that we have a transverse magnetic (TM) wave incident at angle θ_i from vacuum to a WSM as shown in Fig. 5.1(b) where E^i, E^r and E^t (H^i, H^r and H^t) are the incident, reflected and transmitted electric (magnetic) fields, respectively. The transmitted wave propagates toward positive z direction inside WSM, while the reflected wave propagates toward negative z direction. Due to the vanishing ε_{xy} and ε_{zy}, the direction of electric field inside WSM does not rotate. By using Eq. (5.2), we can write down the equation $\mathbf{D} = \hat{\varepsilon}\mathbf{E}$ for the TM wave inside the WSM as follows,

$$\begin{bmatrix} D_x^t \\ D_y^t \\ D_z^t \end{bmatrix} = \begin{bmatrix} \varepsilon_1 & 0 & i\varepsilon_2 \\ 0 & \varepsilon_1 & 0 \\ -i\varepsilon_2 & 0 & \varepsilon_1 \end{bmatrix} \begin{bmatrix} E_x^t \\ 0 \\ E_z^t \end{bmatrix} \tag{5.5}$$

where D^t and E^t are the displacement and electric fields inside the WSM. From Maxwell's equations, we get a differential equation for the EM wave as follows;

$$\nabla \times \nabla \times \mathbf{E}^t = -\nabla^2 \mathbf{E}^t + \nabla \left(\nabla \cdot \mathbf{E}^t \right) = \omega^2 \mu_0 \mathbf{D}^t. \tag{5.6}$$

Since the solutions of $\mathbf{E}^t$ and $\mathbf{D}^t$ are proportional to $\exp\left[i\omega n_w/c \ (\mathbf{s}\cdot\mathbf{r})\right]$, where $\mathbf{s} = (\sin\theta_t, 0, \cos\theta_t)$ is the unit wave vector, we can obtain from Eq. (5.6),

$$\frac{1}{\mu_0}\left(\frac{n_w}{c}\right)\left[\mathbf{E}^t - \mathbf{s}\left(\mathbf{s}\cdot\mathbf{E}^t\right)\right] = \mathbf{D}^t. \tag{5.7}$$

From Eqs. (5.5) and (5.7), we get the following relations,

$$E_x^t = \frac{\varepsilon_1 D_x^t - i\varepsilon_2 D_z^t}{\varepsilon_1^2 - \varepsilon_2^2}, \text{ and } \quad E_z^t = \frac{i\varepsilon_2 D_x^t + \varepsilon_1 D_z^t}{\varepsilon_1^2 - \varepsilon_2^2}. \tag{5.8}$$

Inserting Eq. (5.8) to Eq. (5.7), we obtain simultaneous equations of E_x^t and E_z^t as follows:

$$\begin{bmatrix} \mathrm{A}_- & \mathrm{B}_- \\ \mathrm{B}_+ & \mathrm{A}_+ \end{bmatrix} \begin{bmatrix} E_x^t \\ E_z^t \end{bmatrix} = 0, \tag{5.9}$$

where $\mathrm{A}_\pm = (1 - s_x^2)\varepsilon_{1x} s_z \varepsilon_2 - \mu_0 \left(\frac{c}{n_w}\right)^2 \left(\varepsilon_1^2 - \varepsilon_2^2\right)$ and $\mathrm{B}_\pm = \left(1 - s_x^2\right)\varepsilon_2 - s_x s_z \varepsilon_1$. In order to have nontrivial solutions of $\mathbf{E}^t$, the determinant of the 2×2 matrix in Eq. (5.9) should vanish:

$$\frac{\mu_0 c^2 \left(\varepsilon_1^2 - \varepsilon_2^2\right)}{n_w^4}\left[-n_w^2 \varepsilon_1 + c^2 \mu_0 \left(\varepsilon_1^2 - \varepsilon_2^2\right)\right] = 0. \tag{5.10}$$

from which, we obtain n_w,

$$n_w = \pm c\sqrt{\mu_0 \left(\varepsilon_1^2 - \varepsilon_2^2\right)/\varepsilon_1} \equiv n_w^{\pm}, \tag{5.11}$$

where the n_w^+ (n_w^-) solution corresponds to the positive (negative) wave vector inside the WSM. If we put $\varepsilon_2 = 0$ in Eq. (5.11), we can obtain the refractive index of NM.

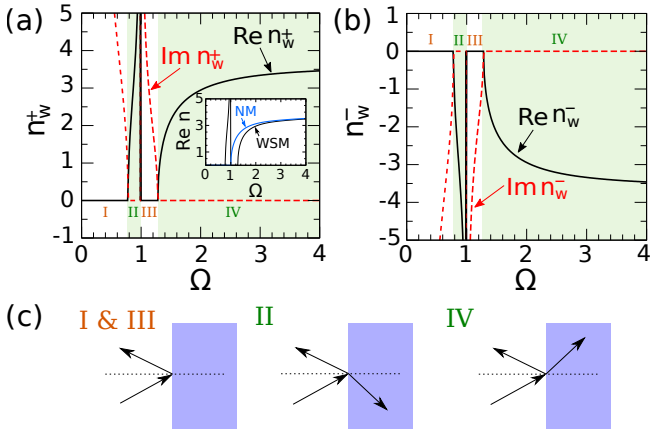

Figure 5.2 (a) The refractive index of WSM for TM wave (n_w) as a function of Ω for the positive solution of Eq. (5.11) (n_w^+). Solid and dashed lines are the real and imaginary parts of n_w^+, respectively. We use $\Omega_b = 0.5$ for the WSM. The plot is divided into four regions. Inset: The real part of refractive index (n) for the WSM compared with a normal metal (NM). (b) The refractive index of WSM for TM wave (n_w) as a function of Ω for the negative solution of Eq. (5.11) (n_w^-). (c) Schematics of EM wave propagations to the WSM for all the four regions of panel (a) and (b).

In Figs. 5.2(a) and (b) we plot n_w as a function of Ω for the positive solution of Eq. (5.11) [Fig. 5.2(a)] and the negative solution of Eq. (5.11) [Fig. 5.2(b)]. The solid and the dashed lines correspond to the real and imaginary parts of n_w, respectively. It is noted that $n_w^\pm$ at each frequency is either purely real or purely imaginary, because we neglect the effects of the impurity and scattering of charge in Eq. (5.3). Therefore, the wave vector $\omega n_w^\pm/c$ can be either real or imaginary depending on $n_w^\pm$. The real (imaginary) wave vector represents a propagating (decaying) wave.

From Fig. 5.2(a), it is important to point out that we may have a propagating wave even at frequencies smaller than plasmon frequency ($\Omega < 1$), in the shaded region II, which is in contrast with NM where an EM wave can propagate if $\Omega > 1$ [see inset of Fig. 5.2(a)]. As shown in the inset of Fig. 5.2(a), the refractive indices of WSM and NM differ only near $\Omega \simeq 1$. At $\Omega \gg 1$, they both converge to the value of $n \approx \sqrt{\varepsilon_b}$. It is important to note that the negative solution of Eq. (5.11) (n_w^-) is assigned to have propagating wave toward positive z direction in the region II, which will be shown later. Let us calculate the reflection and transmission spectra. In NM with applied external magnetic field, the polarization of EM wave undergoes rotation as it enters the material if the direction of propagation is parallel to the direction of applied external magnetic field making the wave polarization not linear. In our case of WSM, we choose the propagation direction of *the purely TM wave* ($E_y = 0$) to be *perpendicular* to the "effective applied magnetic field", which is in the direction of the $\mathbf{b} = b\hat{\mathbf{y}}$. Therefore, we expect no rotation of polarization and the wave polarization keeps linear as TM wave. This fact can also be deduced from the vanishing ε_{xy} and ε_{zy}. As shown in Fig. 5.1(b), the incident, reflected, and transmitted electric fields $\mathbf{E}_i$, $\mathbf{E}_r$ and $\mathbf{E}_t$ can

Fig. 5.2: Fig/Fig2c.eps

be written as

$$\begin{aligned}
\mathbf{E}^i(z) &= (\cos\theta_i, 0, -\sin\theta_i)\, E_0^i \exp(ik_{vz}z),\\
\mathbf{E}^r(z) &= (-\cos\theta_i, 0, -\sin\theta_i)\, E_0^r \exp(-ik_{vz}z),\\
\mathbf{E}^t(z) &= (\cos\theta_t, 0, -\sin\theta_t)\, E_0^t \exp(ik_{wz}^{\pm}z),
\end{aligned} \tag{5.12}$$

with $k_{vz} = (\omega/c)\ \cos\theta_i$ and $k_{wz}^{\pm} = \omega(n_w^{\pm}/c)\ \cos\theta_t$. The angles θ_i and θ_t are related each other by the Snell's law $\sin\theta_i = n_w^{\pm}\sin\theta_t$. The magnetic fields in the y direction can be obtained from the relations $H_y^{i,r} = i\omega\int \varepsilon_0 E_x^{i,r} dz$ and $H_y^t = i\omega\int D_x^t dz$, where $D_x^t = \varepsilon_1 E_x^t + i\varepsilon_2 E_z^t$ is obtained from Eq. (5.5). Then, the magnetic fields can be written as

$$\begin{aligned}
\mathbf{H}^i(z) =& \frac{\omega\varepsilon_0}{k_{vz}}\,(0, \cos\theta_i, 0)\, E_0^i \exp(ik_{vz}z),\\
\mathbf{H}^r(z) =& \frac{\omega\varepsilon_0}{k_{vz}}\,(0, \cos\theta_i, 0)\, E_0^r \exp(-ik_{vz}z),\\
\mathbf{H}^t(z) =& \frac{\omega}{k_{wz}^{\pm}}\,(0, \varepsilon_1\cos\theta_t - i\varepsilon_2\sin\theta_t, 0)\, E_0^t\\
&\times \exp(ik_{wz}^{\pm}z).
\end{aligned} \tag{5.13}$$

After defining the EM fields in both media, we can write down boundary conditions of the EM wave at incidence surface ($z = 0$) as follows,

$$E_0^i\cos\theta_i - E_0^r\cos\theta_i = E_0^t\cos\theta_t, \tag{5.14}$$

and

$$\frac{\omega\varepsilon_0}{k_{vz}}\left(E_0^i\cos\theta_i + E_0^r\cos\theta_i\right) = \frac{\omega}{k_{wz}^{\pm}}\left(\varepsilon_1 E_0^t\cos\theta_t - i\varepsilon_2 E_0^t\sin\theta_t\right), \tag{5.15}$$

where Eqs. (5.14) and (5.15) describe the continuity for the tangential components of electric fields and magnetic fields at $z = 0$, respectively. Reflection coefficient $r = E_0^r/E_0^i$ and transmission coefficient $t = E_0^t/E_0^i$ are given by

$$r = 1 - t\frac{\cos\theta_t}{\cos\theta_i}, \tag{5.16}$$

and

$$t = \frac{2k_{wz}^{\pm}\varepsilon_0\cos\theta_i}{k_{vz}\left(\varepsilon_1\cos\theta_t - i\varepsilon_2\sin\theta_t\right) + k_{wz}^{\pm}\varepsilon_0\cos\theta_t}. \tag{5.17}$$

5.3 Results

We are interested in frequency range, in which the EM wave is transmitted not perfectly reflected. The interesting frequency ranges are shown as region II ($\Omega_- \le \Omega \le 1$) and region IV ($\Omega_+ \le \Omega$), where $\Omega_\pm$ are frequencies that give $n_w = 0$ [Eqs. (5.3), (5.4), (5.11)].

$$\Omega_\pm = 1/2\left(\pm\Omega_b + \sqrt{4 + \Omega_b^2}\right). \tag{5.18}$$

The reflection coefficient r in Eq. (5.16) can be written as follows,

$$\begin{aligned} r &= \frac{A - B - iC}{A + B - iC} \\ &= r_1 + ir_2, \end{aligned} \tag{5.19}$$

where $A = \varepsilon_1 \cos\theta_i \cos\theta_t$, $B = n_w^{\pm}\varepsilon_0 \cos^2\theta_t$, $C = \varepsilon_2 \cos\theta_i \sin\theta_i$. The reflection probability can be obtained from $R = |r|^2 = r_1^2 + r_2^2$, where we define

$$r_1 = \frac{(A+B)(A-B) + C^2}{(A+B)^2 + C^2}, \tag{5.20}$$

$$r_2 = \frac{2CB}{(A+B)^2 + C^2}. \tag{5.21}$$

$R > 1$ if either $r_1 > 1$ or $r_2 > 1$. Let us investigate the case of r_1. From Eq. (5.20), we can define the requirement in order to have $r_1 < 1$ giving us physically sound $R < 1$, otherwise we will have unphysical $R > 1$,

$$|A - B| < |A + B| \tag{5.22}$$

or

$$\left|\varepsilon_1 \cos\theta_i - n_w^{\pm}\varepsilon_0 \cos\theta_t\right| < \left|\varepsilon_1 \cos\theta_i + n_w^{\pm}\varepsilon_0 \cos\theta_t\right|. \tag{5.23}$$

To better visualize Eq. (5.23), we plot $|A - B|$ and $|A + B|$ as a function of Ω. From Fig. 5.3(a), where n_w^+ is selected, $|A - B| > |A + B|$ in region II, which does not fulfill Eq. (5.23) giving the unphysical $R > 1$. On the other hand, from Fig. 5.3(b), where n_w^- is selected, $|A - B| < |A + B|$ in region II, which fulfills Eq. (5.23) and we can have physically correct $R < 1$. This negative solution (n_w^-) should be selected only for region II, because if we apply n_w^- to region IV, we have an unphysical $R > 1$, which is shown by Fig. 5.3(b), in which $|A - B| > |A + B|$ for region IV. We argue later that the reason why n_w^- is selected in region II for having transmitted wave toward positive z-direction, is due to the energy conservation.

The negative refractive index of WSM in region II will cause the wave refracted negatively, which means that the refracted angle θ_t is negative. The refractive index also means that the wave vector of transmitted wave (k_{wz}^-) is negative. The negative wave vector does not mean that the transmitted wave propagates backward, which violates the conservation of energy. The direction of propagation is better determined by the direction of the Poynting vector. The power per unit cross section transmitted in the direction of z can be expressed as

$$\begin{aligned} I_t &= \mathbf{S}_t \cdot \hat{\mathbf{z}} \\ &= \frac{1}{2}\mathrm{Re}\left[\mathbf{E}^t(0) \times \mathbf{H}^{*t}(0)\right] \cdot \hat{\mathbf{z}} \\ &= \frac{c\,|t|^2 \left|E_0^i\right|^2}{2n_w^{\pm}}\varepsilon_1 \cos\theta_t, \end{aligned} \tag{5.24}$$

In order to have transmitted power propagate toward positive z direction, Eq. (5.24) should have a positive value. Since $\varepsilon_1 < 0$ in region II [Eq. (5.3)], while $|t|^2$, $\left|E_0^i\right|^2$, and $\cos\theta_t > 0$, $n_w^{\pm}$ has to be *negative* (n_w^-) in order to have $I_t > 0$. On the other hand, n_w^+

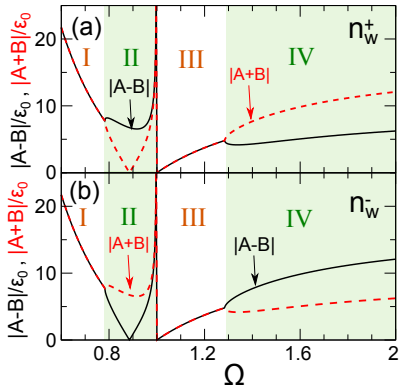

Figure 5.3 $|A-B|$ and $|A+B|$ as a function of Ω if we use (a) n_w^+ and (b) n_w^-. In region II, n_w^- is selected to fulfill Eq. (5.23), while in region IV, n_w^+ is selected. Otherwise, we will have unphysical $R > 1$ in both region.

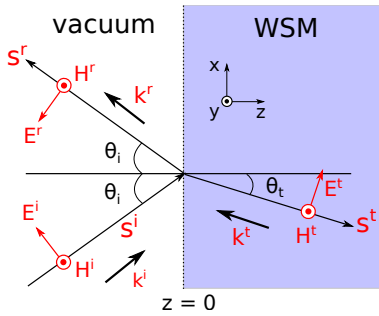

Figure 5.4 The negative refraction in WSM. $\mathbf{S}_t$ is the transmitted Poynting vector. $\mathbf{k}_i, \mathbf{k}_r, \mathbf{k}_t$ are incident, reflected and transmitted wave vectors, respectively.

is selected in region IV, because $\varepsilon_1 > 0$. We refer the transmitted wave as backward wave because the transmitted wave vector points towards negative z-direction shown by Fig. 3.6, otherwise it is forward wave. In short, the negative refraction is needed for the propagation of the EM wave with frequency smaller than the plasmon frequency to *conserve energy*. To show the negative refraction more explicitly, we calculate the tangential component of the transmitted Poynting vector with respect to the interface. The tangential component of Poynting vector is given by,

$$\begin{aligned}\mathbf{S}_t \cdot \hat{\mathbf{x}} = &= \frac{1}{2}\mathrm{Re}\left[\mathbf{E}^t(0) \times \mathbf{H}^{*t}(0)\right] \cdot \hat{\mathbf{x}} \\ &= \frac{c\,|t|^2\,\left|E_0^i\right|^2}{2(n_w^{\pm})^2}\varepsilon_1 \sin\theta_i. \end{aligned} \tag{5.25}$$

Because at region II, $\varepsilon_1 < 0$ and all other terms are positive, then $\mathbf{S} \cdot \hat{\mathbf{x}} < 0$, which means that we have negative refraction. Therefore, at region II, we expect the light is transmitted as backward wave with negative refraction shown by Fig. 5.4.

Fig. 5.3: Fig/Fig4c.eps
Fig. 5.4: Fig/Fig5c.eps

Using Eq. (5.24), the transmission probability T is given by

$$T = \frac{I_t}{I_i} = \frac{1}{n_w^{\pm}} \frac{\varepsilon_1}{\varepsilon_0} \frac{\cos\theta_t}{\cos\theta_i} |t|^2 , \tag{5.26}$$

where $I_i = (c/2)\left|E_0^i\right|^2 \varepsilon_0 \cos\theta_i$ is the incident intensity. The reflection probability R is given by $R = |r|^2$. In Figs. 5.5(a) and 5.5(b) we show the R and T spectra for region II ($\Omega = 0.85$) and region IV ($\Omega = 3$), where the EM wave propagation is allowed. In the case of region II, we adopt the n_w^-, while in the case of region IV, we adopt n_w^+. In region IV, the WSM acts as a NM for $\Omega > 1$. Figure 5.5(b) shows $R = 0$ at $\theta_i = \arctan\ n_w$, which corresponds to the Brewster angle. In both cases, we found $R + T = 1$. In Fig. 5.5(c), we plot the R and T spectra as a function of Ω at a fixed incident angle $\theta_i = 20°$. In region II, we expect that the negative refraction can take place. In NM, all EM wave is reflected in the region II due to the imaginary transmitted wave vector. The region II of WSM, the R gradually decreases with increasing Ω because the transmitted wave vector acquires real value, which signifies the transmission of the incident wave to WSM. After reaching the minimum of R at $\Omega = 0.9$, the reflection probability increases gradually up to $R = 1$ at $\Omega = 1$, above which the transmitted wave vector has only imaginary value that makes $T = 0$. It is important to note that the negative refraction in WSM occurs only in region II, which has frequency range close to ω_p.

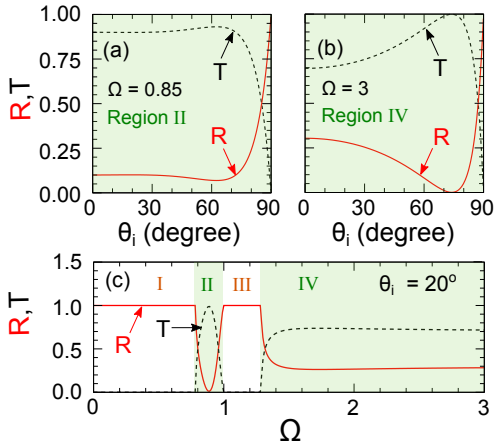

Figure 5.5 The R and T spectra as a function of θ_i shown as solid and dashed line, respectively, for (a) region II ($\Omega = 0.85$), (b) region IV ($\Omega = 3$). In (a) the negative solution of n_w is used, while in (b) the positive one is used. In both cases, $R + T = 1$. (c) The R and T spectra as a function of Ω with fixed $\theta_i = 20°$. In shaded regions II and IV, the wave is transmitted. However, only in region II we expect that negative refraction could occur.

Fig. 5.5: Fig/Fig6c.eps

Chapter 6

Summary

In this thesis, we present the study of electromagnetic (EM) surface wave propagating on the surface of two-dimensional materials, such as graphene and silicene. As the first subject, we investigate the existence of transverse electrin (TE) surface wave on silicene. We found that silicene is theoretically proved to be a versatile platform for utilizing TE surface wave. We have shown that silicene supports the TE surface wave propagation and it exhibits more preferable surface wave properties compared with those of graphene, such as the tunable broadband frequency and smaller confinement length. The TE surface wave in silicene is tunable by the Fermi energy as well as by the external electric field. These characteristics originate from the two-dimensional buckled honeycomb structure.

For the second subject, we study the quantum description of surface plasmon excitation by light in graphene. Surface plasmon can be considered as transverse magnetic (TM) surface wave. The excitation appears as a peak in the optical absorption spectrum, if the resonant conditions for frequency and wave vector are fulfilled. To explain the necessity of satisfying resonant conditions, we quantize the surface plasmon and calculate the excitation probability by using Fermi's golden rule through the surface plasmon - photon interaction. We show that the wave vector matching is needed to obtain non zero interaction matrix element and the frequency matching is needed to have resonant in formulation of Fermi's golden rule. By using Fermi's golden rule, we show that the excitation of surface plasmon will create a peak in absorption spectrum. We also explain that the absorption of light comes from the single particle excitation of electron. However, when the resonant conditions are fulfilled, the electrons are excited collectively known as surface plasmon.

Appendix A

The electron-photon interaction

A.1 Hamiltonian of electron-photon interaction near K-point

In this section, we will derive the Hamiltonian of electron-photon interaction near K-point. The momentum of electron can be expressed by $\hbar\mathbf{p} = -i\hbar\nabla + e\mathbf{A}$, where $\mathbf{A}$ is the vector potential of photon. It is noted that $\mathbf{p}$ is the wave vector of an electron, while $\hbar\mathbf{p}$ is the momentum. The total Hamiltonian of an electron in the presence of $\mathbf{A}$ can be expressed by,

$$\begin{aligned} H_K &= \sum_j \hbar v_{\mathrm{F}} \boldsymbol{\sigma} \cdot \mathbf{p}_j \\ &= \sum_j v_{\mathrm{F}} \boldsymbol{\sigma} \cdot (-i\hbar\nabla_j) + v_{\mathrm{F}} \boldsymbol{\sigma} \cdot e\mathbf{A}(r_j, t), \end{aligned} \tag{A.1}$$

where j is the index of electron. The second term of Eq. (A.1) is called the perturbation Hamiltonian of electron-photon interaction, which is given in Eq. (4.8). Since the total Hamiltonian is linear to $\mathbf{p}$, we do not have the quadratic term of H, which appears for $H = \hbar^2(k + eA)^2/2m$.

A.2 Absorption probability of electron due to the interband transition

The perturbation Hamiltonian of electron-photon interaction near the K point can be written in second quantization form as,

$$H_{\text{e-op}} = \sum_{ll'pp'} \langle l'p' | ev_{\mathrm{F}} \boldsymbol{\sigma} \cdot \mathbf{A} | lp \rangle \, c^\dagger_{l'p'} c_{lp}, , \tag{A.2}$$

where the $c^\dagger_{lp}$ and c_{lp} are the creation and annihilation operators of electron in state $|lp\rangle$, respectively. $l = +1(-1)$ denotes the conduction (valence) band and $p(p')$ denotes the wave vector of electron measured from the K point. $\langle l'p' | ev_{\mathrm{F}} \overrightarrow{\sigma} \cdot \mathbf{A} | lp \rangle$ in Eq. (A.2)

can be calculated as follows,

$$\begin{aligned}
\langle l'p'|ev_{\mathrm{F}}\boldsymbol{\sigma}\cdot\mathbf{A}|lp\rangle =& \sum_{\mathbf{k}}\frac{ev_{\mathrm{F}}}{2}\sqrt{\frac{\hbar}{2V\omega_k\varepsilon_0}}(1+r_p)\begin{bmatrix}1 & l'e^{-i\theta_{p'}}\end{bmatrix}e^{-i\omega_k t}\\
&\times\begin{bmatrix}0 & b_k\cos\theta\\ b_k\cos\theta & 0\end{bmatrix}\begin{bmatrix}1\\ le^{i\theta_p}\end{bmatrix}\int e^{-i\mathbf{p}'\cdot\mathbf{r}}e^{i\mathbf{k}\cdot\mathbf{r}}e^{i\mathbf{p}\cdot\mathbf{r}}\delta(z)dr\\
=&\sum_{\mathbf{k}}\frac{ev_{\mathrm{F}}}{2}\sqrt{\frac{\hbar}{2V\omega_k\varepsilon_0}}\left[le^{i\theta_p}+l'e^{-i\theta_{p'}}\right](1+r_p)\\
&\times\int e^{i(\mathbf{p}+\mathbf{k}_\parallel-\mathbf{p}')\cdot\mathbf{r}}dxdy\int\delta(z)e^{ik_z z}dze^{-i\omega_k t}\\
=&\sum_{\mathbf{k}}\frac{ev_{\mathrm{F}}}{2}\sqrt{\frac{\hbar}{2V\omega_k\varepsilon_0}}\left[le^{i\theta_p}+l'e^{-i\theta_{p'}}\right](1+r_p)\cos\theta\\
&{}_k\delta_{p',p+k_\parallel}e^{-i\omega_k t},
\end{aligned}\tag{A.3}$$

where we assume that the eigen vector $|lp\rangle=\frac{1}{\sqrt{2}}(1\ \ le^{i\theta_k})^t$ is normalized and graphene is purely two-dimensional system (we put delta function $\delta(z)$). Equation (A.2) can be written as,

$$H_{\text{e-op}}=\sum_{ll'pk}(1+r_p)\frac{ev_{\mathrm{F}}}{2}\sqrt{\frac{\hbar}{2V\omega_k\varepsilon_0}}\cos\theta\left[le^{i\theta_p}+l'e^{-i\theta_{p+k_\parallel}}\right]c^\dagger_{l'p+k_\parallel}c_{lp}b_k e^{-i\omega_k t}.$$

In interband transition, we consider vertical transition of $\mathbf{k}$ ($k_\parallel=0$). Therefore, the absorption rate is given by the Fermi golden rule as follows,

$$\begin{aligned}
\gamma_k^{e,\text{inter}}=&\frac{2\pi}{\hbar}\sum_{ll'p}\left|\langle 1_{+1p},0_{-1p},0_k|H_{\text{e-op}}|0_{+1p},1_{-1p},1_k\rangle\right|^2\delta(\hbar\omega_k-2\hbar v_{\mathrm{F}}p)\\
=&\frac{\pi}{V\omega_k\varepsilon_0}|1+r_p|^2\cos^2\theta(v_{\mathrm{F}}e)^2\sum_p\sin^2\theta_p\delta(\hbar\omega_k-2\hbar v_{\mathrm{F}}p)\\
=&\frac{S}{V\omega_k\varepsilon_0}|1+r_p|^2\cos^2\theta(v_{\mathrm{F}}e)^2\int p\delta(\hbar\omega_k-2\hbar v_{\mathrm{F}}p)\\
=&\frac{S}{V\varepsilon_0}|1+r_p|^2\cos^2\theta\frac{e^2}{4\hbar},
\end{aligned}\tag{A.4}$$

The optical absorption probability for graphene surrounded by vacuum $A_{\text{e,inter}}$ can be obtained by dividing $\gamma_k^{e,\text{inter}}$ with photon flux,

$$A_{\text{e,inter}}=\frac{\gamma_k^{e,\text{inter}}}{c\frac{S}{V}\cos\theta}\tag{A.5}$$

$$\begin{aligned}
=&\frac{|1+r_p|^2}{c\varepsilon_0}\ \mathrm{Re}[\sigma_E(\omega_k)]\cos\theta\\
=&\frac{4Z_0\cos\theta\ \mathrm{Re}[\sigma_E(\omega_k)]}{|2+Z_0\cos\theta\sigma_E(\omega_k)|^2},
\end{aligned}\tag{A.6}$$

where $Z_0 \equiv (c\varepsilon_0)^{-1} = 377\ \Omega$ is the impedance of vacuum and $\mathrm{Re}[\sigma_E(\omega_k)] = e^2/4\hbar$ is the real part of interband conductivity. For the normal incident of light, we have

$$A_{\mathrm{e,inter}} = \frac{4Z_0\ \mathrm{Re}[\sigma_E(\omega_k)]}{\left|2 + Z_0\sigma_E(\omega_k)\right|^2} \approx \pi\alpha = 2.3\%, \tag{A.7}$$

where $\alpha = e^2 Z_0/4\pi\hbar$ is the fine structure constant. We return to the well-known interband absorption probability of graphene, which is 2.3%. Equation (A.6) is similar to Eq. (4.16), with the intraband conductivity replaced by interband conductivity.

Appendix B

Velocity matrix

In this chapter, we will derive the velocity matrix given by Eq. 3.3. The velocity matrix $\widehat{v}(k)$ of Eq. 3.3 is the velocity of electron in band representation defined by $\widehat{v}(k) = U^{-1}\ (\partial H_{\varsigma\eta}(\mathbf{k})/\hbar\partial\mathbf{k})\ U$,where U is the unitary matrix which diagonalize $H_{\varsigma\eta}$. $\partial H_{\varsigma\eta}(\mathbf{k})/\hbar\partial\mathbf{k}$ is the velocity of electron in the representation of atomic site, which is given by,

$$\frac{\partial H_{\varsigma\eta}(\mathbf{k})}{\hbar\partial\mathbf{k}} = v_{\mathrm{F}}\begin{bmatrix} 0 & \widehat{\mathbf{x}} - \widehat{\mathbf{y}}i\eta \\ \widehat{\mathbf{x}} + \widehat{\mathbf{y}}i\eta & 0 \end{bmatrix}. \tag{B.1}$$

The U matrix can be obtained by solving for the eigenvector of $H_{\varsigma\eta}$. The U matrix is given as follows,

$$U = \begin{bmatrix} \hbar v_{\mathrm{F}}k\sqrt{\frac{1}{2\epsilon_{\varsigma\eta}(\epsilon_{\varsigma\eta}+\frac{1}{2}\Delta_{\varsigma\eta})}} & \hbar v_{\mathrm{F}}k\sqrt{\frac{1}{2\epsilon_{\varsigma\eta}(\epsilon_{\varsigma\eta}-\frac{1}{2}\Delta_{\varsigma\eta})}} \\ e^{i\eta\theta}\sqrt{\frac{\epsilon_{\varsigma\eta}+\frac{1}{2}\Delta_{\varsigma\eta}}{2\epsilon_{\varsigma\eta}}} & -e^{i\eta\theta}\sqrt{\frac{\epsilon_{\varsigma\eta}-\frac{1}{2}\Delta_{\varsigma\eta}}{2\epsilon_{\varsigma\eta}}} \end{bmatrix}, \tag{B.2}$$

where $\epsilon_{\varsigma\eta} = \sqrt{(\hbar v_{\mathrm{F}}k)^2 + \frac{1}{4}\Delta_{\varsigma\eta}^2}$. By using Eqs. (B.1) and (B.2), we obtain the $\widehat{v}(k)$ as follows,

$$\widehat{v}(k) = \frac{\hbar v_{\mathrm{F}}^2 k}{\epsilon_{\varsigma\eta}}\begin{bmatrix} \widehat{\mathbf{x}}\cos\theta + \widehat{\mathbf{y}}\eta\sin\theta & -Z_-\{\widehat{\mathbf{x}}(-\Gamma_- + \mathrm{A}_-) - \widehat{\mathbf{y}}i\eta(\mathrm{B}_- - \mathrm{I}_-)\} \\ Z_+\{\widehat{\mathbf{x}}(\Gamma_+ + \mathrm{A}_+) - \widehat{\mathbf{y}}i\eta(\mathrm{B}_+ + \mathrm{I}_+)\} & -\widehat{\mathbf{x}}\cos\theta - \widehat{\mathbf{y}}\eta\sin\theta \end{bmatrix}, \tag{B.3}$$

where we define $\beta_\pm = \epsilon_{\varsigma\eta} \pm 1/2\Delta_{\varsigma\eta}$, $Z_\pm = (\beta_\pm/\beta_\mp)^{1/2}$, $\Gamma_\pm = \Delta_{\varsigma\eta}\cos\theta/\beta_\pm$, $\mathrm{A}_\pm = i2\epsilon_{\varsigma\eta}\sin\theta/\beta_\pm$, $\mathrm{B}_\pm = 2\epsilon_{\varsigma\eta}\cos\theta/\beta_\pm$, and $\mathrm{I}_\pm = i2\Delta_{\varsigma\eta}\sin\theta/\beta_\pm$. Here θ is the angle between k and k_x. Eq. (B.3) is Eq. (3.3) of the main text.

Appendix C

Calculation program

Most of the calculation in this thesis was done analytically and the results were plotted using plotting software. But there are some numerical calculations, which were done by using Mathematica, such as the calculation of optical conductivity of silicene with non-zero temperature and the exact solution of dispersion of the surface plasmon. Here, we give the location of the program, which can be found in the FLEX workstation.

Optical conductivity of silicene with $T \neq 0$

This program calculates the optical conductivty of silicene with non-zero temperature. This program uses the built in function of numerical integration in Mathematica (`NIntegrate`). This program also calculates the propagation length of TE or TM surface wave after calculation of optical conductivity.

Program location: `~shoufie/for/mathematica/silicenesigma.nb`
Inputs:

1. EF: The Fermi energy in Joule.
2. T: The temperature in Kelvin.
3. Δ_z: The energy gap due to the electric field in unit of Δ_{SO}.
4. Γ: The scattering of electron in Joule.

Outputs:

1. opt.dat: The optical conductivity
2. prop.dat: The propagation length

The dispersion of surface plasmon

This program calculates the dispersion of surface plasmon in graphene surrounded by a medium with dielectric constant ε. This Mathematica program solves the Eq. (2.96) for frequency as a function of wave vector numerically using `NSolve`.

Program location: `~shoufie/for/mathematica/plsd.nb`
Inputs:

1. EF: The Fermi energy in Joule.
2. ε: The dielectric constant of surrounding medium.

Outputs:

1. plsd.dat: The dispersion of surface plasmon.

Appendix D

Publication list

Papers related to this thesis

1. C. B. Reynold, **M. S. Ukhtary**, R. Saito, Absorption of THz electromagnetic wave in two mono-layers of graphene, J. Phys. D, 49, 195306, (2016).

2. **M. S. Ukhtary**, A. R. T. Nugraha, E. H. Hasdeo, R. Saito, Broadband transverse electric surface wave in silicene, Appl. Phys. Lett. 109, 063103 (2016).

3. Y. Harada, **M. S. Ukhtary**, M. Wang, S. Srinivasan, E. H. Hasdeo, A. R. T. Nugraha, G. Noe, Y. Sakai, R. Vajtai, P. M. Ajayan, R. Saito, J. Kono, Giant terahertz-wave absorption by monolayer graphene in a total internal reflection geometry, ACS Photonics, 4, 121-126 (2017)

4. **M. S. Ukhtary**, A. R. T. Nugraha, R. Saito, Negative Refraction in Weyl Semimetals, J. Phys. Soc. Jpn. 86, 104703 (2017).

5. **M. S. Ukhtary**, R. Saito, Quantum description of surface plasmon excitation by light in graphene, Physica Status Solidi b, 1800181 (2018).

Other papers

1. **M. S. Ukhtary**, E. H. Hasdeo, A. R. T. Nugraha, R. Saito, Fermi energy-dependence of electromagnetic wave absorption in graphene, APEX, 8, 055102, (2015). (During master course)

2. H. Liu, **M. S. Ukhtary**, R. Saito, Hidden symmetries in N-layer dielectric stacks, J. Phys. Condens. Matter, 29, 455303 (2017).

3. S. A. Nulli, **M. S. Ukhtary**, R. Saito, Significant enhancement of light absorption in undoped graphene using dielectric multilayer system, Appl. Phys. Lett. 112, 073101 (2018).

4. L. Ding, **M. S. Ukhtary**, M. Chubarov, T. H. Choudury, F. Zhang, R. Yang, A. Zhang, J. A. Fan, M. Terrones, J. M. Redwing, T. Yang, M. Li, R. saito, S. Huang, Understanding Interlayer Coupling in TMD-hBN Heterostructure by Raman Spectroscopy, IEEE Transactions on Electron Devices 99, (2018).

Conferences

Oral presentations

1. **M. S. Ukhtary**, H. Liu, S. A. Nulli, R. Saito: Optical properties of multilayer of dielectric media. Presented in ATI 2017 Nano-Carbon Meeting and Zao17 Meeting (2017.08.09-10), Yamagata-Zao, Japan.

2. **M. S. Ukhtary**, E. H. Hasdeo, A. R. T. Nugraha, R. Saito: Fermi energy-dependence of electromagnetic wave absorption in graphene. Presented in Autumn meeting of JSAP 2017 (2017.09.05-09), Fukoka, Japan.

3. **M. S. Ukhtary**, H. Liu, S. A. Nulli, R. Saito: Optical properties of multilayer of dielectric media. Presented in Autumn meeting of JSAP 2017 (2017.09.05-09), Fukoka, Japan.

4. **M. S. Ukhtary**, E. H. Hasdeo, A. R. T. Nugraha, R. Saito: Transverse Magnetic and Transverse Electric Surface Waves in Silicene. Presented in ATI 2018 Nano-Carbon Meeting and Zao18 Meeting (2018.08.01-02), Yamagata-Zao, Japan.

Poster Presentations

1. **M. S. Ukhtary**, A. R. T. Nugraha, E. H. Hasdeo, R. Saito: Broadband transverse electric surface wave in silicene. Presented in NT16: The Fiftenth International Conference on the Science and Application of Nanotubes (2016.05.07-13), Vienna University, Austria.

2. **M. S. Ukhtary**, A. R. T. Nugraha, E. H. Hasdeo, R. Saito: Transverse magnetic and transverse electric surface wave in silicene. Presented in 51st Fullerene-Nanotubes-Graphene General Symposium of Nanotubes (2016.09.07-09), Kaderu Sapporo, Japan.

3. **M. S. Ukhtary**, A. R. T. Nugraha, E. H. Hasdeo, R. Saito: Physical picture of reflection, transmission and absorption of electromagnetic wave in graphene. Presented in A3 Symposium of Nanotubes (2016.11.01-03), Buyeo, South Korea.

4. **M. S. Ukhtary**, H. Liu, R. Saito: Hidden symmetries in N-layer dielectric stacks. Presented in 52nd Fullerene-Nanotubes-Graphene General Symposium of Nanotubes (2017.03.01-03) , Tokyo University, Japan.

5. **M. S. Ukhtary**, A. R. T. Nugraha, R. Saito: Negative Refraction in Weyl Semimetals. Presented in NT17: The Fiftenth International Conference on the Science and Application of Nanotubes (2016.06.25-30), Belo Horizonte, Brazil.

6. **M. S. Ukhtary**, H. Liu, S. A. Nulli, R. Saito: Optical properties of multilayer of dielectric media: Hidden symmetries and application. Presented in A3 Symposium of Nanotubes (2017.10.27-29), Suzhou, China.

7. **M. S. Ukhtary**, R. Saito: Second quantization of surface plasmon in graphene and the applications. Presented in 54nd Fullerene-Nanotubes-Graphene General Symposium of Nanotubes (2017.03.10-12), Tokyo University, Japan.

Bibliography

[1] AN Grigorenko, Marco Polini, and KS Novoselov, Nature photonics 6(11), 749–758 (2012).

[2] R. Saito, G. Dresselhaus, and M. S. Dresselhaus, Physical Properties of Carbon Nanotubes (Imperial College Press, London, 1998).

[3] H-S Philip Wong and Deji Akinwande, Carbon nanotube and graphene device physics (Cambridge University Press, New York, 2010).

[4] Eddwi Hesky Hasdeo. Electronic Raman spectroscopy of metallic carbon nanotubes. Ph. D. thesis, Tohoku University, Department of Physics, June 2013.

[5] Phaedon Avouris, Nano letters 10(11), 4285–4294 (2010).

[6] AH Castro Neto, F Guinea, NMR Peres, Kostya S Novoselov, and Andre K Geim, Reviews of modern physics 81(1), 109 (2009).

[7] KS Novoselov, P Blake, and MI Katsnelson, Encyclopedia of Materials: Science and Technology pages 1–6 (2001).

[8] Stefan Alexander Maier, Plasmonics: fundamentals and applications: fundamentals and applications (Springer Science & Business Media, Bath, 2007).

[9] S A Mikhailov and K Ziegler, Physical Review Letters 99(1), 016803 (July 2007).

[10] Sergey G Menabde, Daniel R Mason, Evgeny E Kornev, Changhee Lee, and Namkyoo Park, Scientific Reports 6(1), 21523 (February 2016).

[11] III Wendell T Hill and Chi H Lee, Light-Matter Interaction (John Wiley & Sons, Weinheim, Germany, June 2008).

[12] John Polo, Tom Mackay, and Akhlesh Lakhtakia, , May 2013).

[13] John Weiner and Frederico Nunes, , February 2017).

[14] H Liu, D A Genov, D M Wu, Y M Liu, J M Steele, C Sun, S N Zhu, and X Zhang, Physical Review Letters 97(24), 243902 (December 2006).

[15] Motohiko Ezawa, New Journal of Physics 14(3), 033003 (March 2012).

[16] N D Drummond, V Zolyomi, and V I Fal'ko, Physical Review B 85(7), 075423 (February 2012).

[17] Tianrong Zhan, Xi Shi, Yunyun Dai, Xiaohan Liu, and Jian Zi, Journal of Physics: Condensed Matter 25(21), 215301 (May 2013).

[18] Choon How Gan, Applied Physics Letters 101(11), 111609 (September 2012).

[19] Hong Liu, Bing Wang, Eunice S P Leong, Ping Yang, Yun Zong, Guangyuan Si, Jinghua Teng, and Stefan A Maier, ACS Nano 4(6), 3139–3146 (June 2010).

[20] F Ramos-Mendieta, J A Hernández-López, and M Palomino-Ovando, AIP Advances 4(6), 067125 (June 2014).

[21] YU V BLUDOV, AIRES FERREIRA, N M R PERES, and M I VASILEVSKIY, International Journal of Modern Physics B 27(10), 1341001 (April 2013).

[22] J B Pendry, L Martin-Moreno, and F J Garcia-Vidal, Science 305(5685), 847–848 (August 2004).

[23] Stefan A Maier, Mark L Brongersma, Pieter G Kik, Scheffer Meltzer, Ari AG Requicha, and Harry A Atwater, Advanced Materials 13(19), 1501–1505 (2001).

[24] Ashkan Vakil and Nader Engheta, Science 332(6035), 1291–1294 (2011).

[25] Dmitry Yu Fedyanin, Alexey V Krasavin, Aleksey V Arsenin, and Anatoly V Zayats, Nano Letters 12(5), 2459–2463 (April 2012).

[26] Bing Wang and Guo Ping Wang, Optics letters 29(17), 1992–1994 (2004).

[27] Liu Liu, Sailing He, and Zhanghua Han, Optics Express 13(17), 6645–6650 (August 2005).

[28] Sergey I Bozhevolnyi, Frontiers in Optics 2008/Laser Science XXIV/Plasmonics and Metamaterials/Optical Fabrication and Testing (2008), paper MWD3 page MWD3 (October 2008).

[29] William L Barnes, Alain Dereux, and Thomas W Ebbesen, Nature 424(6950), 824–830 (August 2003).

[30] Bo Johnsson, Stefan Löfås, and Gabrielle Lindquist, Analytical Biochemistry 198(2), 268–277 (November 1991).

[31] Kevin A Tetz, Lin Pang, and Yeshaiahu Fainman, Optics Letters 31(10), 1528–1530 (May 2006).

[32] Kathryn M Mayer and Jason H Hafner, Chemical Reviews 111(6), 3828–3857 (June 2011).

[33] R C Jorgenson and S S Yee, Sensors and Actuators B: Chemical 12(3), 213–220 (April 1993).

[34] JiřÄśÌĄ Homola, Sinclair S Yee, and Günter Gauglitz, Sensors and Actuators B: Chemical 54(1-2), 3–15 (January 1999).

[35] Bo Liedberg, Claes Nylander, and Ingemar Lunström, Sensors and Actuators 4, 299–304 (January 1983).

[36] Jiří Homola, Chemical Reviews 108(2), 462–493 (January 2008).

[37] U Jönsson, L Fägerstam, B Ivarsson, B Johnsson, R Karlsson, K Lundh, S Löfås, B Persson, H Roos, and I Rönnberg, BioTechniques 11(5), 620–627 (November 1991).

[38] C Kittel, P McEuen, and P McEuen. Introduction to solid state physics. 1996.

[39] Dror Sarid and William Challener, Modern introduction to surface plasmons: theory, Mathematica modeling, and applications (Cambridge University Press, Cambridge, 2010).

[40] Tengpeng Guan, Wei Chen, Xiaoliu Zuo, and Zhijun Sun, Optics Express 22(4), 4714–4722 (February 2014).

[41] David J Griffiths, Introduction to Electrodynamics (Cambridge University Press, Cambridge, June 2017).

[42] Jackson, CLASSICAL ELECTRODYNAMICS, 3RD ED (John Wiley & Sons, New York, January 2007).

[43] Xiao Yong He and Rui Li, IEEE Journal of Selected Topics in Quantum Electronics 20(1), 62–67 ().

[44] Qiaoliang Bao, Han Zhang, Bing Wang, Zhenhua Ni, Candy Haley Yi Xuan Lim, Yu Wang, Ding Yuan Tang, and Kian Ping Loh, Nature Photonics 5(7), 411–415 (July 2011).

[45] Boubekeur Lalmi, Hamid Oughaddou, Hanna Enriquez, Abdelkader Kara, Sébastien Vizzini, Bénidicte Ealet, and Bernard Aufray, Applied Physics Letters 97(22), 223109 (December 2010).

[46] Matthew J Allen, Vincent C Tung, and Richard B Kaner, Chemical Reviews 110(1), 132–145 (January 2010).

[47] Geim, A K, Science 324(5934), 1530–1534 (June 2009).

[48] A K Geim and K S Novoselov, Nature Materials 6(3), 183–191 (March 2007).

[49] A H Castro Neto, F Guinea, N M R PERES, K S Novoselov, and A K Geim, Reviews of Modern Physics 81(1), 109–162 (January 2009).

[50] C J Tabert and E J Nicol, Physical Review B 88(8), 085434 (August 2013).

[51] Abdelkader Kara, Hanna Enriquez, Ari P Seitsonen, L C Lew Yan Voon, Sébastien Vizzini, Bernard Aufray, and Hamid Oughaddou, Surface Science Reports 67(1), 1–18 (January 2012).

[52] M Houssa, A Dimoulas, and A Molle, Journal of Physics: Condensed Matter 27(25), 253002 (June 2015).

[53] C J Tabert and E J Nicol, Physical Review B 89(19), 195410 (May 2014).

[54] L Stille, C J Tabert, and E J Nicol, Physical Review B 86(19), 195405 (November 2012).

[55] Gian G Guzmán-Verri and L C Lew Yan Voon, Physical Review B 76(7), 113 (August 2007).

[56] B Van Duppen, P Vasilopoulos, and F M Peeters, Physical Review B 90(3), 035142 (July 2014).

[57] Marinko Jablan, Hrvoje Buljan, and Marin Soljačić, Physical Review B 80(24), 245435 (December 2009).

[58] E H Hwang and S Das Sarma, Physical Review B 75(20), 205418 (May 2007).

[59] George W Hanson, Journal of Applied Physics 103(6), 064302 (March 2008).

[60] L A Falkovsky and A A Varlamov, The European Physical Journal B 56(4), 281–284 (May 2007).

[61] M. Shoufie Ukhtary, Eddwi H Hasdeo, Ahmad R T Nugraha, and Riichiro Saito, Applied Physics Express 8(5), 055102 (May 2015).

[62] Marinko Jablan, Marin Soljačić, and Hrvoje Buljan, Proceedings of the IEEE 101(7), 1689–1704 (2013).

[63] Hai-Yao Deng and Katsunori Wakabayashi, Physical Review B 92(4), 045434 (July 2015).

[64] B Wunsch, T Stauber, F Sols, and F Guinea, New Journal of Physics 8(12), 318–318 (December 2006).

[65] Hrvoje Buljan, Marin Soljačić, and Marinko Jablan, Optics Express 19(12), 11236–11241 (June 2011).

[66] Yuliy V Bludov, Daria A Smirnova, Yuri S Kivshar, N M R PERES, and Mikhail I Vasilevskiy, Physical Review B 89(3), 035406 (January 2014).

[67] M. M. Vazifeh and M. Franz, Phys. Rev. Lett. 111(2), 027201 (2013).

[68] J. Hofmann and S. Das Sarma, Phys. Rev. B 93(24), 241402 (2016).

[69] A. A. Zyuzin and A. A. Burkov, Phys. Rev. B 86(11), 115133 (2012).

[70] A. A. Burkov and L. Balents, Phys. Rev. Lett. 107(12), 127205 (2011).

[71] A. A. Zyuzin and V. A. Zyuzin, Phys. Rev. B 92, 115310 (2015).

[72] A. G. Grushin, Phys. Rev. D 86(4), 045001 (2012).

[73] A. A. Zyuzin, S. Wu, and A. A. Burkov, Phys. Rev. B 85(16), 165110 (2012).

[74] Pavan Hosur and Xiaoliang Qi, C. R. Phys. 14(9), 857–870 (2013).

[75] Radi A Jishi, Feynman Diagram Techniques in Condensed Matter Physics (Cambridge University Press, Cambridge, 2013).

[76] H Bruus K Flensberg and H Bruus, Many-body quantum theory in condensed matter physics (Oxford University Press New York, Oxford, 2004).

[77] Cheng-Cheng Liu, Hua Jiang, and Yugui Yao, Physical Review B 84(19), 195430 (November 2011).

[78] Cheng-Cheng Liu, Wanxiang Feng, and Yugui Yao, Physical Review Letters 107(7), 076802 (August 2011).

[79] C J Tabert and E J Nicol, Physical Review Letters 110(19), 197402 (May 2013).

[80] Motohiko Ezawa, Physical Review Letters 109(5), 055502 (August 2012).

[81] Cole B Reynolds, M. Shoufie Ukhtary, and Riichiro Saito, Journal of Physics D: Applied Physics 49(19), 195306 (May 2016).

[82] Sophocles J Orfanidis, Electromagnetic waves and antennas (Rutgers University, New Brunswick, 2002).

[83] Alexandre Archambault, François Marquier, Jean-Jacques Greffet, and Christophe Arnold, Physical Review B 82(3), 035411 (July 2010).

[84] M. Shoufie Ukhtary, Ahmad R T Nugraha, Eddwi H Hasdeo, and Riichiro Saito, Applied Physics Letters 109(6), 063103 (August 2016).

[85] Na Liu, Shaunak Mukherjee, Kui Bao, Yang Li, Lisa V Brown, Peter Nordlander, and Naomi J Halas, ACS Nano 6(6), 5482–5488 (May 2012).

[86] L A Falkovsky, Journal of Physics: Conference Series 129(1), 012004 (2008).

[87] Marco Finazzi and Franco Ciccacci, Physical Review B 86(3), 035428 (2012).

[88] M. Shoufie Ukhtary, Nugraha Ahmad R T, and Saito Riichiro, Journal of the Physical Society of Japan 86(10), 104703 (September 2017).

[89] V. G. Veselago, Phys. Usp. 10, 509–514 (1968).

[90] J. B. Pendry, Phys. Rev. Lett. 85(18), 3966 (2000).

[91] Vadim V Cheianov, Vladimir Fal'ko, and BL Altshuler, Science 315(5816), 1252–1255 (2007).

[92] D. R. Smith, J. B. Pendry, and M. C. K. Wiltshire, Science 305, 788–792 (2004).

[93] A. Ishikawa, T. Tanaka, and S. Kawata, Phys. Rev. Lett. 95, 237401 (2005).

[94] HO Moser, BDF Casse, O Wilhelmi, and BT Saw, Phys. Rev. Lett. 94(6), 063901 (2005).

[95] Filiberto Bilotti, Alessandro Toscano, and Lucio Vegni, IEEE Trans. Antennas. Propag. 55(8), 2258–2267 (2007).

[96] Mikito Koshino and Intan Fatimah Hizbullah, Phys. Rev. B 93(4), 045201 (2016).

[97] A. B. Sushkov, J. B. Hofmann, G. S. Jenkins, J. Ishikawa, S. Nakatsuji, S. Das Sarma, and H. D. Drew, Phys. Rev. B 92, 241108 (2015).